AFRL-HE-BR-TR-2001-0172

UNITED STATES AIR FORCE
RESEARCH LABORATORY

SIMULATING THE EFFECTS OF LASER DAMAGE TO THE RETINA

Conceptual MindWorks, Inc.
4318 Woodcock Drive, Suite 210
San Antonio, Texas 78228-1316

HUMAN EFFECTIVENESS DIRECTORATE
DIRECTED ENERGY BIOEFFECTS DIVISION
Optical Radiation Branch
8111 18th Street
Brooks AFB, Texas 78235-5104
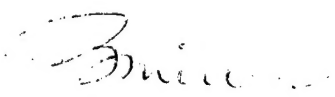
December 2001

20020213 080

NOTICES

This report is published in the interest of scientific and technical information exchange and does not constitute approval or disapproval of its ideas or findings.

Using Government drawings, specifications, or other data included in this document for any purpose other than Government procurement does not in any way obligate the US Government. The fact that the Government formulated or supplied the drawings, specifications, or other data does not license the holder or any other person or corporation; or convey any rights or permission to manufacture, use, or sell any patented invention that may relate to them.

For the most part, this report is published as it was received from the contractor. It has been reviewed for content and is approved for publication.

LEON N. McLIN, Lt Col, USAF, BSC
USAF Contract Monitor

RICHARD L. MILLER, PhD
Chief, Directed Energy Bioeffects Division

REPORT DOCUMENTATION PAGE

Public reporting burden for this collection of information is estimated to average 1 hour per response, including the time for reviewing instructions, searching existing data sources, gathering and maintaining the data needed, and completing and completing and reviewing the collection of information. Send comments regarding this burden estimate or any other aspect of this collection of information, including suggestions for reducing this burden, to Washington Headquarters Services, Directorate for information Operations and Reports, 1215 Jefferson Davis Highway, Suite 1204, Arlington, VA 22202-4302, and to the Office of Management and Budget, Paperwork Reduction Project (0704-0188), Washington, DC 20503.

1. AGENCY USE ONLY (Leave blank)	2. REPORT DATE	3. REPORT TYPE AND DATES COVERED
	December 2001	Final: 3 Sep 93 – 31 Jul 96

4. TITLE AND SUBTITLE
Simulating the Effects of Laser Damage to the Retina

5. FUNDING NUMBERS
C – F41624-93-C-9015
PE – 65502F
PR – 3005
TA – OL
WU – 31

6. AUTHOR(S)
Conceptual MindWorks, Inc.

7. PERFORMING ORGANIZATION NAME(S) AND ADDRESS(ES)
Conceptual MindWorks, Inc.
4318 Woodcock Drive, Suite 210
San Antonio, TX 78228-1316

8. PERFORMING ORGANIZATION REPORT NUMBER

9. SPONSORING/MONITORING AGENCY NAME(S) AND ADDRESS(ES)
Air Force Research Laboratory
Human Effectiveness Directorate, Directed Energy Bioeffects Division
Optical Radiation Branch
8111 18th Street
Brooks AFB, TX 78235-5215

10. SPONSORING/MONITORING AGENCY REPORT NUMBER

AFRL-HE-BR-TR 2001-0172

11. SUPPLEMENTARY NOTES

12a. DISTRIBUTION/AVAILABILITY STATEMENT

Approved for public release; distribution is unlimited.

12b. DISTRIBUTION CODE

13. ABSTRACT (Maximum 200 words)

This Phase II SBIR brought vision and signal processing researchers from the Air Force, academia and the public sector together to develop a visualization tool for modeling laser damage to the retina. The research resulted in experimental results, innovative models and two commercial products.

14. SUBJECT TERMS
Laser damage; model development; retina damage; VisionProbe

15. NUMBER OF PAGES

146

16. PRICE CODE

17. SECURITY CLASSIFICATION OF REPORT	18. SECURITY CLASSIFICATION OF THIS PAGE	19. SECURITY CLASSIFICATION OF ABSTRACT	20. LIMITATION OF ABSTRACT
Unclassified	Unclassified	Unclassified	UL

NSN 7540-01-280-5500

Table of Contents

*Note: These items have been withdrawn from the published report. They are available for review at AFRL/HEDO, Building 803, Brooks Air Force Base, TX.

Simulating the Effects of Laser Damage to the Retina
Final Report

List of Figures
Summary Section

Simulating the Effects of Laser Damage to the Retina
A Detailed Review

1. Introduction

The Air Force's interest in eye damage caused by exposure to intense light began with the dawn of the atomic bomb. Atomic bomb flashes emitted a bright light that caused visual damage to observers. Presently, eye damage due to intense light exposure is more likely to be caused by lasers than by atomic bombs. This is because lasers have become prevalent in the military; they are used for both aiming devices and weapons. Both accidents and direct enemy action result in pilots being particularly vulnerable to eye damage from accidents and direct enemy action.

Laser damage to the eye can result in a number of injuries. Hemorrhages can occur if arteries are hit by lasers and even blindness can occur if there is strong laser blow to the to the optic disk which destroys the optic nerve. Since the topic of laser damage is so vast, this Phase II effort focused on retinal receptor drop out due to heat or occlusion by blood. It was assumed that no underlying nerves were affected and that retinal loss was "all or nothing."

The present Phase II combined Air Force, university and CMI to research the effects of laser eye damage on pilots' performance. The research produced exciting experimental results, innovative models (biologically plausible, visualization and signal processing) and two commercial products. The experimental results came from two sets of psychophysical experiments performed at Conceptual MindWorks, Inc. (CMI) and the University of Texas at San Antonio (UTSA), VEP experiments performed at the University of Texas Health Science Center at San Antonio (UTHSC) and biological experiments performed at UTSA. The biologically plausible model resulted from a collaboration between Dr. Wilson Geisler at the University of Texas at Austin (UTA) and CMI. The visualization model was a result of a collaboration between Brooks Air Force Base and Conceptual MindWorks, Inc., and the signal processing model resulted from work performed at UTSA. The combination of data collection, modeling and commercial products has resulted in the following Phase II report.

2. Evolution of Phase II

Phase I resulted in a model that demonstrated the decrease in acuity due to a laser lesion in the foveal region. The model was called the "Geisler" VEP model and was based on Visual Evoked Potential (VEP) data from rhesus monkeys with laser lesioned eyes. Phase II proposed extensions of the "Geisler" model and a new signal processing model from Phase II. The proposed extensions included incorporating VEP data from humans with normal vision, VEP data from humans with eye diseases whose effects were similar to those of laser damage and VEP data from humans whose vision was altered by artificial scotomas. Another proposed extension was to develop a visualization tool programmed in C that allowed pilots and vision researchers to view what a scene would look like if he/she had incurred laser eye damage. This tool was also used to produce a commercial visualization product that allowed patients and their families to view how the

diseased eye viewed a scene. The proposed signal processing model was to investigate the modeling of retinal neurons and their signal processing properties. This was to result in a better understanding of how damage to specific photoreceptors in the retina has secondary effects on the surrounding sensory outputs.

Over the course of the Phase II project, a number of changes were made to the original proposal. These changes were due to advancements in knowledge and technology as well as the changing needs of the Air Force. All of the changes were made with approval and feedback from the Air Force contract monitor. First, the "Geisler" VEP model was replaced by the Inhomogenous Retino-Cortical (IRC) model. Psychophysical experiments were collected for the Inhomogenous Retino-Cortical models (IRC). VEP data of diseased and normal subjects were collected in addition to the psychophysical data collection. See Appendix IV for the results and conclusions. Second, the visualization model (the AVS/Concentric ring model) was implemented in AVS so that the tool could be incorporated into a larger set of Air Force tools called ILPEM. Also three of the four research projects at UTSA were oriented to aid in the new model development. Third, the Inhomogenous Retino-Cortical (IRC) model was used to estimate the detectability of objects such as airplanes in the sky.

Other deviations from the Phase II proposal were in the form of additions. A second commercial product, called the VisionProbe, was added to the Phase II work.

3. Psychophysical Data Collection for Model

The psychophysical experiments were designed to generate a complete set of contrast sensitivity functions (CSF) and to test performance effects of laser eye damage. Two sets of stimuli were used, the first was a set of Gabor patches and the second was an airplane picture that was perturbed by different artificial scotoma. Both sets o stimuli were presented at various eccentricities, the goal of which was to determine the visual capabilities at various eccentricities. The Gabor patches were also used to measure the spatial summation of the third harmonic of gratings with a without the presence of a fundamental frequency. A more detailed description of the psychophysical experiments can be found in Appendix II. The results of the psychophysical experiments were used to calibrate both the AVS/Concentric Ring Model and the IRC. Results from the IRC and the psychophysical experiments were then compared in order to validate the IRC as a model of visual performance.

4. Model Development

4.1 VEP Model

The visual damage modeling effort began in Phase I with the "Geisler" VEP model. The model was based on VEP data collected from rhesus monkey's who had their eyes damaged by controlled laser blasts. VEP measurements were taken before and after the blasts. The model basically divided the retina into a series of imaginary concentric rings. Each ring is assigned a mathematically derived weight value based on ganglion cell densities. Initially, all the weights were set to one. When a pattern, such as a sine wave pattern, is passed through the model, the first operation is to calculate the pattern's contrast sensitivity for each ring. Then, the responses for all the rings are summed. Since there is considerable variation between one subject's and another's VEP data, the

summed ring responses are multiplied by a subject weight. The model is trained for each subject using a minimization of least squares algorithm. Please refer to Appendix II for the results and conclusions of the Phase I effort.

4.2 AVS Concentric Ring Model

In Phase II, a visualization tool was developed to display the maximal amount of information available at each point in a receptive field for a person with a laser eye injury or a disease that causes photoreceptor drop out. To display the image, the AVS/Concentric Ring Model was used. For displaying a scene as an undamaged eye would see it, the user must first choose a foveation point in the image. Then, like the "Geisler" VEP model, a series of rings representing different eccentricities from the foveation point are superimposed on the scene. A contrast sensitivity function is defined for each ring based on either the literature or the data collected at CMI and described in the Psychophysical Experiments section. A low pass filter that corresponds to the contrast sensitivity function is applied to the pixels in the corresponding region. Therefore, the blur increases ring to ring as the image moves radically outward from the foveation point. To simulate the effect of laser damage, total photoreceptor dropout is assumed. To simulate this, the damaged region is replaced by the average illumination in the total image. This basic technique may also be applied to multiple foveation points. For a more detailed description of the model, please refer to Appendix I. A user's guide is presented in Appendix V.

4.3 IRC Model

The Inhomogenous Retino-Cortical (IRC) model is based on Ideal Observer theory. Ideal Observer theory takes well-established scientific facts about vision and puts them into one model. The facts include physical properties of light, the optics of the eye and absorption of spectra of pigments. The resulting Ideal Observer depicts what the physical properties of the eye are capable of seeing or detecting and illustrates where information is lost in the visual system. A d' measure is used to quantify the ability to see or detect an object. The model does not, however, do a good job of modeling what is actually seen by a person. This is thought to be due to the fact that a human's vision is based on not only the physics of the eye but also cortical functions. In layman's terms, your brains are constantly changing and adapting the information our eyes send. Therefore, what our eyes see and what we perceive are two very different things.

The IRC takes the ideal observer theory and adds floating parameters so that actual visual performance of a subject can be modeled. The parameters are fit using a set of contrast sensitivity curves. To this end, we collected a series of contrast sensitivity curves using psychophysical experimentation, see section 2.0 Psychophysical Experiments. Once the parameters have been fit, the IRC model can be tested to discover how well it modeled a subject's ability to detect an object. For a more detailed description of the model, please refer to Appendix II. A user's guide is presented in Appendix VI.

5. Commercial Products

5.1 VisionProbe

5.1.1 Description

The VisionProbe is a high-speed, high-resolution, computer-based graphics subsystem especially configured for applications in vision research that can reside on any AT compatible computer. It is capable of producing color and monochrome patterned stimuli. A separate graphics co-processor is used to produce the graphics. It resides on a separate board that plugs into the AT compatible bus. This is an advantage because once the graphics processor has been instructed on the type of stimulus patterns to display, the host computer can devote all of its resources to other tasks such as data acquisition and analysis while the graphics board produces the graphics. Because of this independence, VisionProbe integrates smoothly with the DataWave Systems' Experimenter's WorkBench™ so that each product can perform all of its functions at full capacity. This enables an experimenter to collect and analyze data on the same machine, a feature that no other visual stimulator on the market shares.
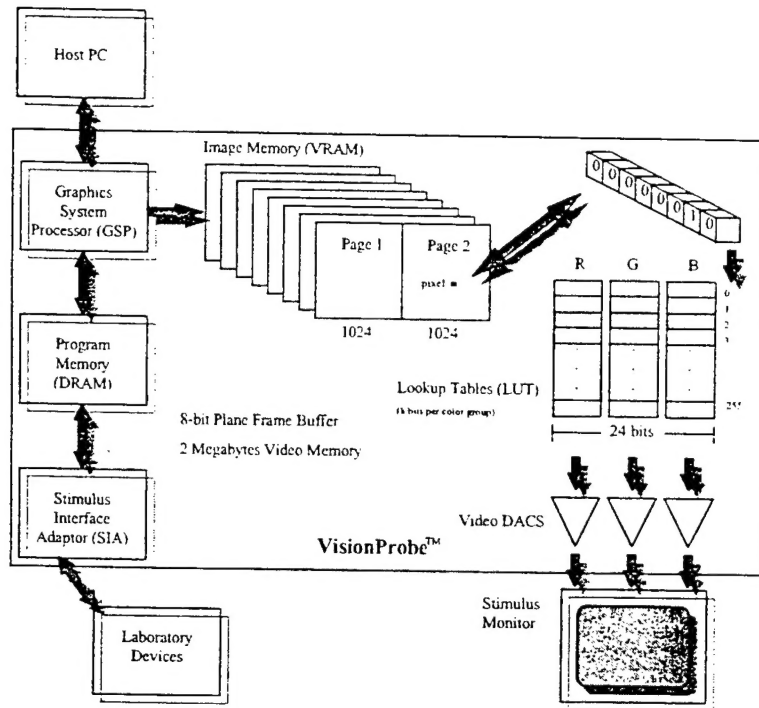
5.1.2 System Configuration

VisionProbe contains the following components when assembled in standard configuration:

- Graphics processor board (OmniComp TEXAN ET)

- I/O adapter board (Conceptual MindWorks ViPSIA/1)

- High-resolution, 21" color CRT

- STIM software which generates the stimulus patterns and controls the graphics processor

- ViP software which is the command level interface by which the user communicates with the graphics board.

- Integrated photometer (UDT Model 265 or equivalent)

The graphics engine itself is the Texas Instruments 34020. The graphics processor board includes 2 Mb of video RAM for holding the video images and 4 Mb of dynamic RAM for holding the STIM software. Video output to the CRT is accomplished through three 8-bit video digital to analog converters (DACs). This permits each of the three color guns (red, green, and blue) in the display to be set to one out of a maximum of 256 luminance levels. The maximum and minimum luminance levels are set by the operator. The ViPSIA/1 adapter board provides for input to and output from the stimulator system. These signals allow for synchronization of the stimulator with external data acquisition and display devices.

An optional, although strongly recommended, component of the VisionProbe is the integrated photometer. When present, the photometer permits VisionProbe to perform automatic gamma correction of the CRT display. Gamma correction is necessary to make the luminance gain function of the display linear and to balance the output of the three color guns so that colors are produced correctly. The user is also able to use the photometer to verify brightness of the display. If an external photometer is available, the display brightness can be measured with that instrument, and gamma correction can be accomplished manually.

Host PC

Image Memory (VRAM)

Graphics System Processor (GSP)

Page 1   Page 2

pixel ■

1024   1024

R   G   B

Program Memory (DRAM)

Lookup Tables (LUT)
(8 bits per color group)

8-bit Plane Frame Buffer

2 Megabytes Video Memory

24 bits

Stimulus Interface Adaptor (SIA)

Video DACS

VisionProbe™

Laboratory Devices

Stimulus Monitor

5.1.3 VisionProbe Development Tasks

5.1.3.1 Background

The VisionProbe was originally developed in the late 1980s by Krug Life Sciences, Inc. to provide a source of visual stimuli for vision researchers. The product was sold to several vision researchers and is still being used by some of them. This product was designed based upon then-state-of-the-art graphics processors. Since that time the graphics card (National Design, Inc. 1288, NDI 1288) has become obsolete, National Design, Inc. has gone out of business and the CPU that the software was designed for has been enhanced (The TMS34010 has been replaced by the TMS34020). The Krug version of the VisionProbe was integrated with a data acquisition system, DataWave Technologies (formerly BrainWave, Technologies) Experimenter's WorkBench. The unavailability of the VisionProbe has left the Experimenter's WorkBench without an integrated visual stimuli system. Our research into the world of vision research has determined that there is still a need for a product similar to the vision probe, especially in situations where the Experimenter's WorkBech system is utilized for data collection in vision experiments. The following sections discuss the tasks that were performed to return the VisionProbe to a production state.

5.1.3.2 Evaluation Of Design

The first step to determine if the VisionProbe Design could be produced with commercially available parts was to perform an evaluation and get familiar with the existing VisionProbe Design. The graphics cards were contacted. OmniComp, Inc

located in Houston, TX had a second generation product, the Texan ET which would support the vision probe function.

5.1.3.3 Existing VisionProbe Evaluation, Assessment And Familiarization

The VisionProbe source code and users manuals were reviewed and the responsible engineers became familiar wit the design of the system. Design notes from the latest versions of the VisionProbe were compared to the source code to determine the last production baseline of the VisionProbe product. This baseline would be the basis for the new VisionProbe product to be developed. Enhancements and added capabilities would be considered as time and resources permitted. The source code was compiled into an executable and operated on the hardware to ensure that all software components were accounted for.

5.1.3.4 VisionProbe Update Planning

The VisionProbe can be divided into three components for planning purposes. The software which was originally written for a TMS34010 based processor required modifications due to processor differences. A large portion of the software could be transferred to the TMS34020 system with only small revisions for Input/Output and memory usage. The graphics board was purchased from a vendor and configured properly for the VisionProbe application. The daughter card (ViPSIA) was redesigned based upon the new graphics card interfaces, new physical envelope, and the latest components commercially available (some of the ViPSIA parts have become obsolete since the original design was completed).

5.1.3.5 Software Development

Software development for the VisionProbe focused on the conversion of the software written fro the NDI 1288 board, TMS34010 processor to the OmniComp Texan ET, TMS34020 processor. The software required revisions for the following functional areas:

- 34010 versus 34020 differences.

- Graphics Card differences such as VRAM wrap, bulk clearing of VRAM, etc.

- Palette chip differences

- ViPSIA design differences including addresses and provisions for expanded signals

- Host Communication Differences (see section 5.1.3.13)

5.1.3.6 Hardware Development

Hardware development for the VisionProbe consisted of producing the VisionProbe Stimulus Interface Adapter (ViPSIA) circuit card. The block diagram for the ViPSIA is shown below.

9

Figure 2: ViPSIA Block Diagram
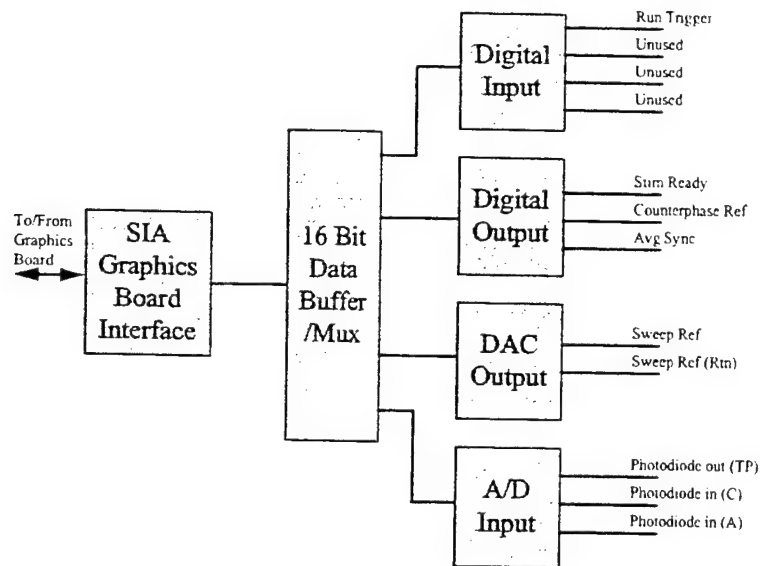
5.1.3.7 Define Interface Between The Texan ET And The ViPSIA

The NDI 1288 based VisionProbe interfaced with the ViPSIA through a memory connector provided on the NDI 1288 board. This connector was not available on the OmniComp Texan ET board. Several alternatives were considered: connect through the PCs motherboard, modify the Texan ET to provide data and address connectors, or utilize the floating point unit (FPU) socket that is provided on each Texan ET for a co-processor option. The FPU socket option was selected due to its suitability to the design. The PC bus option was ruled out due to the overall requirement to allow the VisionProbe to be co-located with the data acquisition software. The FPU socket provided all the necessary signals required fro the ViPSIA with the exception of three. These signals will be routed from elsewhere on the Texan ET to FPU socket unused pins. power and ground for the ViPSIA will be provided from the FPU socket as well.

5.1.3.8 Define Schematic For ViPSIA

The schematic for the updated ViPSIA was derived from the Krug ViPSIA. The basic design for the analog Input/Output portion of the card remained the same. The digital portion of the design was repackaged into a Field Programmable Gate Array (FPGA) for space, power consumption, component availability and flexibility reasons. The modified schematic was developed to support procurement of the circuit card as well efforts to prototype the card.

5.1.3.9 Breadboard ViPSIA

Validation of the design concept was demonstrated by creating a wire wrap version of the ViPSIA digital section. Discrete components were utilized with wire wrap sockets to create a logical representation of the digital portion of the circuit card. Once the design was operating as required the refined schematic was delivered to the ViPSIA manufacturer for card layout and construction.

5.1.3.10 Develop, Design and Manufacture The ViPSIA

Estimates from three sources to develop the layout, design the circuit card and manufacture initial products were received. A local company, Galactic Technologies,

Inc. was selected based upon their cost, hardware design experience and design recommendations, to build the ViPSIA. The layout for the board was completed, design for the FPGA was generated based upon the logical design contained in the design input, the printed circuit board was procured and the board was manufactured and tested.

5.1.3.11 Test The ViPSIA

Once the ViPSIA was manufactured the circuit card was integrated with the Texan ET and tested to ensure that all functions operated correctly. The configuration was tested in TBD different configurations to demonstrate compatibility of the VisionProbe with various manufacturer's PCs.

5.1.3.12 Cable Design And Manufacture

Cables for the VisionProbe products were designed and manufactured. A Cable is required between the ViPSIA PC connector and the data acquisition system and an internal cable is required between the ViPSIA circuit card and the PC connector plate.

5.1.3.13 Data Acquisition Interface Development

Discussions between DataWave Technologies and CMI engineers revealed that the Experimenters WorkBench software included some VisionProbe routines which supported direct communications between the two products. Examination of this software determined that it communicated with the NDI 1288 board directly through it's TMS34010 host interface. This type of host interface is not supported in the TMS34020. Recall that one of the primary design requirements for the VisionProbe development of this product was to not require DataWave to have to make changes to their product. Initial descriptions of the VisionProbe stated that the Experimenter's WorkBench/VisionProbe communication was performed via an ASCII or binary file. We began thinking of ways to simulate the old host communications, but this approach would cause problems. The problem is that the host communication with the 34010 is tied in with the hardware, (the GSP could detect a read or a write to it's HSTDATA register) this means that the PC could write or read as fast as it wanted to. A software solution would introduce errors because we would not be able to tell when the PC has read or written to the GSP memory, thus resulting in data loss. The solution to this problem is to use the new host interface and make the appropriate changes to the DataWave code. These changes will not be major because they all occur in functions that are easily replaceable. The new functions were developed by CMI so that it will recognize TMS34010 or TMS34020 based VisionProbe and set the communications protocol accordingly. DataWave must only recompile their Experimenter's WorkBench product to contain the new source code. The interface has been tested at DataWave's facility and is operating correctly. The VisionProbe configuration that utilizes the DataWave data acquisition system is shown in below.

Figure 3: Swept Stimulus Operation Example
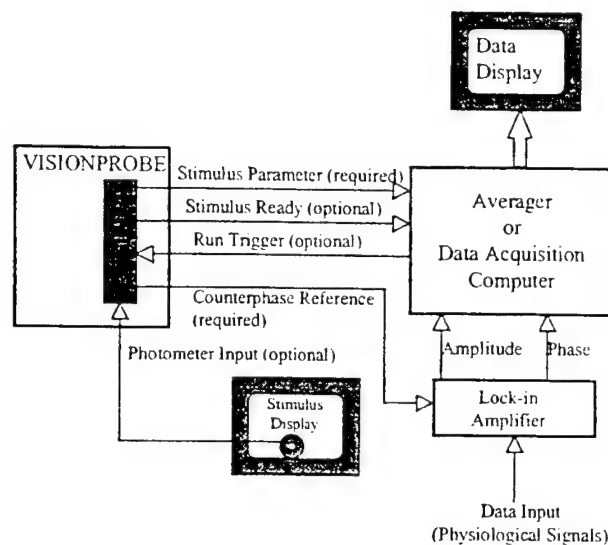
5.1.4 Commercialization

The sale of the VisionProbe to vision researchers will be conducted with two primary emphasis. The first emphasis will be to market the VisionProbe product with DataWave's Experimenter's WorkBench. The VisionProbe is fully integrated with the Experimenter's WorkBench and already has developed a list of potential customers based upon their use of the previous version of the VisionProbe. Plans are currently being made to show the VisionProbe with the Experimenter's WorkBench at the Neuroscience convention this fall. The VisionProbe is also available as a standalone vision stimulator to be utilized in various research application requiring a variety of programmable, controlled visual stimuli.

5.2 Educational Tool

5.2.1 Description

The Educational Tool product will provide the clinician or technician a method to display the effects of certain diseases on the human vision system to patients and their families. The purpose of the educational tool is to provide the ability to view a scene through the eyes of an individual with visual degradation due to disease or other factors. The tool will be utilized as a teaching tool to show people how the vision system of someone with eye disease expresses itself. It is based on the AVS/Concentric Ring model described earlier in the report.

The educational tool shall have the ability to display pictures of representing general cases of diseases specified. Their shall also be options to enter specific disease parameters. (i.e. damaged areas of the retina). The basis of the educational tool shall be the Vision Model developed for the AVS environment for the SBIR Phase II project.

The diseases listed below will be modeled within the educational tool. Specific details of each of the models were developed based upon discussions with subject matter experts.

- Glaucoma
- Photo Toxicity

5.2.2 System Configuration

12

5.2.2 System Configuration

The Educational tool is an PC application software package under Windows 3.1 or higher environment. No special hardware or system configuration is required to install or operate the tool.

5.2.3 Educational Tool Development Tasks

5.2.3.1 Porting the AVS Model to the PC

The Vision model developed for laser damage in the SUN/AVS environment was re-hosted to the PC environment to allow a broad group of users access to the program. All of the display and data entry routines were either developed or converted from the SUN/AVS software developed for this project.

5.2.3.2 Define Disease Parameters

In order to adequately model the various diseases of the eye in the educational tool, interviews and research was conducted. Vision experts at the University of Texas Health Science Center were contacted and provided tutorials to the design engineers regarding the diseases of interest, how they affect an individuals vision and how the disease progresses. Descriptions of each of the diseases to be modeled were provided to the software engineers for use in the implementation of the models. The models used for the diseases largely resembled the AVS/Concentric Ring model presented in this report.

5.2.3.3 Design and Implement the Disease Models

Each of the disease models were translated into a software design. The design was coded in C++ and integrated with the AVS converted software (see 1.2.3.1 above).

5.2.4 Remaining Development Tasks

The following tasks remain to be completed in order to make the Educational Tool a fully marketable commercial product.

- Full testing must be conducted on the software.
- Detailed Disease descriptions, Help features, and Users Guides must be completed.
- Additional diseases may be included into the tool.
- User evaluation and recommendations must be sought in order to improve the product.

6. Concurrent Research Topics

As a part of the Phase II project, basic multi-disciplinary research at UTSA was performed. Dr. Desai of the electrical engineering department developed a signal processing model for the effects of laser damage on acuity. Dr. Tsin of the biology department conducted experiments on the effects of a simulated retinal hemorrhage on the level of photopigment bleaching in light adapted bovine eyes. Dr. Dykes of the psychology department study the effect of simulated retinal hemorrhage in the form of electronic noise on psychophysical detection experiment performance. Dr. Gokhman of the mathematical department investigated the generation of Wavelets as possible stimuli (other than Gabor patches) and looked into the modeling of the effect of blood as a

scattering media in the vitreous humor. All the reports have been included in Appendix III.

7. Summary

The present Phase II brought together researchers in vision and signal processing from UTSA, UTA, UTHSC, CMI and Brooks Air Force Base. This research resulted in four sets of experimental results, three models and a visualization tool which may be used at Brooks Air Force Base for modeling laser eye damage. In addition, two commercial tools were developed and a vendor has been established for one tool while a vendor is being sought for the other.

Appendix I

The Visualization Tool Description

Simulating the Effects of Laser Damage to the Retina

List of Figures

16

The Visualization Tool Description

GOAL:

This model was conceived as a visualization tool to illustrate the effect on a scene as viewed by a person with normal vision, a laser lesion, or disease. For the Air Force this model has been implemented with AVS (so that it will interact with the existing ILPIM model at the laser lab) and for the commercial package it has been implemented on a PC with windows.

The model will be explained in a series of three stages. The first will explain how we perturb a natural scene with a series of low pass filters to resemble what a person sees who has normal vision and only focuses at one point on the scene. The second stage will explain how we further degrade the image to reflect the damaged retina (laser lesion or disease). The third stage will assume that the user has selected several foviation points and explain how a resultant image is arrived at that represents the total information viewed by the person.

STAGE 1:

A digital image is obtained. The user selects any pixel in the image and assumes this is the center of the region in the field of view that is focused on the fovea (herein called the foviation point). The user then selects up to 15 eccentricities that may extend up to 30 degrees from the fovea. The distance between the retina and the ring is called eccentricity. A source of contrast sensitivity functions is selected, either from the literature or the CMI experiments. A genetic algorithm is used to interporlate the contrast sensitivity data, generating a 3-D surface with contrast sensitivity as the amplitude and eccentricity and frequency as the independent axis. For each of the eccentricities selected by the user, a contrast sensitivity function is arrived at from the surface that was just fit to the experimental data. Next a low pass filter is developed that has the frequency response of the corresponding CSF curve. For each of the eccentricities chosen, a copy of the original image is filtered with the low pass filter that corresponds to the CSF function for that eccentricity (this eliminates any boundary effects that would occur if one to filter only part of the image with the corresponding low pass filter). Now a composite image is formed. Each pixel in the original image lies is in one and only one eccentricity and there is one and only one filtered image that corresponds to that eccentricity. Therefore the ij^{th} pixel in the original image can be replaced by the ij^{th} pixel in the filtered image that corresponds to the correct eccentricity. This results in an image that is increasingly blurred outward from a user selected foviation point and represents the loss in resolution of the retina due to decreased sampling density with distance from the fovea. This scene is as would be seen by a person with normal vision.
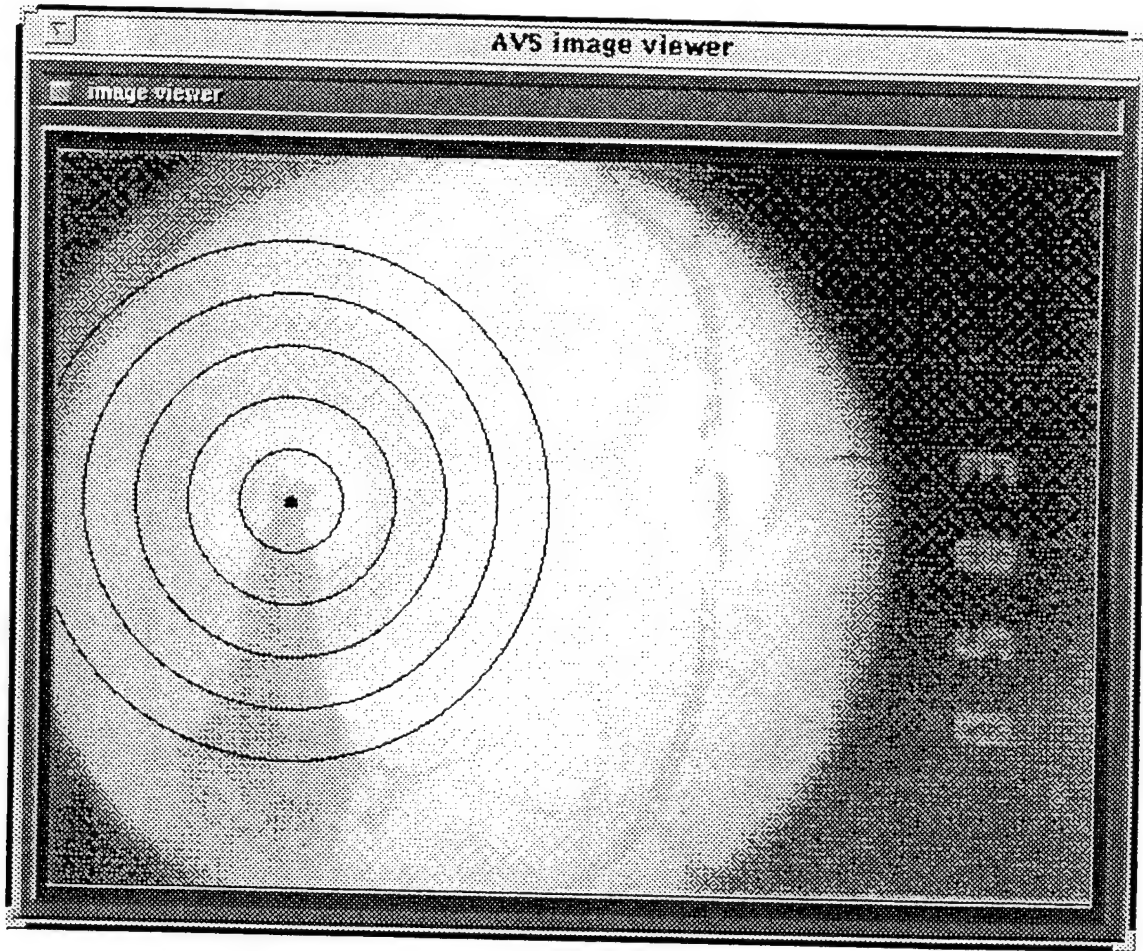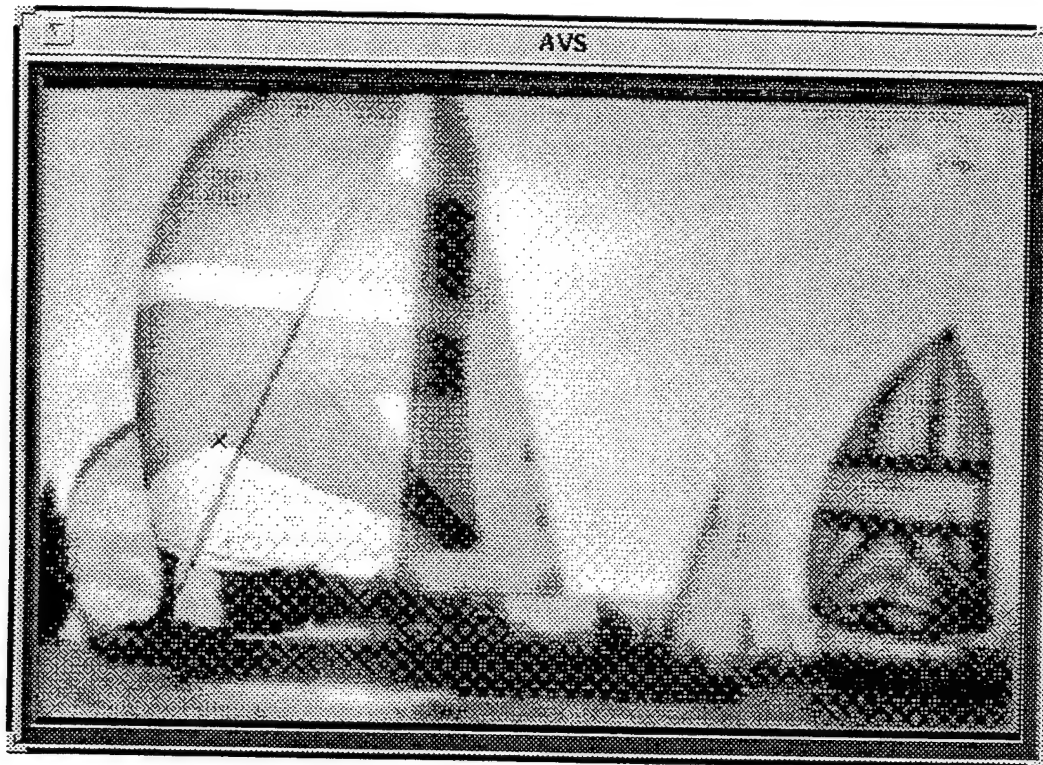
FIGURE 1. RETINAL IMAGE WITH CONCENTRIC RINGS

FIGURE 2. FILTERED SCENE DUE TO NATURAL DEGREDATION. (X INDICATES FIXATION POINT.)

STAGE 2:

When the image of a retina is displayed and the person selects the eccentricities, they are also ask to select damaged regions on the retina with the mouse. These may be user selected or the retinal image may be of a damaged retina with the user only outlining the actual damaged region. For laser lesions and certain diseases (macular degeneration, phototoxicity, glaucoma, etc.) the damaged region is assumed to have total photoreceptor drop-out and therefore the pixels in the damaged region are replaced with the average illumination in the total image. For Glaucoma we use the Humphry field map to arrive at decreased amplitudes and cutoff points for the low pass filters corresponding to the effected regions. This technique is easily extended to any disease for which one can determine the change in the CSF. The result is a scene as viewed by a person with damaged vision who has only focused his/her eyes at one point.
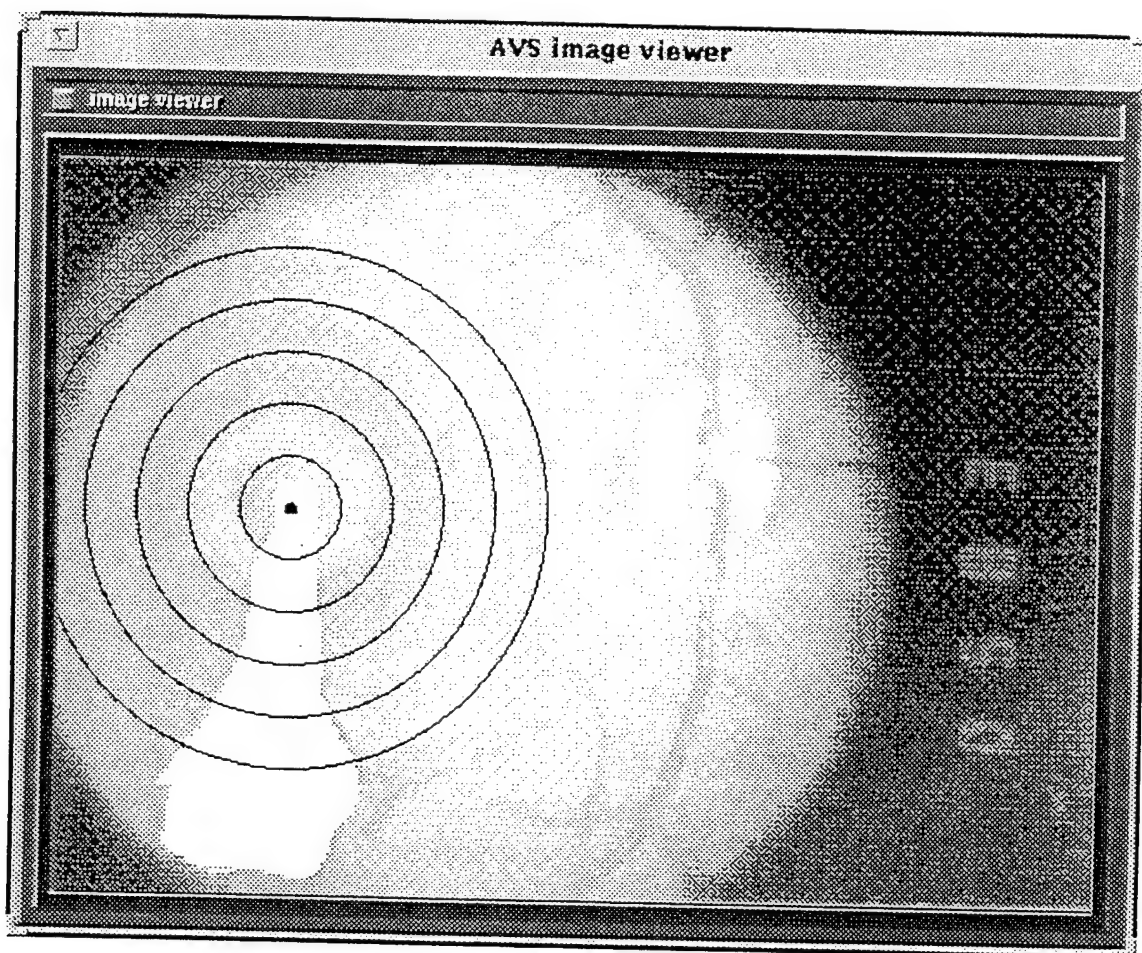
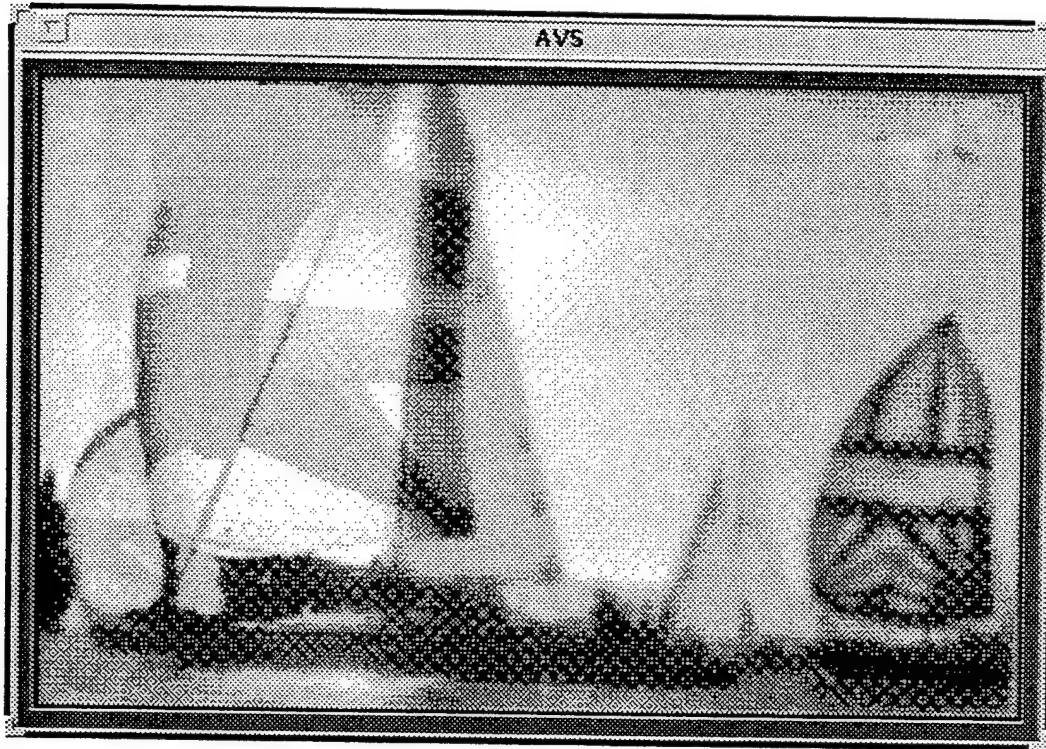FIGURE 3. RETINAL IMAGE WITH MARKED DAMAGE REGION

FIGURE 4. OUTPUT SCENE DUE TO RETINAL DAMAGE

STAGE 3:

This next stage is meant to represent the total amount of information available to a person with normal or damaged vision if they are allowed more time to view the same scene and therefore have several foviation points. We assume the information gained at each neighborhood would be the maximum amount from the different foviations, i.e. the neighborhood that has been blurred the least. Therefore in this stage, stages 1 and 2 are repeated for each foviation point and the resultant image is formed by selecting pixel ij from the scene in which the neighborhood of ij was filtered/blurred the least. This results in a scene which assumes that the person retained the maximum possible information at each foviation point.

Inputs: Natural Scene
            Number of Eccentricities
            Regions of disease or lesion
            One or more foviation points

Output: Scene as viewed by the person normal or afflicted

21

Appendix II

Detailed Description of the Inhomogenous Retinal Cortical Model

Appendix II
Table of Contents

Simulating the Effects of Laser Damage to the Retina
Final Report

List of Figures

I. Introduction

1.1 Purpose of Study

The purpose of this project is to calculate loss of visual acuity due to retinal receptor dropout. The idea of modeling visual acuity has grown from military and clinical necessity. Since the dawn of the Atomic Age, the Air Force has been interested in eye damage caused by intense light which originally came from atomic bomb flashes. Later, however, a much more common threat appeared, laser light. Lasers have become widely used in the military both as aiming devices and weapons. There is constant eye danger due to deliberate enemy action as well as accidents. Even relatively weak laser light is concentrated on a small part of the retina by the optics of the eye and can cause burns.

Laser damage can take many forms. For example, hemorrhages can result if arteries are hit. A strong, direct hit to the optic disk could presumably destroy the entire optic nerve blinding the eye. Since the topic of laser eye damage is so vast, the scope of this study will be limited. This study assumes retinal loss due to heat or occlusion by blood but without underlying nerves being affected. Furthermore, retinal loss has hitherto been treated as either "all or nothing," though some of the models being developed would allow partial losses to be incorporated without modification.

The possibility of modeling partial damage leads to another use for the models being developed: the calculation of acuity loss due to various eye diseases which damage the retina e.g. glaucoma, retinitis pigmentosa, etc.). Presently no disease modeling has been done; however the possibility is open for future work.

1.2 Measures of Visual Performance

Modeling the effects of retinal damage requires metrics for the quality of vision. We have already chosen visual acuity as our means of measurement, but unfortunately there is no single definition for this term. Two important types of acuity are Snellen, or the ability to read an eye chart, and grating, the ability to detect sinusoidal intensity variations on a background of otherwise constant intensity. These and other kinds of visual acuity are described below in section [2.5.4]. The important point here is to distinguish the concept of acuity as a metric for visual performance with the actual measurement of acuity. This measurement sounds like a simple process, as easy as having a patient read an eye chart. Unfortunately, this is not nearly accurate enough to be of use in this study. Two general methodologies are available to measure acuity (among many other

things); the visual evoked potentials (VEP) and psychophysics. Both are complex and have strengths and weaknesses.

VEP are a class of weak electrical signals that are emitted by the brain in response to visual stimuli. It has been known for many years that the brain emits tiny electrical signals summed from a great numbers of neurons; some of the signals are related to vision. The VEP are taken via external electrodes placed on the back of a subject's skull near the visual cortex while the subject is watching a timed image of varying stimuli. These signals, though a very noisy sum, can be related to the image the subject sees, and used to give a measure of visual acuity by testing a series of patterns, and determining which give a response and which do not.

The other methodology to measure visual performance is psychophysics. Psychophysics is a very broad term meaning the study of quantitative relationships between stimulus and perception. It can pertain to measurement of any of the senses. For example, seminal psychophysical experiments were used to study the ability of an observer to distinguish between two different weights. Generally, psychophysics requires the use of cooperative subjects able to understand language, implying humans at least a few years old. However, animals with special training have also been used.

II. Literature Review

This section (sixty-six pages) has been withdrawn from this report. It is available for review at the AFRL/HEDO offices at Brooks Air Force Base, Texas.

III. Research performed

3.1 VEP Model

3.1.1 Introduction

In a previous study, a VEP based model of retinal damage measurements was developed. The model used data taken in previous research performed by the Air Force. In a series of experiments, rhesus monkeys had their eyes damaged by controlled laser blasts. The monkeys' retinas were studied and photographed before and at various times after the exposures, in increasing periods from days to months. A secondary set of experiments endeavored to measure the monkey's visual acuity before and after the laser exposures. As explained in section [2.2], the only way to measure an animal's vision without special training is through the taking of VEP signals. VEP studies were made at approximately the same time as the photographs, using the counterphasing grating stimuli described in equation [11]. Several studies were made on each monkey before the laser exposure, to establish a baseline for normal vision. Each study consisted of a series of VEP readings taken at differing spatial frequencies. Acuity was estimated by measuring the highest spatial frequency which gave measurable VEP signals.

A simple model was developed to simulate the acuity loss and thus perhaps alleviate the need for monkey experiments. The original goal of the VEP model was to calculate loss in visual acuity from the retinal damage as judged from the photographs. Since the only available way to estimate acuity was based on VEP amplitudes, the goal was later simplified. It became the calculation of VEP amplitudes in a damaged retina and comparing them with actual recorded values.

3.1.2 Methods

The easiest way to explain the VEP model is to first show the methodology for a normal eye, then see the effect of retinal damage. The theoretical basis for the model is the fact that VEP are a noisy, approximate, sum of signals in the visual cortex. Mathematically, the model, shown in block diagram form in figure [32], is similar to a simple neural network. Functionally, it divides the retina into a series of imaginary concentric rings. Each ring is given a weight, the determination of which will be explained below. The terms called "ring fraction good" are all set to one. A pattern such as a sine wave grating being passed though the model would have its contrast sensitivity calculated, (generally by interpolation as explained in section [3.3]), for each ring. The responses for all the rings are then summed. VEP is known to have considerable variation between different subjects, so the summed ring responses are multiplied by a subject weight. The

system is trained, independently for each subject, with a simple minimization of least squares algorithm. Input spatial frequency, measured VEP amplitude, and a subject ID are entered. The error term, the difference between the output and measured VEP amplitudes is squared and summed, separately for each subject. Jogging the subject weight and recalculating gives a slightly changed error, allowing the calculation of a derivative of error with respect to weight. This derivative is used to recalculate the subject weight in a direction that reduces the error. Baseline data are input to the model and the model's outputs compared with measured ones. The subject weight is adjusted to give the least square error.

$$R = Sw_s \sum_{i=0}^{n} w_{ri} g_{ri} CSF_i \qquad [66]$$

Equation [66] describes the calculations. S is the strength of the input signal, w_s is the subject weight, w_{ri} is the weight for the ith ring, g_{ri} is the good fraction for the ith ring (set to 1 for a healthy eye), and CSF_i is the contrast sensitivity function for the ith ring.

The model has certain underlying assumptions and simplifications. Firstly, contrast sensitivity (CS) is used as an estimator for VEP response. Theoretical justification for this is tenuous. One may argue that high CS is an indication of high sensitivity of the visual system and likely implies a high VEP response and visa versa. CS was used because of the large variety of data in the vision literature. Secondly, CS is assumed to be equal at any point on any concentric ring. This is of course not true, CS is known to vary at different positions around the eye. The VEP data supplied by the Air Force were so noisy that the concentric assumption was perfectly good, and as will be seen below, the use of CS curves worked as well as could be hoped.

Figure [33] shows an example of how retinal damage is applied to the model. The upper left of [33] shows a photograph of a damaged retina. The upper right is the same picture with damaged and blood occluded areas outlined by hand. The optic disk is also blanked out. Its effect on the VEP summation is negligible because of its eccentricity. Its real use in this implementation is to calibrate the photographs, which have no other means of relating pixels to degrees. A computer program next separates out the damaged areas, as shown in the lower left picture. The damage is scaled and placed on the concentric rings shown in the lower right. The inner most rings are totally occluded, in this case and the ones further out, only partially so.

The cortical magnification factor or (CMF) (Wilson, Levi, Maffei, Rovamo, De Valois, 1990)
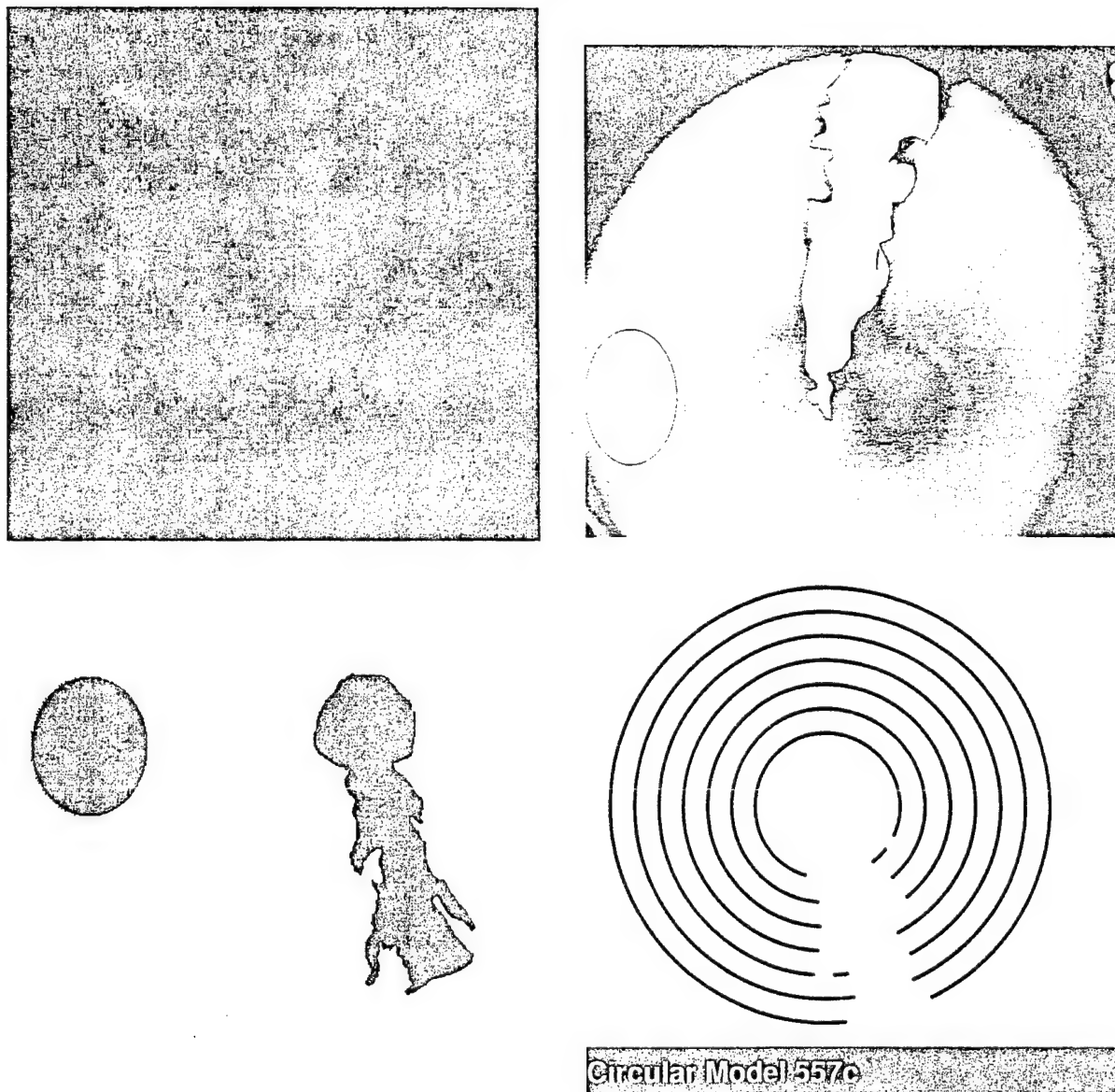
FIGURE 33. Steps in VEP Model.

describes the mapping between the retina and visual cortex. This is the ratio of the length of a tiny portion of the cortex divided by that of the length of the retina that maps to it. In some literature, CMF is defined as a ratio of areas instead of lengths. The CMF varies with eccentricity, or distance from the fovea, or center of the retina, in degrees.

$$M_C(\Theta) = M_F / (1 + \frac{\Theta}{E_2}) \qquad [67]$$
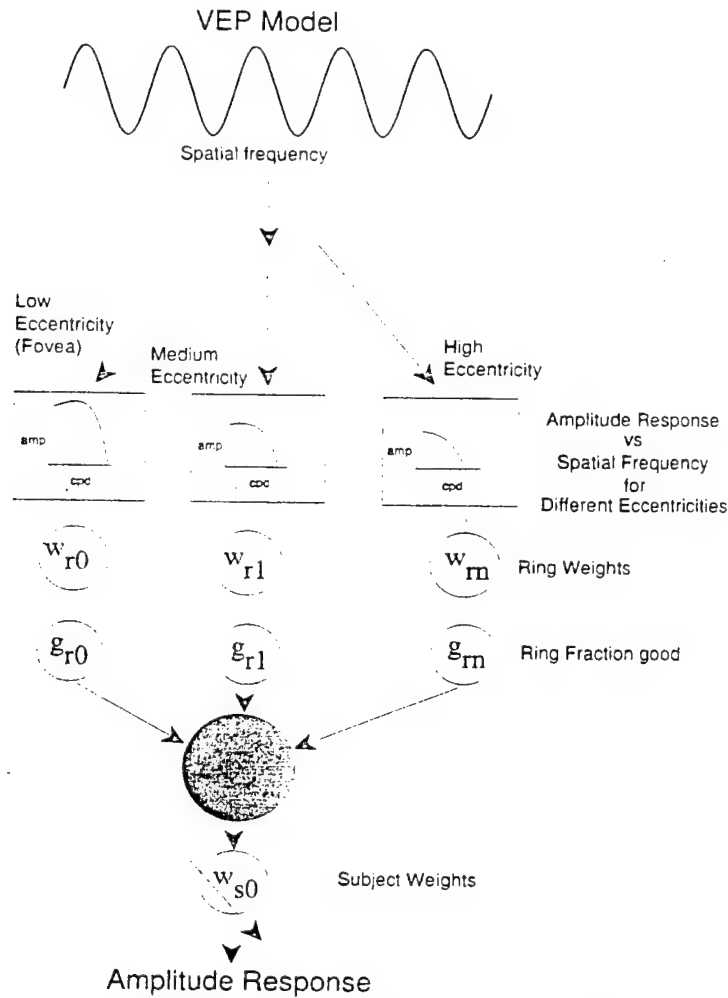
FIGURE 32. Data flow through VEP model

After the damaged areas have been superimposed on the rings, equation [66] is again used to give the VEP response predicted by the model. The only difference from the training case with undamaged eyes, is that the g_{ri} term for each ring is set equal to the fraction of the ring remaining.

Finally, the calculation of the ring weights must be explained. The original idea was to calculate them and the subject weights with a single algorithm, similar to a backpropagation neural network (Widrow & Stearns, 1985). This method proved impractical because the training data were too noisy, as is seen in the top chart of figure [34]. Another way to calculate the ring weights was developed, using cortical magnification factors.

Equation [67] is a formula commonly found in the literature to describe the change in CMF with eccentricity. $M_C(\Theta)$ is the cortical magnification factor as a function of eccentricity, Θ is the eccentricity, M_F is the magnification found in the fovea. The parameter called E_2 is the eccentricity where the cortical magnification drops to half the value at the fovea. M_C is a dimensionless ratio so E_2 must have the same units as Θ, generally degrees. Unfortunately, there is no agreement on a value for E_2, or even on a narrow range of values. It varies drastically with the nature of what is being measured. According to Wilson et al. (1990) there are two ranges of values for E_2, depending on what is being measured. One range was from .3 to .9 degrees, the other 1.5 to 4.

Once a value for E_2 has been selected, the ring weights are calculated by multiplying the area of each ring by the square of the cortical magnification factor. This squaring converts a linear measure to an area measure. The effect of the E_2 parameter is to set the relative weight of the fovea versus the rest of the retina. The lower the value for E_2, the faster the dropoff with eccentricity and the higher the relative weight of the fovea. Conferring with Dr. Randolf Glickman, (1993, personal communication) one of the scientists who had taken the original VEP measurements, it was learned that the fovea is responsible for "almost half the VEP signal strength." To translate this statement into a value for E_2, Mathematica was used to calculate the first thirty ring values and the fraction that fell inside the fovea, assumed here to be a circle of radius 2.5 degrees.

3.1.3 Results

Figure [34] shows some results of the model. The top graph shows the fit to an undamaged eye. Note that the peak of the solid curve matches the peak value of the experimental points. Because of the extreme noisiness of the data points, as evident in that graph, a different training algorithm was developed. Instead of minimizing the squared errors, the subject weights were set so that the peak of the curve for undamaged data matched the peak of the raw data points. The center graph shows a predicted curve versus. experimental points taken just after exposure. The third graph shows predicted and actual data for two weeks after the exposure, when blood had time to be reabsorbed into the body, slightly improving sight.

3.1.4 Conclusions

The results show promise, as can be seen in figure [34], but the work was hampered by the extreme noisiness of the original data supplied by the Air Force. Work on this model was dropped in favor of the psychophysical modeling described in the rest of this paper. If new VEP studies were to be undertaken, care should be taken to make the measurements as repeatable as possible. There is anecdotal evidence that the researchers in the original studies were not interested in amplitudes, only in the presence or absence of a signal. The ring weights would also be worthy of further study. It should be possible to vary the E_2 parameter to improve the fit and to include some data from damaged eyes in the training. One could also return to the original scheme of calculating the ring weights by training.

3.2 Best Remaining Model

Another way to look at the vision damage problem could be called the "Best Remaining Model." This model is based on the fact that most of the visual acuity is based on the center of the fovea where the cones are most dense. As the eyes move around, the fovea is fixated on points of interest. If part of the retina is destroyed by a lesion, the loss in acuity will depend on the position of the lesion. According to this model, if it misses the fovea, no loss in acuity will result If the lesion destroys the fovea, the loss will depend on the observer's reaction. If he/she looks directly at the scene of interest, the best remaining portions of the retina will not be focused on the target but at some distance from it. Later, the observer may teach himself/herself to look away from what he/she is trying to see, thus placing the best remaining part of the retina on the target of interest.

This model, though totally different from the VEP model, also suffers from severe weaknesses. It implies that a large lesion will do no damage to vision if it misses the fovea, even by a small amount. Even if the lesion traversed the center of the fovea, the best remaining model would imply that vision would be unimpaired. Intuitively, this seems hard to believe. Furthermore, it does not take into account eye motion or any other temporal effects. If the observer focuses the best remaining part of his retina on a target, he will not be able to keep his eye motionless. It seems likely that the eye will at certain times move into a position such that the target is focused on the damaged part of the retina. Clearly, the best remaining model is no solution to this problem, it is at best, a guideline for attacking it.

3.3 Interpolation of Contrast Sensitivity

Both the VEP and psychophysical vision damage models require interpolation of contrast sensitivity. CS measurements are expensive and slow, so only relatively few are done in any study. Both models require CS points to be available for any combination of eccentricity and SF.

There are two basic ways to approach the CSF interpolation problem. One is to try to find an analytic function that describes the shape of the curves, possibly with theoretical justification. Such a formula would have parameters to be fitted to the data by minimizing a sum of squares, giving an equation for CSF given the eccentricity and SF. The second way is simple interpolation such as a spline fit.

One such function attempted is shown in equation [68].

$$CSF = aSF^b e^{-(cSF^d)} \qquad [68]$$

This equation fitted CSF to SF for a fixed eccentricity. Four parameters, a,b,c,d were calculated using a least squares routine. This worked fairly well for curves at a single eccentricity. One approach to extend it to two dimensions was to calculate the four parameters for each different eccentricity, then interpolate each parameter, for eccentricities not given. This worked for one set of data, the Rovamo shown here in figure [35], but failed with other sets of data. The problem was that some of the parameters would change sign during interpolation causing instabilities. This approach was finally abandoned for a double spline fit. Each SF curve for a fixed eccentricity was interpolated by spatial frequency using cubic splines, giving a curve with many evenly spaced SF points. A second series of spline fits was done across the eccentricities for each SF. The resulting data were put into a table and read into a program to give fast access. Recently, a new method has been tried. The frequency response of a Difference of Gaussian filter was studied and it was noted that it had a considerable resemblance to a CSF curve. This was clearly no surprise, because the retina is believed to be full of DoG filters converting input signals from the retina to the ganglion cells. The main difference was that an unmodified DoG filter is band pass and transmits no DC signal what so ever. A CSF curve, on the other hand, may show drop off at low frequencies but not cutoff. Some CSF curves show virtually no dropoff at low frequencies. It was therefore decided to try to simulate a CSF curve with a DoG by shifting the latter in the frequency domain.

Equation [69] shows the Fourier transform of a DoG multiplied by A, an amplitude parameter to be determined. The term f_s represents the frequency shift. A zero value for fs indicates that both terms go to one when SF goes to zero, a non-zero value will cause CSF to go positive or negative (a meaningless case) when SF is zero.

$$CSF = A \left(e^{\left(-(SF + f_s)^2 \sigma_1^2 \right)} - e^{\left(-(SF + f_s)^2 \sigma_2^2 \right)} \right)$$

[69]

The parameters fs, s1, s2, and A were fit with a genetic algorithm, described in section [2.3.3.1] using minimizing least square error between experimental and calculated data points. Results from fits on the Banks data are shown in figure [36]. To date, attempts to extend this method to three dimensions (CSF versus eccentricity and SF) have failed, though other techniques can be used to interpolate between eccentricities.
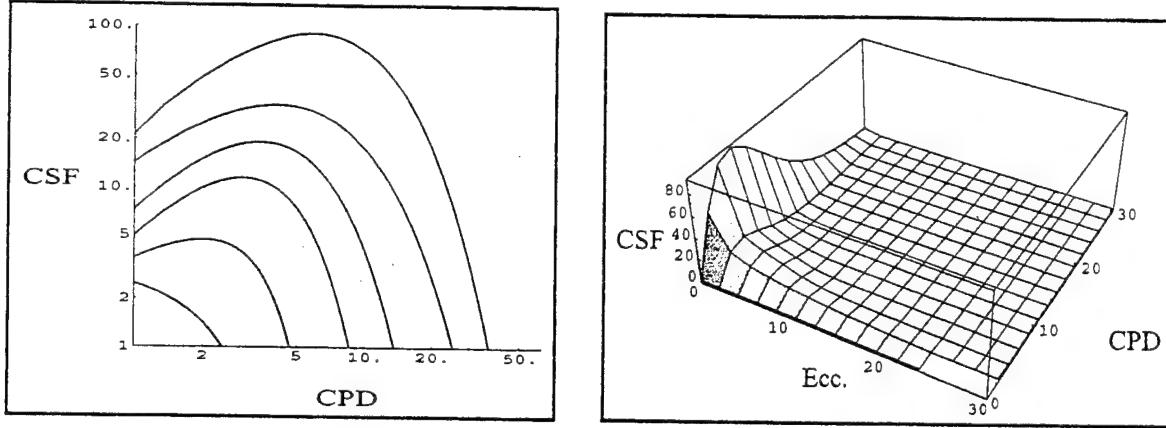
FIGURE 35. Family of Curves from Rovamo. 2 and 3d plots.
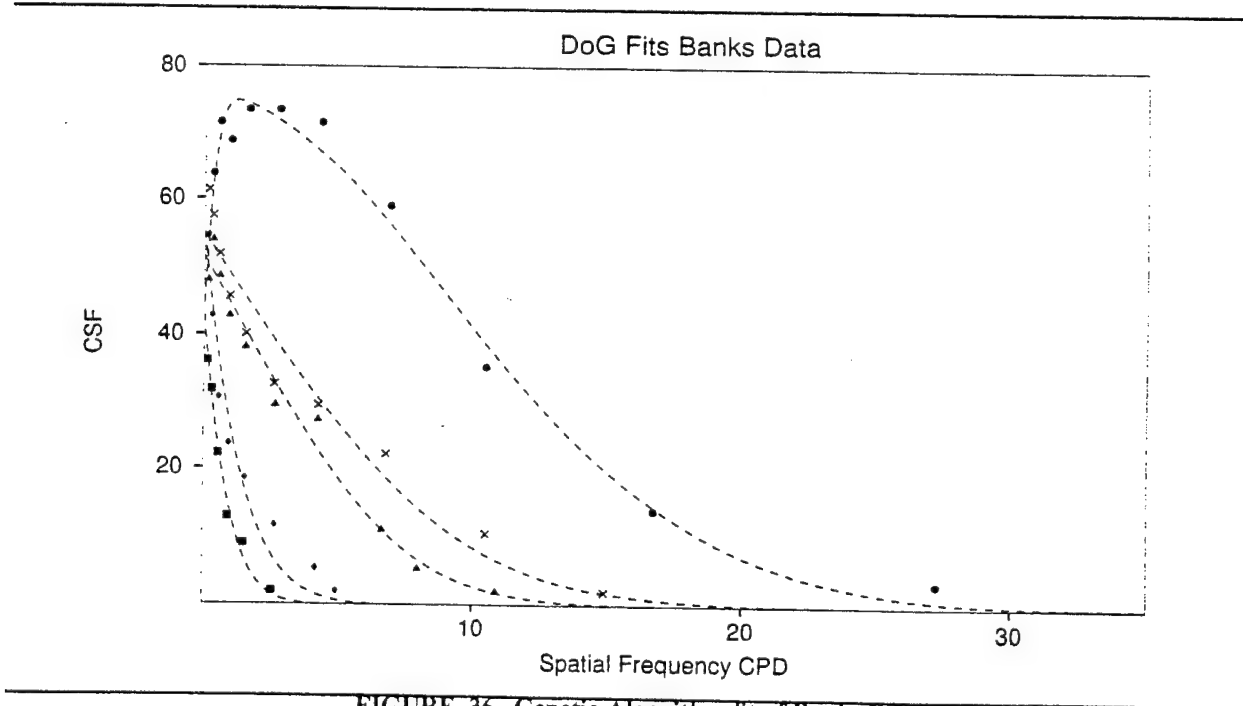
FIGURE 36. Genetic Algorithm fit of Banks Data

IV. Models, Experiments, and Comparisons.

4.1 IRC model

4.1.1 Relationship with ideal observer theory

As explained above, ideal observer theory does not provide an accurate simulation of human vision, nor is it intended to. Yet one might ponder the question: "since ideal observer theory is based on the best known information about the vision system as well as known principles of physics and statistics, why could it not be applied to vision modeling?" The Inhomogeneous Retino-Cortical (IRC) model has been developed by professor Wilson Geisler to modify ideal observer theory to this end. The concept is to deviate from the ideal as little as possible while allowing certain parameters to float as necessary to match actual performance for a particular subject. Once the parameters have been fit, the model can be tested.

The IRC model in its current state simulates the optics of the eye, the sampling density of the retina and ganglion cells, parvo cell responses, cortical non-linearities and an ideal detector. Each of these has been dealt with in sections [2.5] and [2.7]. The optics and sampling density are as described by Campbell and Gubish (1966) and Curcio et al. (1990). The ganglion cell responses are described with spatial DoGs following the work of Enroth-Cugell and Croner and Kaplan (1995). IRC deviates from ideal theory here, however. As mentioned above, there is a time delay between the center and surround that changes the shape of CSF curves according to the temporal shape of the stimulus. Rather than complicate the model by simulating these temporal effects directly, the relative weights between center and surround are arrived at through parameter fitting. Continuous or slowly changing stimuli show low frequency dropoff in the CSF and have center and surround weights close to .5. Faster changing stimuli show little low frequency dropoff and have center weights much higher than surround.

The cortex is not modeled except for two non-linearities. The first is rectification. Cortical cells unlike ganglion cells, have a low spontaneous firing rate and thus cannot transmit a negative signal. The other is the contrast exponent described above in section [2.7.6]. The exponent is one of the parameters to be fit.

A d' is calculated with the same method as figure [31]. Ganglion cell responses are calculated and the cortical factors applied. The process is repeated for two images and the results passed to a d' calculator. This d' calculator uses a noise distribution that is assumed to have a variance propor-

tional to the mean. A Poisson distribution is characterized by variance equal to the mean. Currently, the variance is set to 1.2 times the mean. One might call this a "Poisson like" distribution.

4.1.2 Summation of d'

The models described below need a means of summing many values for d'. d' will be calculated by comparing cortical cell responses for two images. A value of d' is calculated for each individual cell. These d' values are of no use by themselves and must be summed to provide an overall d' between the two images. To sum d', one uses its definition as distance divided by standard deviation. If all cell outputs are assumed to be independent, distance is calculated in the standard Euclidian way, the square root of the sum of the squares. Likewise, the variance of a random variable which is the sum of other random variables is the some of the variances of those variable. Equation [70] gives the final result, where a_i is the output of the ith cell for one image, b_i is the output of the same cell for the other image.

$$d' = \sqrt{\frac{\sum_i (a_i - b_i)^2}{\sum_i var(a_i) + var(b_i)}}$$ [70]

4.1.3 Computer Simulation of IRC model for Gabor patch CSF curves

A computer simulation of the IRC will be used to calculate the d' values for various patterns placed on a simulated retina. This program, developed in FORTRAN 77 by Professor W. Geisler, uses the IRC model to calculate ganglion cell outputs. It has been slightly modified for the purpose of the present work, to handle large, complex, images It starts by assuming Poisson distributed noise for each receptor in the retina as described in the Ideal Observer section, [2.7.8]. A simulated retina is used for the spatial distribution of the inputs. The layout is based on the data from Curcio (1990), and spatial irregularities in the hexagonal sampling matrix are also modeled. Optical blurring in the eye is simulated with a point spread function and ganglion cell outputs are simulated by means of difference of Gaussian formulas, who's sizes also change with eccentricity. A value for d' for a stimulus versus a blank image is calculated, according to formula [70].

This simulation will be run on various stimuli being tested with psychophysical experiments on human observers, especially on the third harmonic cycle summation series of experiments.

4.2 Psychophysical experiments

4.2.1 Design details and experimental protocol

Since the main thrust of the project is estimating visual acuity under performance conditions, the VEP has been determined to be a poor measure for the reasons stated. A new psychophysical study is being proposed to provide performance data. This study generated a complete set of CSF curves. By generating a new set of CSF curves, our stimulus conditions can be compared with those of CSF curves in the literature to provide some idea of how stimuli may effect other parts of the experiment.

Several sets of stimuli were used to develop models of the loss of vision from laser damage. This model of vision loss was used to develop visualization tools of scenes after laser damage has occurred. The proposed stimuli will be used to:

- measure contrast sensitivity at various eccentricities under the same stimuli conditions as a VEP experiment, so that a comparison of the two methods can be made
- measure contrast sensitivity for Gabor patches at various eccentricities in order to determine the visual capabilities of the retina at various eccentricities
- measure the ability to detect a natural object in the scene at various eccentricities
- measure spatial summation of the third harmonic of gratings with and without the presence of a fundamental frequency

4.2.2 Method

All experiments will be conducted in a quiet room, and the experiments will be conducted using a VMI monitor driven by a MicroVAX II computer with Parallax graphics cards.

An additional four bits of resolution have been added to the brightness values of the stimuli, bringing the total resolution of the stimuli to twelve bits. This is accomplished by building a circuit which adds the signals from the red gun to that of the green gun, which is the main output.

Viewing distances have been determined to be:
- 114.6 cm for spatial frequencies of 0.5, 1, and 2 cycles per degree (CPD)
- 229.2 for spatial frequencies of 4 and 8 CPD
- 458.4 cm for spatial frequencies of 16 CPD
- 573 cm for spatial frequencies of 32 CPD

Subjects: Three volunteers, one female aged 31, and two males, aged 24 and 31 have participated in this study. Each participant was given an ophthalmological examination to ensure normal

vision. Each participants has visual acuity corrected to at least 20/20, normal visual fields and color vision, and is not hypersensitive to light.

This section describes all experiments except when noted otherwise. Subject has a chin rest to control the distance to the screen. The computer communicates with the subject via a voice synthesizer. At the start of each experiment, the synthesizer says, "start." Next there are two stimulus intervals of 200 milliseconds (ms) each with a 500 ms pause between them. Finally, there is a variable timed response interval. This experiment is referred to as a two-interval, forced-choice experiment (shown in Figure [37]). The method used to determine the contrast threshold involves a three down/one up staircase with reversals.[25]

Two-Interval, Forced-Choice Experiment (4 seconds per trial with 1 second rest)
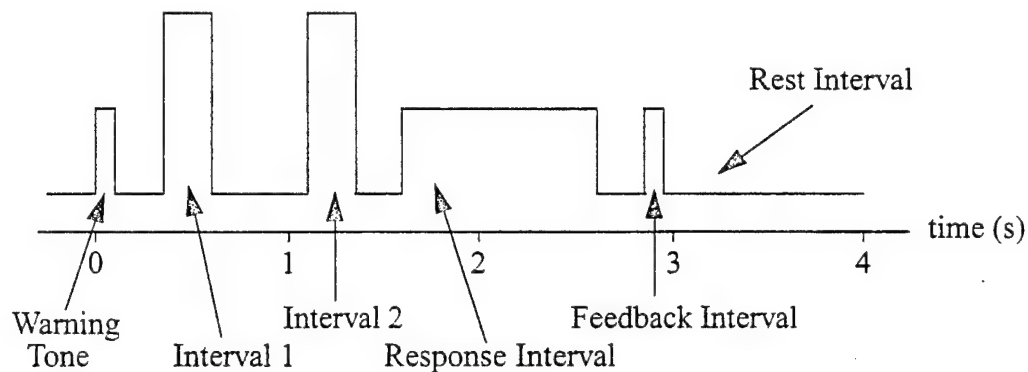
FIGURE 37. Timing of the two-interval, forced-choice experiment.

For both the first and second sets of stimuli, during the first interval a pattern of stripes (either horizontal or vertical) appears on the screen. Then, during the second interval a second pattern, orthogonal to the first, appears. The third set of stimuli will use a pseudo-natural scene (an aircraft) in place of the stripes used previously. Just as before, the aircraft will appear at two orthogonal orientations

During the response interval for the first three sets of stimuli, the subject presses a key to indicate which pattern appeared in the first interval. The voice synthesizer responds with "correct" or "wrong" depending on the response given. The response interval varies from a fraction of a second if the response is given while the patterns are still up, to about 1.5 seconds if no response is made. At that point the response is automatically declared wrong.

The third set of stimuli differs conceptually from the others. The fundamental pattern will extend across the screen and will not change during the experiment. The number of fundamental cycles will be fixed, but the number of harmonic cycles will vary. In this case, all patterns will be hori-

zontal. The subject will be only trying to detect the presence of the additional harmonic. During the response interval, the subject presses a key to indicate if the pattern was detected.

There are three sets of experimental stimuli which are detailed below.

The first set of stimuli Table 1 consists of a series of Gabor patches at varying eccentricities used to produce CSFs at varying eccentricities. These will be compared to the literature to check for the effects of different stimuli conditions. Gabor patches will have 5 cycles contained in 2 standard deviations of the Gaussian envelope.

Table 1 Psychophysical Experiments -- Gabor Patches

Stimulus Shape	Eccentricity	Spacial frequency	Number of points
Entire Screen	n/a	1,2,4,8,16,32	6
Gabor Patches on Temporal Meridian	0,2,5,10,30	cutoff/powers of 2	~22
Gabor patches on Nasal Meridian	5,10,30	cutoff/powers of 2	15

The second set of stimuli (Table 2) will consist of aircraft images with and without missing areas to measure the effects of loss of parts of the retina on the ability to detect objects in a scene.

Table 2 Psychophysical Experiments -- Pseudo-Natural Scenes

Stimulus Shape	Eccentricity	Scotoma size	Number of points
Aircraft: 1.25° long	0	0	1
Aircraft: 1.5° long	0	0	1
Aircraft: 2.0° long	0	0	1
Aircraft: 2.5° long	0	0	1
Aircraft: 5.0° long	0	0	1
Aircraft: 6.0° long	0	0	1
Aircraft: 1.25° long	0	1	1
Aircraft: 1.5° long	0	1	1
Aircraft: 2.0° long	0	1	1
Aircraft: 2.5° long	0	1	1
Aircraft: 3.0° long	0	1	1
Aircraft: 5.0° long	0	1	1

Table 2 Psychophysical Experiments -- Pseudo-Natural Scenes

Stimulus Shape	Eccentricity	Scotoma size	Number of points
Aircraft: 2.0° long	0	2	1
Aircraft: 3.0° long	0	2	1
Aircraft: 5.0° long	0	2	1
Aircraft: 6.0° long	0	2	1

The third set of stimuli (Table 3) will consist of a set of experiments to measure grating summation in the presence of a fundamental. This will allow fine tuning of the current theories of spatial frequency channels, and, thus, be useful in perfecting the psychophysical model of vision loss. Cycle summation data has been measured for Gabor patches [26], but to our knowledge, it has never been measured for a harmonic in the presence of its fundamental.

The reasoning behind this fourth set of stimuli is based on the decomposition of an image into spatial frequency channels. Recall that an edge transforms into a series of odd harmonics in the frequency domain. Furthermore, there is a well known effect of cycle summation. A grating of two cycles is more visible than one of one cycle and a grating of 5 cycles is more visible yet. Above about five to seven cycles, however, the grating no longer becomes more visible. What is not known yet, however, is if this cycle summation effect remains unchanged for an odd harmonic in the presence of its fundamental.

Most natural scenes are full of edges, therefore, any model for detection of objects that depends on spatial frequency channels requires information about how odd harmonics sum in the presence of a fundamental. The experiments described in Table 4 should provide at least part of this information.

Table 3 Psychophysical Experiments -- Grating Summation

Stimulus Shape	Eccentricity	Spatial Frequency	Number of Cycles	Number of Points
Grating + Third Harmonic	0	1,2,4	1,2,3,5,10	45
Third Harmonic Only	0	3,6,12	1,2,3,5,10	45

4.2.3 Airplane studies.
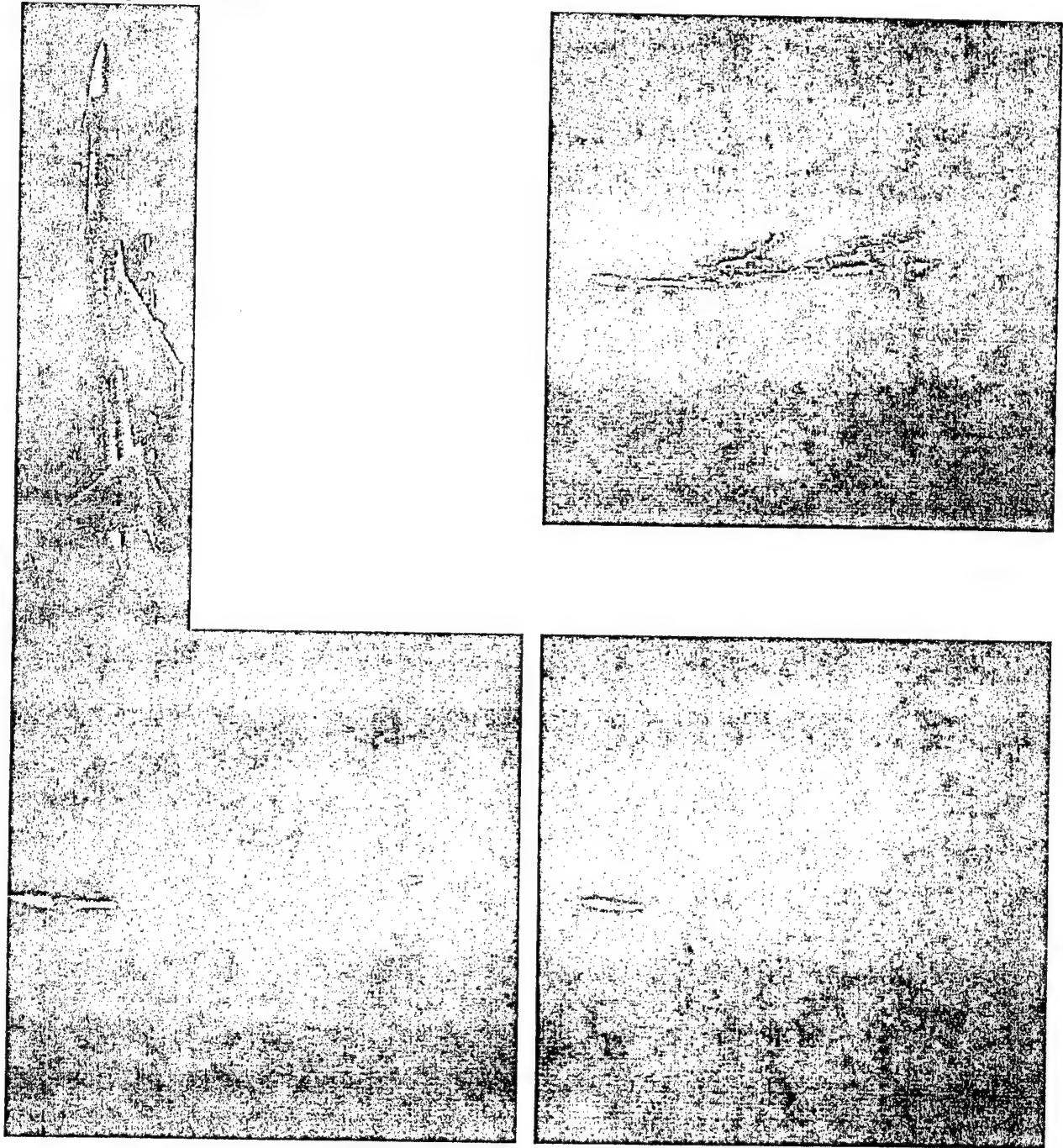
FIGURE 38. Airplane Stimuli.

Figure [38] shows the generation of the airplane stimuli. The upper left shows the original picture of the plane. The background has been made black with manual retouching. In the upper right, the figure has been centered and placed in a background of intensity equal to the average brightness of the plane. In the two lower figures, artificial scotomas of different sizes are shown.

The section on artificial scotomas [2.6.1] describes a series of methods to stabilize portions of images on the retina, creating the effect of a scotoma or dead zone. The experiment described here achieves a similar effect without any special equipment. As described above, it uses a stimulus presentation which is short enough (200 ms) that the eye will not move during that interval, thus no stabilization is needed.

The airplane experiments consist of contrast sensitivity measurement of the airplane versus a blank background of the same intensity. It would have been possible to do 90 degree rotations of the airplane, as was done on the gratings. This was not done for two reasons. The airplane experiments are meant to be simulations of natural scenes, whereas the Gabor gratings are not. Rotating the airplane 90 degrees is artificial and not compatible with the concept of simulation of a natural scene. The other reason is that rotating a long, thin, object such as an airplane would expose widely different parts of the retina to the image. Nothing on the vertical meridian has been tested in these experiments, so there is no information available to calibrate a model, other than on the horizontal meridian.

Cycle Summation at 0° Eccentricity
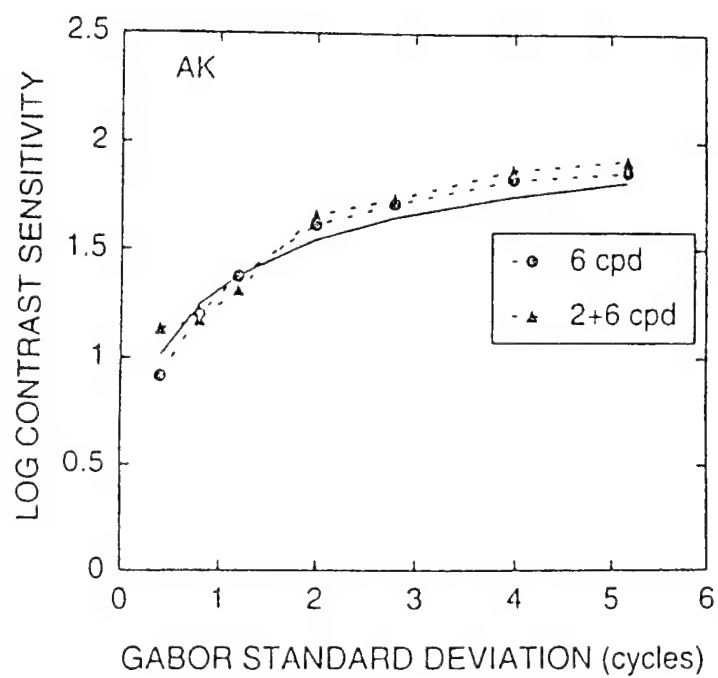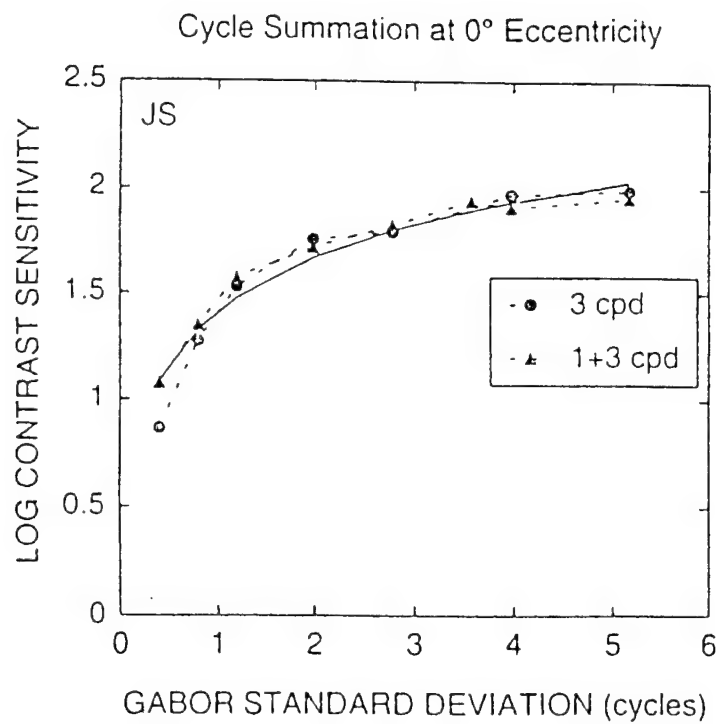
FIGURE 39. Third Harmonic curves. Dark Lines represent IRC simulations. Triangles represent presence of fundamental, Circles, its absence.

4.2.4 Results
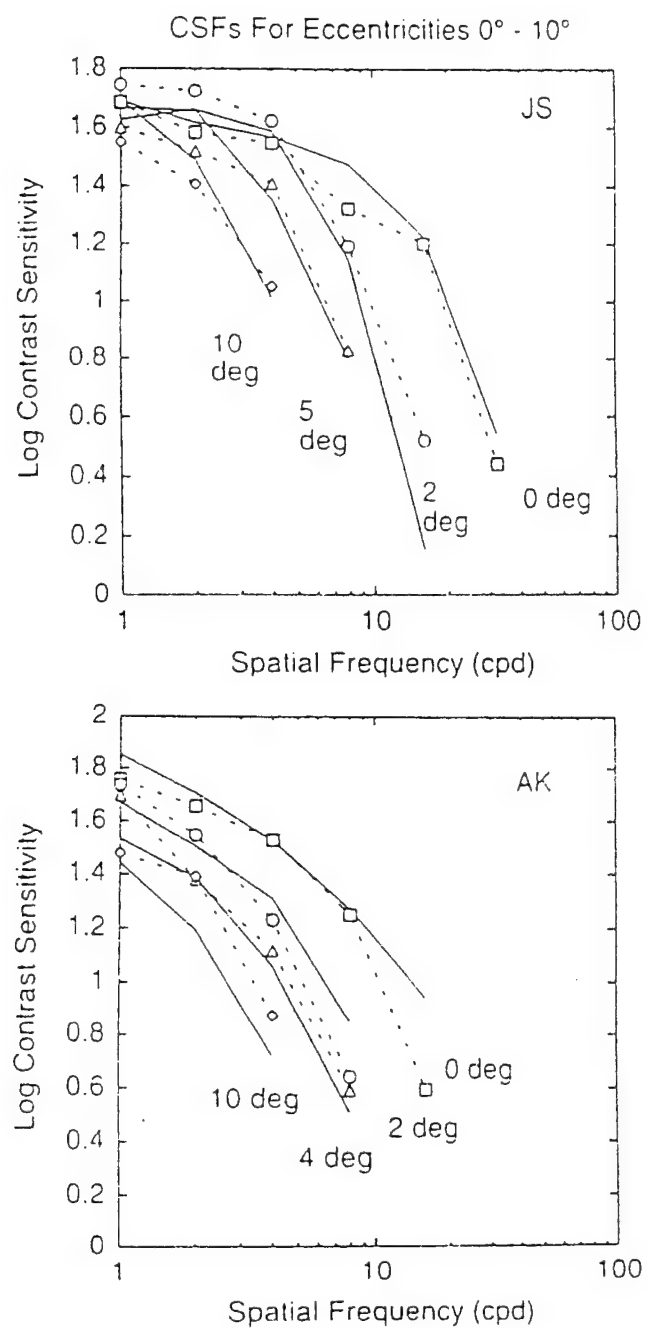
FIGURE 40. CSF Curves. Dark Lines represent IRC simulations.
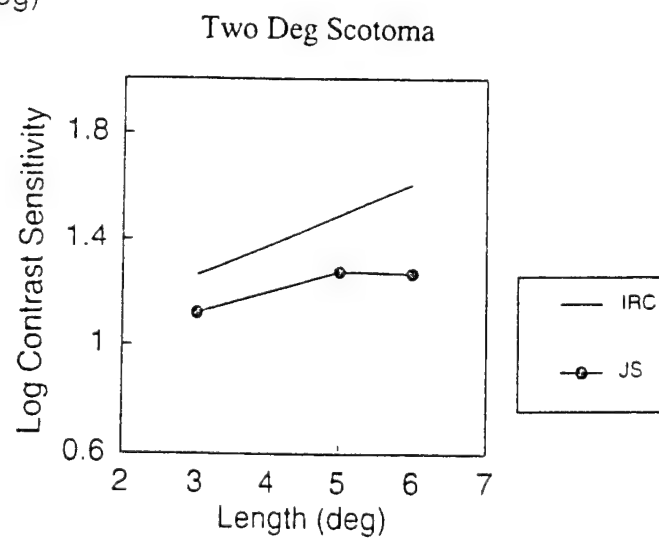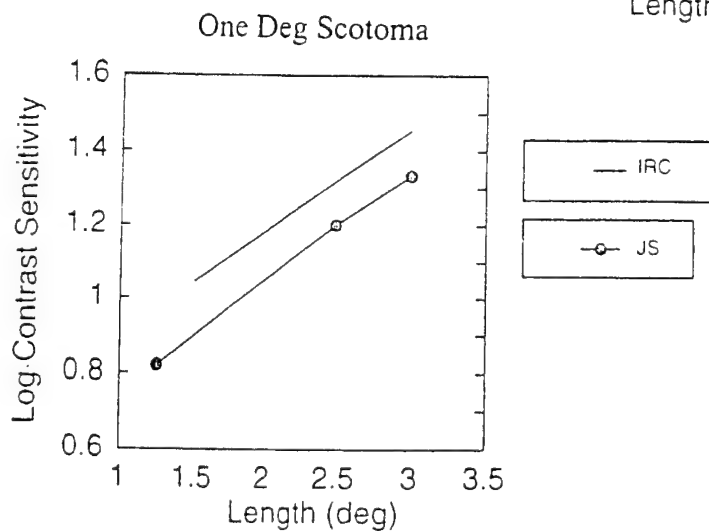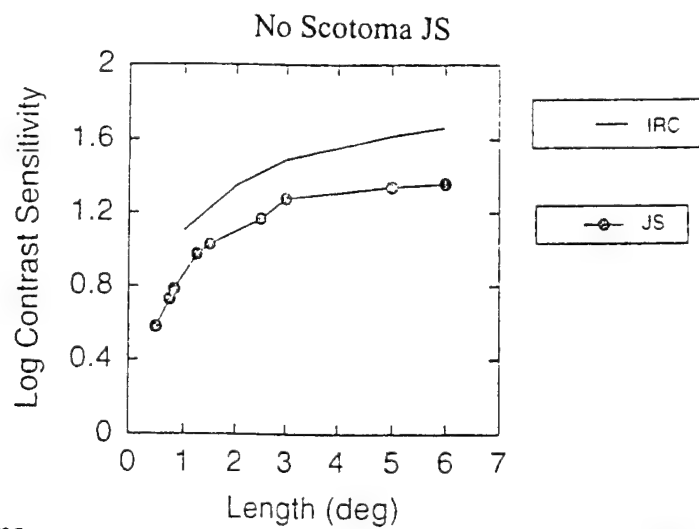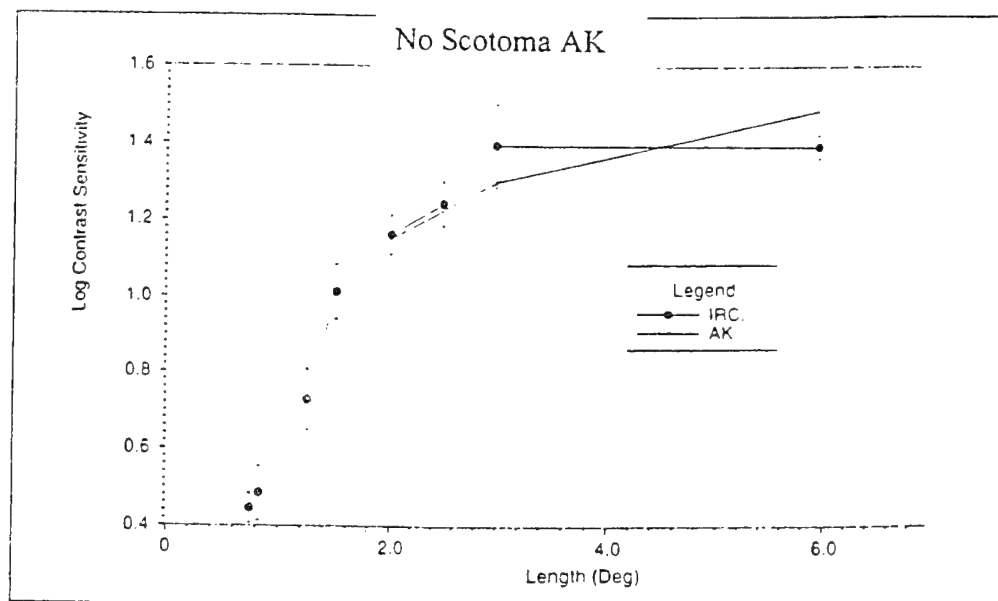
FIGURE 41. Airplane curves. Dark Lines represent IRC simulations. Points represent experiment.

4.3 Alternate model

This alternate model, based on spatial frequency channels, is included to show possible alternatives to the IRC. It was never implemented. The alternate model was an attempt to improve on the VEP and best remaining models, but to be simple enough to be easily implemented on a computer. Like the other models, it ignored temporal effects. Figure [42] illustrates an overview of this spatial frequency channel model. In a similar manner to the IRC model (figure [31]), two stimuli are fed to a routine which calculates a value for d' representing the perceptual difference between the two. Figure [42] shows a block diagram of the processing of each stimulus. The input to the retina passed through non-linearities related to control of sensitivity (section [2.5.2] in the vision system. Next is a large series of tuned and oriented spatial frequency channels (section [2.7.7]) which cover the entire retina, three of which are illustrated. Each channel is simulated as a digital filter which is convolved with a portion of the input image. These outputs are processed further as shown in figure [44] before going to the d' calculator. Note that a provision is made for interactions between other channels, though early implementations of the model will probably ignore these interactions. The output of the filter convolution is passed to cortical contrast acceleration non-linearities as discussed in section [2.7.6].
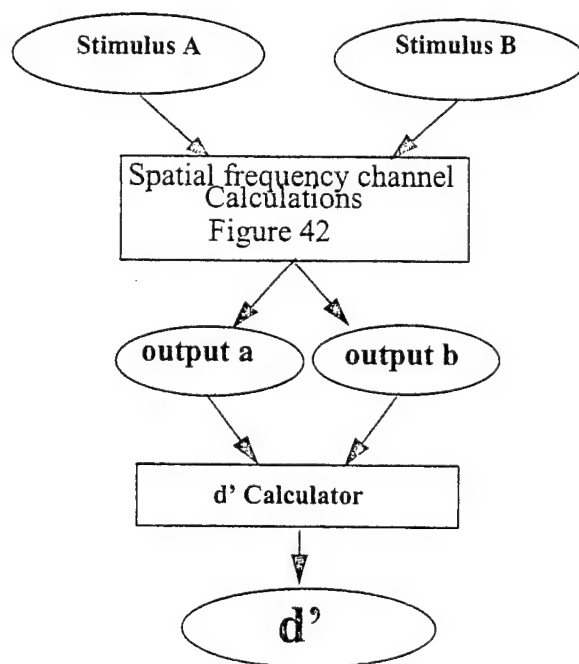
FIGURE 42. Spatial Frequency Channel Model

At the same time, (CS), covered in section [34], is calculated as a function of eccentricity and spatial frequency, in a similar manner to the one described in the VEP model. CS is used as a measure of the gain of each channel and is multiplied by the rectified channel output.
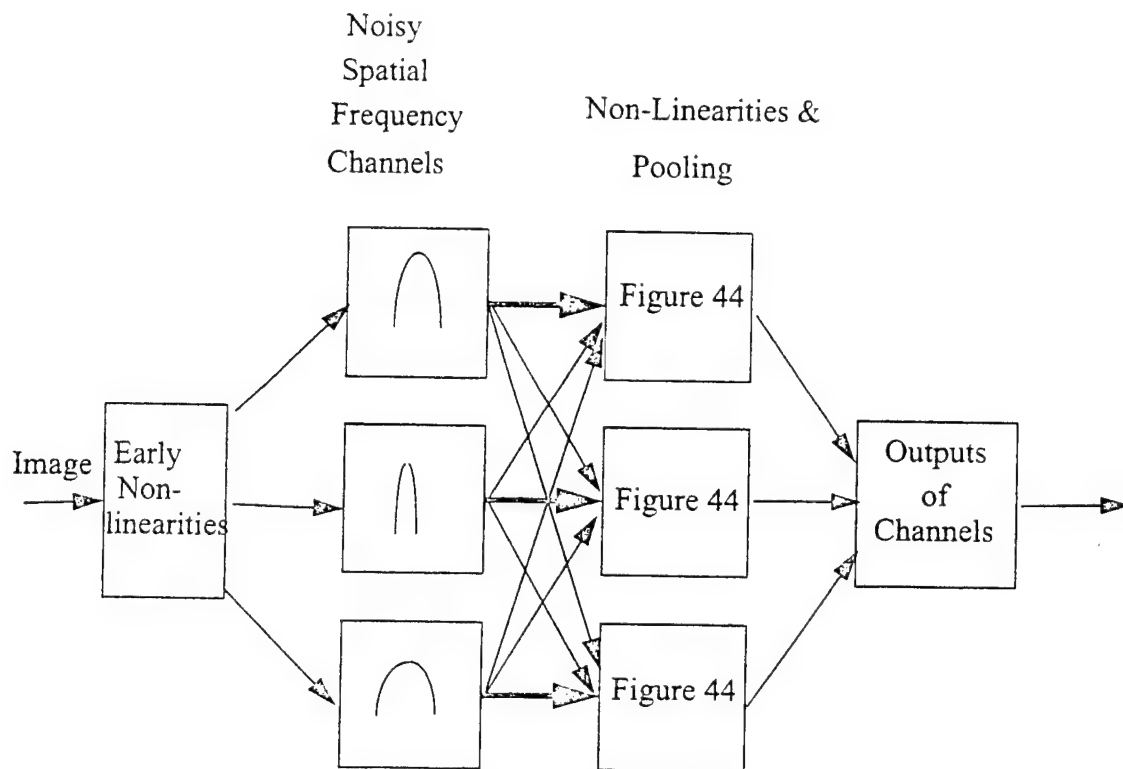
FIGURE 43. Overview of Calculations-Spatial Frequency Channel Model

CS is used here is a simple means of calculating the sensitivity of each channel. To obtain the CS at any desired values of SF and eccentricity, interpolation must be used. This is described below in section [3.3]. Therefore, the model shows a CS calculation routine. One last routine calculates interactions between the given channel and others. This is shown as being multiplied by the outputs, so a value of 1 indicates no interaction effect. This routine would have been added if necessary, after completing the rest of the model.
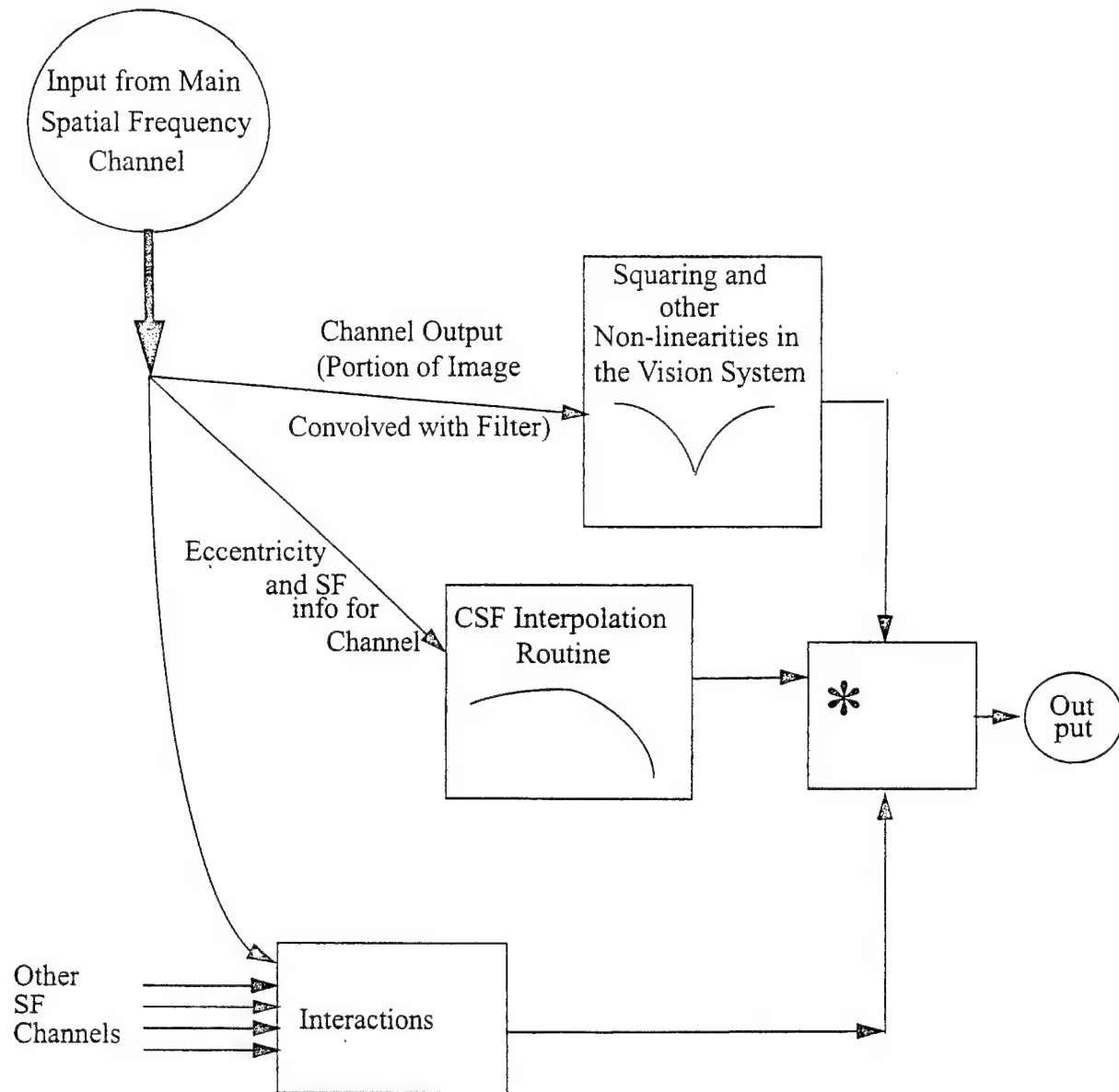
FIGURE 44. Post-Channel Calculations.

The outputs of the channels will be sent back to the d' calculator in figure [42]. One way to convert the outputs to d' is shown in equation [71]. This is based on the Quick Pooling formula of equation [46]. Equation [71] has an exponent, q, as well as a function f. f would have been assumed to be multiplication by an adjustable weight, that weight and q would have been set by fitting against experimental data.

$$d' = f\left(\left|\sum_i |A_i - B_i|^q\right|^{1/q}\right)$$

[71]

To utilize this model in a practical manner to simulate vision loss due to retinal damage, the functions and algorithms taking place in the various boxes must be specified. This can be done by calculating d' values for a series of psychophysical experiments being run and perhaps also from experiments in the literature. Certain effects, such as the early non-linearities shown in figure [42] can probably be safely ignored, assuming linearity for small ranges of illumination changes. Simple grating experiments should excite only one channel at a time, and be easy to simulate in the model. More complicated patterns could be run exciting multiple channels, allowing development of more complex aspects.

V. Conclusions

While the research is still on going, the IRC model shows great promise. It has shown good results fitting CSF and cycle summation curves. The latter is an important result because it shows that cycle summation is not due to some mysterious summation rule or response of spatial channel: it is due to the same d' summation rule for any other pattern. The premise is tantalizing - detection can be modeled by a summation of information.

The spatial frequency channel model as described would have been easy to implement - it is convolutions, CS interpolations, and some other calculations, all of them fairly simple. The model would have suffered from at least one serious flaw, using CS functions to calibrate the channels might work - as long as the same kind of stimulus was used to generate the CS curves as to generate the stimulus under test. It would lack the flexibility of the IRC model which can have its parameters retrained for different kinds of stimuli.In retrospect, it has been realized that this implementation of a spatial frequency channel model does not simulate the channels very well. It would not handle the properties described above in section[2.7.7], because it does not implement channel masking or adaption. Therefore, it does not seem to be a useful exercise to implement this model without major design changes.

The airplane results are somewhat contradictory. One subject shows excellent agrement, the other is about .3 log unit high.

How far will the IRC model take us? Color effects could by added by simulating the positions of the three kinds of cones and their connections to ganglion cells. Temporal effects could be added by simulating the delay between surround and center. This should alleviate the need for using parameter fitting to set the ratio of weights between the center and the surround. Tuned and oriented cortical cells can be added in. The computational requirements of such a model would be considerable.

Of course, the purpose of this project is the simulation of retinal damage. The results are inconclusive, as yet, but show excellent promise.

VI. References

Albrecht, D.G. & Geisler, W. S. Visual cortex neurons in monkey and cat: Contrast response non-linearities and stimulus selectivity. In. T. Lawton (Ed.) Computational Vision Based On Neurobiology SPIE Proceedings 2054, 12-31.

Arnow, T. L. (1991) Comparison of sensor configurations for ANN Pattern Recognition. Master's Thesis, University of Texas at Austin, August 1991.

Azzopardi, P. & A. Cowey. (1993) Preferential representation of the fovea in the primary visual cortex. Nature, 361(25), 719-721.

Banks, M. S.; Sekuler, A. B.; & S. J. Anderson. (1991) Peripheral spatial vision: limits imposed by optics, photoreceptors, and receptor pooling. Journal of the Optical Society of America - Part A, Optics & Image Science, 8(11), 1775-1787.

Banks, M.S., Sekuler, A.B., & Anderson, S.J. (1991). Peripheral spatial vision: limits imposed by optics, photoreceptors, and receptor pooling. Journal of the Optical Society of America - Part A, Optics & Image Science, 8(11), 1775-1787.

Bovik, A. C., Clark, M. & Geisler, W. S. (1990), Multichannel Texture Analysis Using Localized Spatial Filters, IEEE Transactions on Pattern Analysis and Machine Intelligence, 22 55-73.

Bovik, A. C., Gopal, N., & Emmoth, T. & Restrepo, A. Localized Measurement of Emergent Image Frequencies by Gabor Wavelets, IEEE Transactions on Information Theory, 38, 691-712.

Campbell, F. W. & Gubish, R.W. (1966) Optical quality of the human eye. Journal of Physiology, 186 558-578.

Cox, A. J. (1981) Evaluation of Peak Location Algorithms with Subpixel Accuracy for Mosaic Focal Planes. in Processing of Images and Data from Optical Sensors, Carter, W. H. editor., Proceedings SPIE 292. 288-299.

Cox, Allen J. (1987) Point-Source Location Using Hexagonal Detector Arrays, Optical Engineering, 26(1).

Crawford, M. L. J., Andersen, R. A., Blake, R., J., Jacobs, G.H., Neumeyer, C., (1990) Interspecies comparisons in the understanding of human visual perception. In L. Spillman and J. Werner (Eds.) Visual Perception, The Neurophysiological Foundations. (pp. 231-272). San Diego, CA: Academic Press.

Croner, L. J. & Kaplan, E. (1995). Receptive fields of P and M ganglion cells across the primate retina. Vision Research, 35 (1), 7-24.

Curcio, C., Sloan, K.R, Kalina, R.E., &Hendrickson, A.K. (1990) Human photoreceptor topography, The Journal of Comparative Neurology 292, 497-523.

Curcio, C., Sloan, K.R, Packer, O., & Hendrickson, A.K. (1987) Distribution of Cones in Human and monkey retina: individual variability and radial asymmetry, <u>Science 236</u>, 579-581.

De Valois, R. & De Valois, K. (1990) <u>Spatial Vision.</u> New York, N.Y. Oxford University Press.

Enroth-Cugell, C. Robson, J. G., Schweitzer-Tong, & Watson, A.B. (1983) Spatio-temporal interactions in cat retinal ganglion cells showing linear spatial summation. <u>Journal of Physiology 341</u>, 279-307.

Foley-Fisher, J. A. & Murphy, K. St. J. (1987) Simulation of a Retinal Scotoma by a Stabilized Retinal Image, <u>Opthal. Physiol. Opt. 7</u> (4). 495-498.

Gallagher & Wise...

Gegenfurtner, K.R., & Kiper, D.C. (1992). Contrast detection in luminance and chromatic noise. <u>Journal of the Optical Society of America - Part A. Optics & Image Science,</u> 9(11), 1880-8.

Geisler, W. S. & Banks, M. S. (1994) Visual Performance, in <u>Handbook of Optics. 1: Fundamentals. Techniques, & Design. 2nd ed.</u> McGraw Hill.

Geisler, W. S. (1984) Physical limits of acuity and hyperacuity. <u>Journal of the Optical Society of America A.</u> 1(7), 775-782.

Geisler, W. S. (1989). Sequential ideal-observer analysis of visual discrimination. <u>Psychological Review,</u> 96(2), 267-314.

Gescheider, G. A. (1976) <u>Psychophysics Method and Theory,</u> New York John Wiley and Sons.

Ghosh, J. & Bovik, A. C (1991) Neural Networks for Textured Image Processing. In <u>Artificial Neural Networks and Statistical Pattern Recognition Old and New Connections.</u> Eds I.K. Sethi and A.K. Jain, Elsevier Science Publishers, New York, 1991.

Goldberg, D. E. (1989) <u>Genetic Algorithms.</u> Reading, Mass.: Addison-Wesley.

Graham, N. (1989) <u>Visual Pattern Analyzers.</u> New York: Oxford University Press.

Graham, N. Sutter, A, & Venkatesan, C. (1993). Spatial-frequency and orientation-selectivity of simple and complex channels in region segregation. <u>Vision Research, 33,</u> 1893-1911.

Green, D. M. & Swets, J. A. (1966) <u>Signal Detection Theory and Psychophysics.</u> New York: John Wiley and Sons.

Greenlee, M.W., & Thomas, J.P. (1992). Effect of pattern adaptation on spatial frequency discrimination. <u>Journal of the Optical Society of America - Part A. Optics & Image Science. 9</u>(6), 857-862.

Greenlee, M.W., & Thomas, J.P. (1993). Simultaneous discrimination of the spatial frequency and contrast of periodic stimuli. Journal of the Optical Society of America - Part A, Optics & Image Science. 10(3), 395-404.

Hahn, L.W., & Geisler, W. S. (1995) Adaptation mechanisms in spatial vision I: Bleaches and backgrounds. Vision Research. 35, 1585-1594.

Hilz, R. & Cavonius, C. R. (1974) Functional Organization of the Peripheral Retina: Sensitivity to Periodic Stimuli. Vision Research 14 1333-1337.

Kelly, D.H. (1778) Photopic contrast sensitivity without foveal vision. Optics Letters. 2(4), 79-81.

Kelly, D.H. (1779) Motion and vision. I. Stabilized images of stationary gratings. Journal of the Optical Society of America. 69(9), 1266-1274.

Kelly, D.H. (1779) Motion and vision. II. Stabilized spatio-temporal threshold surface. Journal of the Optical Society of America. 69(10), 1340-1349.

Kortum, P. T., & Geisler, W. S. (1995) Adaptation mechanisms in spatial vision II: Flash threshold and background adaptation. Vision Research. 35. 1595-1610.

Kuffler, S.W. (1953) Discharge patterns and functional organization of mammalian retina. Journal of Neurophysiology 16, 37-68.

Kumar, T & Glaser, D. (1993) Initial performance, learning and observer variability for hyperacuity Tasks. Vision Research. 33. 1133-1149.

Legge, G., & Foley, J. (1980). Contrast masking in human vision. Journal of the Optical Society of America. 70(12), 1458-1470.

Levitt, H. (1971) Transformed up-down methods in psychoacoustics. Journal of the Acoustical Society of America. 49(2), 467-477.

Longbotham H. & Glickman, R. (1991) Noninvasive Assessment of the Visual System, Presented at the Noninvasive Assessment of the Visual System Topical Meeting, Santa Fe, New Mexico.

MacMillan, N. A. & Creelman, C. D. (1991) Detection Theory. Cambridge: Cambridge Univeristy Press.

McGinn, D. (1995, May 8). Software au naturel. Newsweek. 125 (19), 70-71.

Merigan, W.H & Maunesll, J.H.R (1993) Annual Review of Neuroscience 16 369-402.

Morgan, M. J. Hyperacuity, in Vision and Visual Disfunction: Spatial Vision. D. Regan (Ed.), 10 87-113, CRC Press, Inc., Boca Raton.

Navarro, R., Artal, P., & Williams, D. (1993) Modulation transfer of the human eye as a function of retinal eccentricity. Journal of the Optical Society of America - Part A. Optics & Image Science, 10(2), 201-212.

Peli, E., Yang, J.A.,Goldstein, R., & A. Reeves. (1991). Effect of luminance on suprathreshold contrast perception. Journal of the Optical Society of America - Part A, Optics & Image Science, 8(8), 1352-1359.

Peli, E.; Yang, J.; & Goldstein, R. B. (1991) Image invariance with changes in size: the role of peripheral contrast thresholds. Journal of the Optical Society of America - Part A, Optics & Image Science, 8(11), 1762-74.

Proakis, J. G. & Manolakis, D. G. (1988) Introduction to Digital Signal Processing, New York, Macmillan.

Regan, D. (1989) Human Brain Electrophysiology: Evoked Potentials and Evoked Magnetic Fields in Science and Medicine. New York: Elsevier Science Publishing.

Regan, D. (1991) A Brief Review of Some of the Stimuli and Analysis Methods Used in Spatiotemporal Vision Research, in Vision and Visual Disfunction: Spatial Vision, D. Regan (Ed.), 10 pp 1-42, CRC Press, Inc., Boca Raton.

Robson, J. G. & Graham, N. (1981) Probability Summation and Regional Variation in Contrast Sensitivity Across the Visual Field. Vision Research 21 409-418.

Rovamo, J. Franssila, & Risto, N. (1992) Contrast sensitivity as a function of spatial frequency, viewing distance, and eccentricity with and without spatial noise. Vision Research, 32(4), 631-637.

Sachtler, W.L., & Zaidi, Q. (1992). Chromatic and luminance signals in visual memory."Journal of the Optical Society of America - Part A, Optics & Image Science, 9(6), 877-894.

SBIR Phase I Final Report. Conceptual MindWorks, Inc., 4318 Woodcock Dr., Suite 210, San Antonio, TX 78228, 1993.

Shapley, R. et. al. (1991) Spatiotemporal Receptive Fields and Direction Selectivity. In Computational Models of Visual Processing Eds M. Landy and A. Movshon, Cambridge Mass.: MIT Press.

Sutter, A. K. & Graham, N. V. Investigating Simple and Complex Mechanisms in Texture Segregation using the Speed-Accuracy Trade-off Method, presented at ARVO 1994.

Grossman, A., Cavanagh, P., Fischer, B., Ramachandran, V, & von der heydt. (1990) Form Perception and Attention: Striate Cortex and Beyond. In L. Spillman and J. Werner (Eds.) Visual Perception. The Neurophysiological Foundations. (pp. 273-316). San Diego, CA: Academic Press.

Wandell, B. A. (1995) Foundations of Vision. Sunderland, Massachusetts: Sinauer Associates Inc.

Walraven, J.,Enroth-Cugell, C., Hood, D.,MacLeod, D. & Schnapf, J. (1990). The Control of Visual Sensitivity. In L. Spillman and J. Werner (Eds.) Visual Perception. The Neurophysiological Foundations. (pp. 53-102). San Diego, CA: Academic Press.

Watson, A. (1991) Neural Contrast Sensitivity. In Computational Models of Visual Processing Eds M. Landy and A. Movshon, Cambridge Mass.: MIT Press.

Watson, A. B. (1983). What does the eye see best? Nature, 302, 419-422.

Watson, A., B. Detection and Recognition of Simple Spatial Forms. 101-114

Webster, M.A., & Mollon, J.D. (1993). Contrast adaptation dissociates different measures of luminous efficiency. Journal of the Optical Society of America - Part A. Optics & Image Science, 10(6), 1332-1340.

Widrow, B. & Stearns, D. (1985) Adaptive Signal Processing. Englewood Cliffs, New Jersey: Prentice-Hall.

Williams, D. R. (1985) Visibility of Interference Fringes Near the Resolution Limit. Journal of the Optical Society of America - Part A. Optics & Image Science. 2(7),.

Williams, D. R. & Coletta, N. J. (1987) Cone Spacing and the Visual Resolution Limit. Journal of the Optical Society of America - Part A, Optics & Image Science, 4(8),.

Wilson, H. & Hujanski, R. (1993) Spatial frequency adaption and contrast gain control. Vision Research, 33, 1133-1149.

Wilson, H. R. (1991) Psychophysical Models of Spatial Vision and Hyperacuity, in Vision and Visual Disfunction: Spatial Vision, D. Regan (Ed.), 10 64-86, CRC Press, Inc., Boca Raton.

Wilson, H., Levi, D., Maffei, L., Rovamo, J., De Valois, Rovamo, J. & Raninen, A. (1990) The perception of form. In L. Spillman and J. Werner (Eds.) Visual Perception, The Neurophysiological Foundations. (pp. 231-272). San Diego, CA: Academic Press.

Appendix III

The Effects of Disease on Signal Processing
Characteristics of the Human Visual System

"A SIGNAL PROCESSING APPROACH TO LASER DAMAGE"

M. Desai

We have developed a signal processing model for the effect of laser damage on visual acuity. Our goal is to explore how laser damage over a small region of the retina (e.g. at or near the fovea) affects vision at other points on the retina. We believe that the destruction of part of the retina may affect acuity elsewhere. The damaged area is modeled to have complete loss of vision, (i.e. zero sensory reception or dead zone). We then model processing of a stimulus with the laser-damaged retina using a linear filter model of the neural receptive fields. The receptive field models are localized, hence the effects of processing are also localized. However, it can be argued that the effects of the laser damage effect the responses of neighboring receptive fields, hence propagating the effects of the damage from the damaged area.

Visual acuity is measured by the responses of the laser-damage model to different inputs. A simple measure of resolution is made using simple point targets (impulses) of small separation as the input to the system. The point targets are then passed through appropriate linear filters, including Gaussian and Gabor filters. A second measure of acuity is based on texture discriminability. In this approach, the input is assumed to be a sum of two sinusoidal gratings. The measure of acuity is based on the discriminability (channel separation) of the gratings in the vicinity of the damaged region.

Using these models, we are able to show that the laser damage reduces visual acuity near the dead zone, in the following sense: the filtered stimuli (neuronal responses) are affected in such a manner that the effective acuity within a given visual channel is reduced. Thus, the filtered stimuli response data that is used by subsequent processing elements may effect processes such as stereopsis and motion field perception both within the damaged region (where it is eradicated), and in the vicinity of the damaged region as well. The extent of the effect is found to depend directly on the effective span (spatial extent) of the channel or receptive field. This implies that large peripheral receptive fields involving a significant (spatial) degree of spatial summation over the retina may be most affected.

We are also able to show that the effect is worsened as the ambient light intensity increases. The analysis we present includes a variety of channel types (Gaussian, Gabor) and also analyzes the effects of varying such parameters as the spatial extent of the reception field (or the filter bandwidth)

123

and the extent of the damage.

A more extensive analysis is then developed that attempts to analyze the effects of damage on a multi-channel (wavelet-like) visual processing system. This analysis encapsulates the effects of variable resolution (sampling density) over the retina, as well as an analysis of how the errors are distributed across channels (hence scales) in a multi-channel scenario. Finally, observations are made on how extensively certain basic low-level visual tasks may be effected by the laser damage. This is accomplished by examining the effect of the flawed, filtered stimulus on computer models of, e.g., stereo, texture, and motion processing.

1. 1-D Signal Processing Model

Our goal in this one-dimensional model is to explore how laser damage over some region of retina (e.g. fovea) affects vision at other points on the retina. In other words, how does the destruction of part of the retina may affect acuity elsewhere. To understand this, first we consider the simple 1-D model, that is equivalent to considering the damage along a single line as illustrated below. For this analysis assume continuous mathematics and uniform sampling. The multiresolution analysis will be addressed in the later sections.
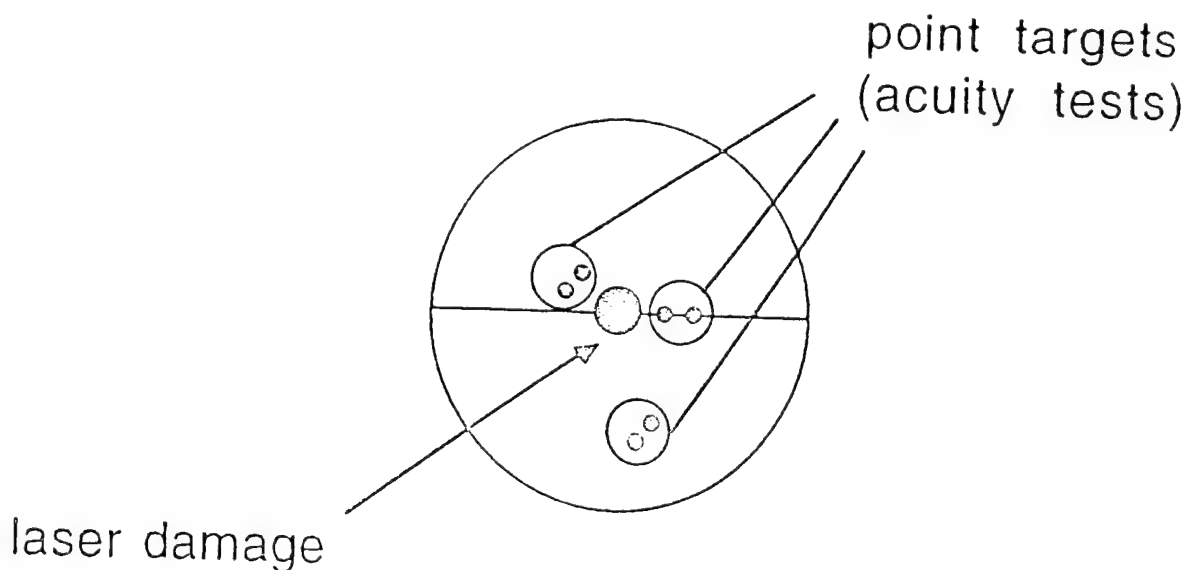
Fovea with laser damaged illustrated as point targets.
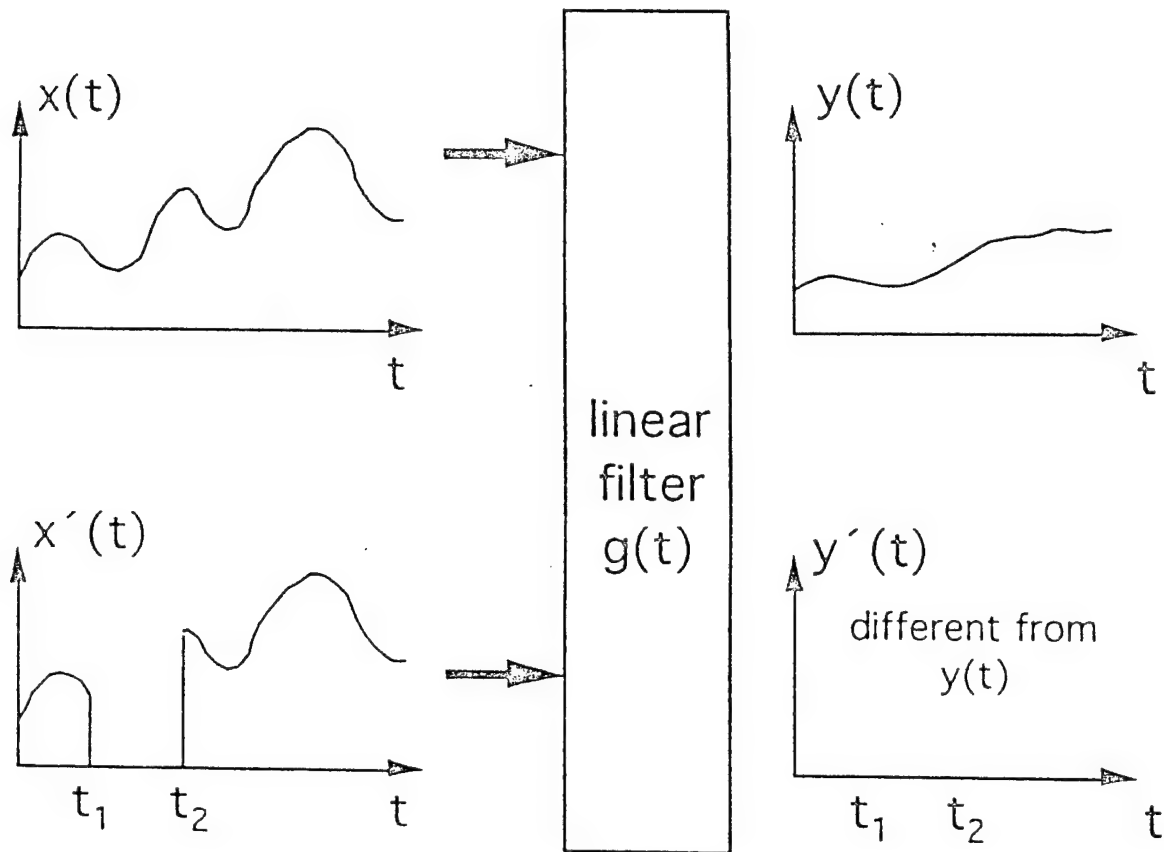
One-dimensional filter model with [t_1 to t_2] being the dead zone or the laser damaged area.

This illustrates the model. First, eliminate a chunk of a signal, then pass the signal through a filter. The result (output) will be changed (differ from the ideal) at places other than in the "dead" zone [t_1, t_2]. In fact, it may be changed everywhere (although likely negligibly with some distance from the damaged point). The "filters" used may be thought of as models for neural receptive fields, which are localized, so the effect will be localized, yet WILL propagate from the damage area. Within a measurable vicinity of the damaged region, there will be pronounced effect on the filter responses.

Now consider an ideal image signal (visual stimulus) $x(t)$. Denote the signal resulting from retinal damage to be $x'(t)$, where the damage results in loss of signal in the interval $[t_1, t_2]$. We can then write:

$$x'(t) = x(t) [u(t_1-t) + u(t- t_2)]$$

where

$$u(t) = \text{unit step}.$$

The outputs of the filter with the two signal inputs (ideal and damaged) are

$$y(t) = x(t) * g(t)$$

and

$$y'(t) = x'(t) * g(t)$$

respectively. As an example of the effect we will assume that the input is a pair of ideal point targets (unit impulses) on a constant non-zero intensity background.

Ideal Point Targets

Now suppose that

$$x(t) = \delta(t - t_3) + \delta(t - t_4) + C$$

where $\delta(t)$ is the Dirac impulse function. We will be using it's integral properties (in convolutions) to model the response to closely-placed point targets. This signal is depicted:
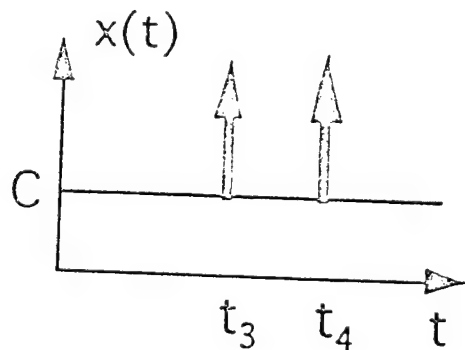
The constant level C which models a non-zero background (constant ambient light flux) is both necessary and realistic. Any realistic scene has a background illumination. Moreover, without it, the

dead zone will not show up! (this has an important implication).

The ideal response is:

$$y(t) = g(t - t_3) + g(t - t_4) + C \int_{R} g(t) \, dt.$$

Make the simple assumption that g is Gaussian (could be Gabor etc). Then we may model the resolution loss at the gaussian channel output (again, no damage yet). The following depicts the classic acuity problem observed at the filter output:
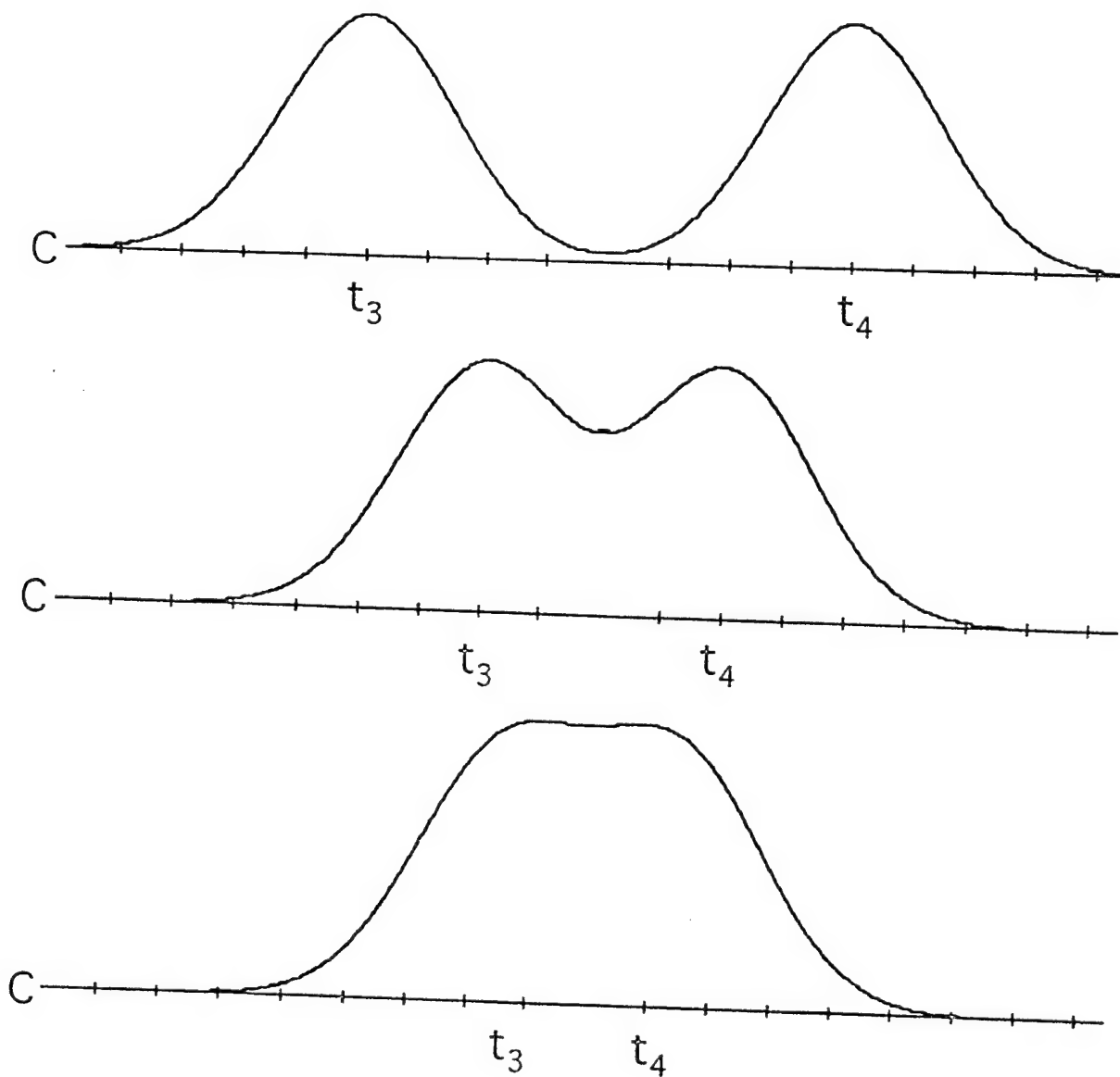
Ideal Point Targets on Damaged Retina

Now we consider the case of a laser-damaged retina. The signal with damage is

$$x'(t) = [\delta(t - t_3) + \delta(t - t_4) + C] \, [u(t_1 - t) + u(t - t_2)]$$

$$= \delta(t - t_3) + \delta(t - t_4) + C \cdot [u(t_1 - t) + u(t - t_2)]$$

(of course t_3, t_4 are not in the dead zone). This is depicted below:
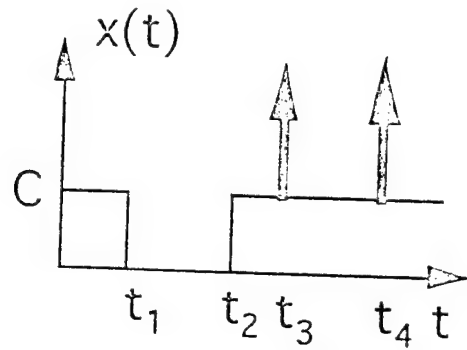
The output is now:

$$y'(t) = g(t - t_3) + g(t - t_4) + C \left\{ \int_{t_1 - t}^{\infty} g(t) \, dt + \int_{-\infty}^{t - t_2} g(t) \, dt \right\}$$

Thus we can model the resolution loss at the gaussian channel output for the case where there has been damage. This is depicted in the following diagram, with comparison to the case where there is no damage:
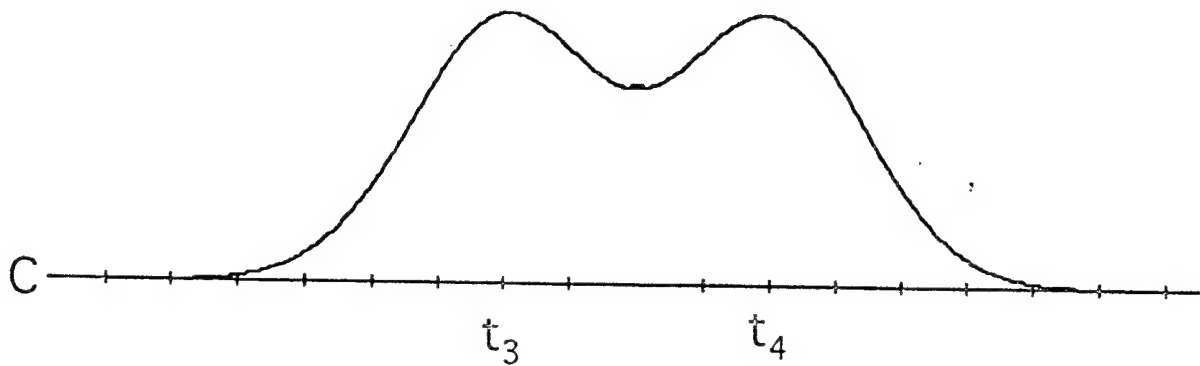
WITHOUT DAMAGE
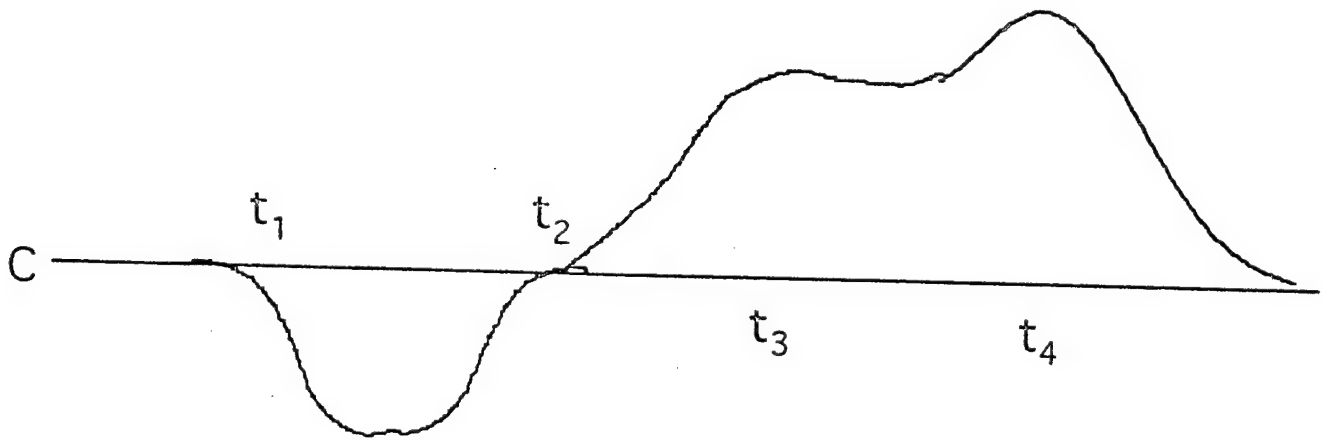
WITH DAMAGE - RESOLUTION REDUCED

The Gaussians still mix, but acuity is further reduced by the proximity of the **response to the dead zone**. This loss in resolution is manifested by a lessening of one of the gaussian peak responses, making it difficult (for example, in an algorithm, or a neural network), to discriminate one peak from another. It could easily, in fact, be interpreted as a single peak.

As might be expected, the effect is worsened as the light ambient intensity increases - the trough is deepened, thus reducing the resolution further:
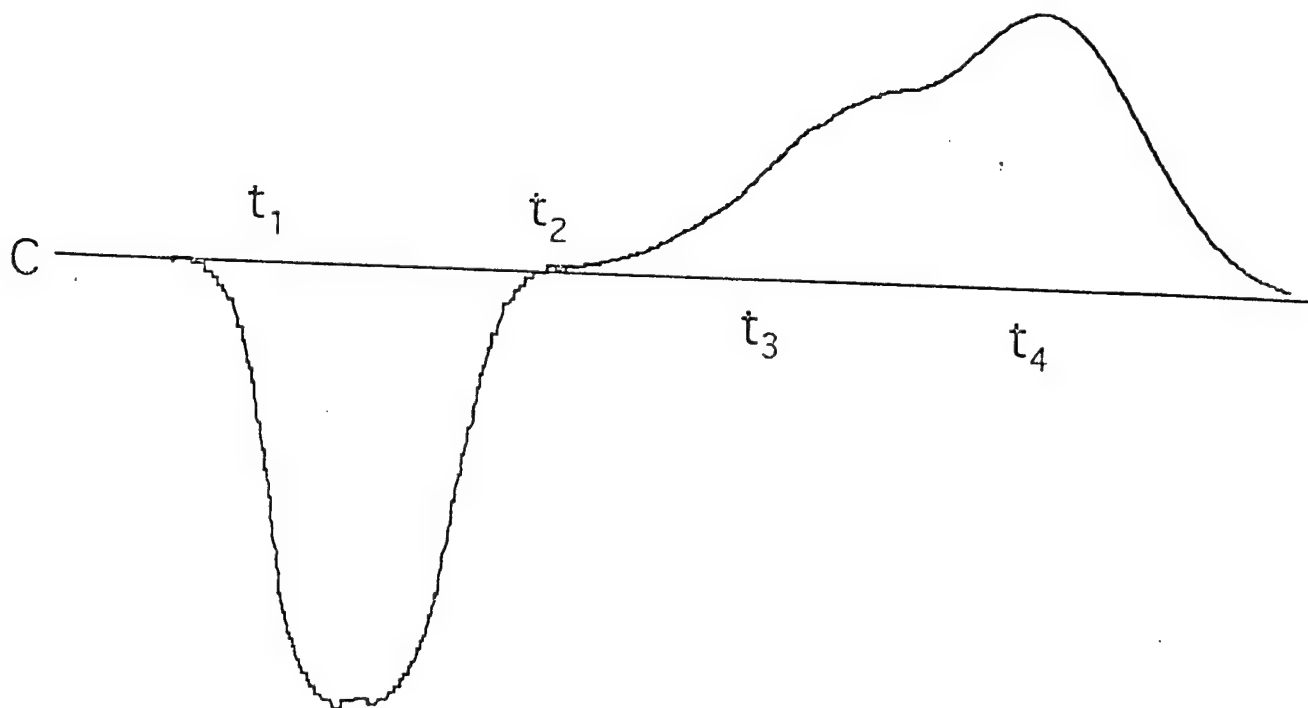
By this simple demonstration, we have shown that when a chunk of a signal is eliminated, then passed through a filter, the output result will be changed at places other than in the "dead" zone [t_1, t_2]. The "filters" are models for neural receptive fields, which are localized, so the effect will be localized, yet WILL propagate from the damage area in a significant way. The extent of the effect depends directly on the effective span (spatial extent) of the channel or receptive field. This implies that large peripheral receptive fields having a lot of spatial overlap over the retina may be most affected. The effect will be more pronounced when the ambient light intensity is higher.

2. Multi-Channel Model

We have performed a preliminary analysis of the effects of laser damage on multiple channels or filters. The multi-channels may be a wavelet-like filter bank, or a network of receptive fields. It is of interest to consider the effects of the damage as it is processed at variable resolutions over the retina. In particular, it would be useful to know how the error is distributed across channels, and how well visual tasks can be accomplished using the flawed data.

130
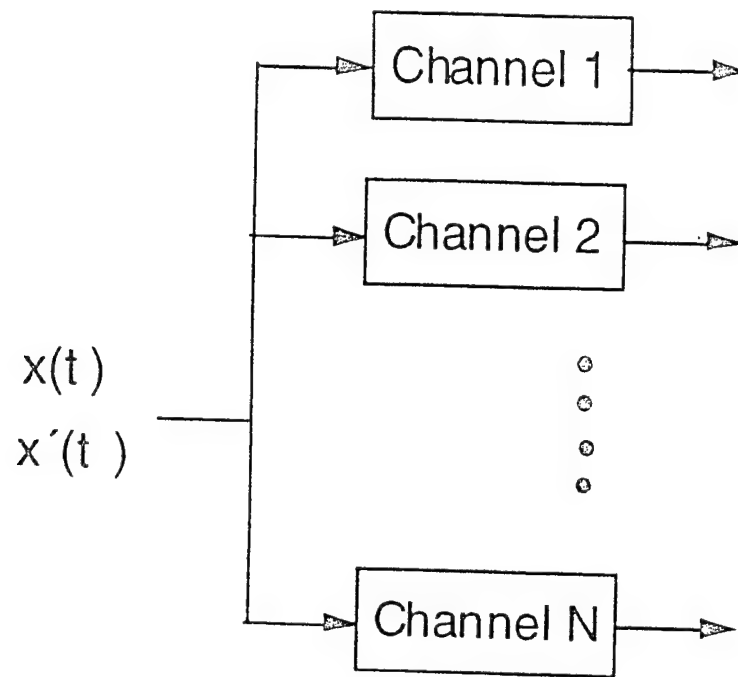
Experimental Results:

We have performed an empirical study of the effects of laser damage on multi-channel filters. We consider five different channel filters which are the Gabor functions. The input in this case will be actual two-dimensional signals (images), i.e, the Lena image reproduced in Figure 1a.

Five Gabor filters are used in the simulations. Each has an orientation along 90°. The bandwidth of each is one octave, in accordance with typical Gabor-shaped receptive fields. The center frequencies vary from about 10 cycles/image to 100 cycles/image in octave increments.

Figures 1b-f shows the responses of these five filters (top image in each case), ranging from low-frequency filter to high-frequency filter. We model the laser eye damage with a square "hole" in the image, i.e., with the image intensities set to zero in the dead zone. The outputs of the five filters for this input is also shown in Figs. 1b-f (middle image in this case). The difference between the filter ideal and filtered damaged image is shown at the bottom of Figs 1b-f. As in the one-dimensional model, the two-dimensional results show that the effect of the damage extends well beyond the damaged region. The extent of the difference appears to increase with decreasing frequency, although the intensity of the difference (away from the dead zone) appears to increase with increasing frequency.

Original Lenna
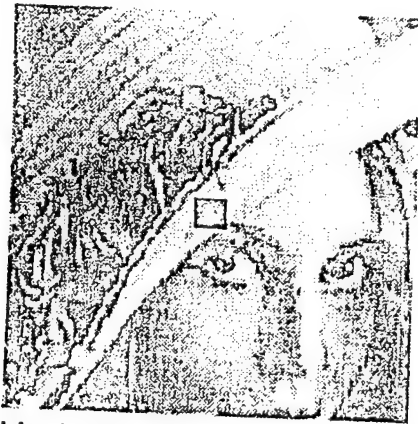
Masked Lenna

Figure 1:a. Unfiltered 256 x 256 Lenna images with and without 20 x 20 mask.
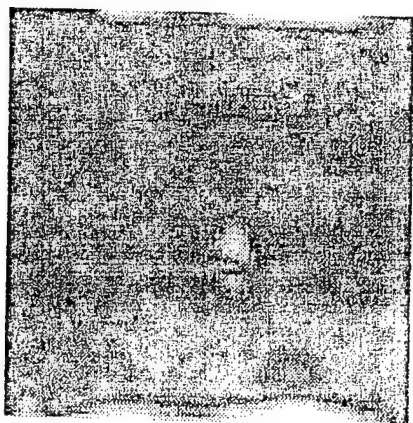
Unmasked Lenna: Channel 2
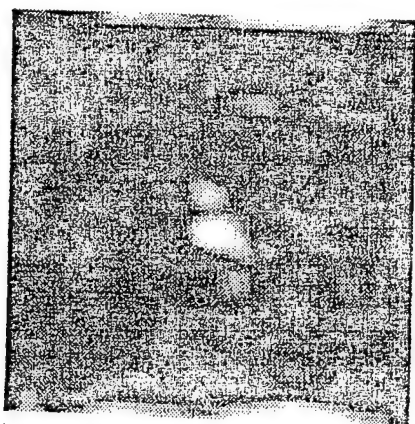
Masked Lenna: Channel 2
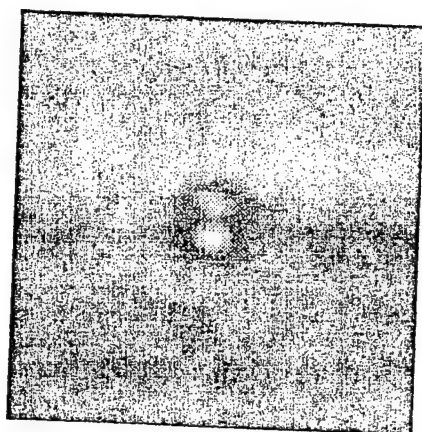
Difference image

Figure 1:c. Channel 2 outputs of Gabor filtered images and their absolute difference.
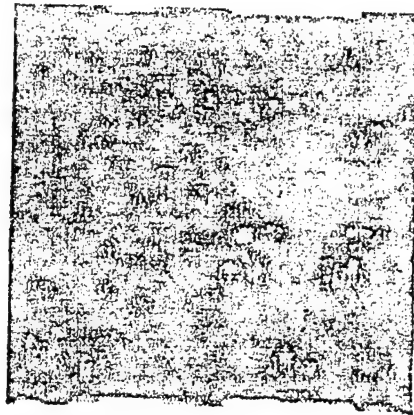
Unmasked Lenna: Channel 3
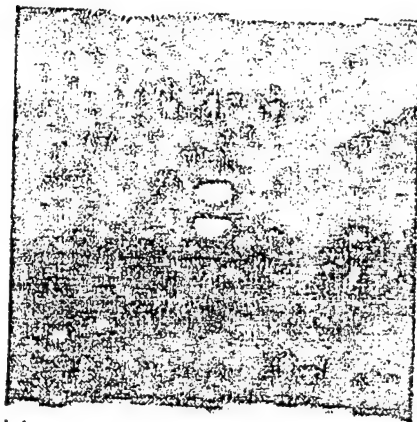
Masked Lenna: Channel 3
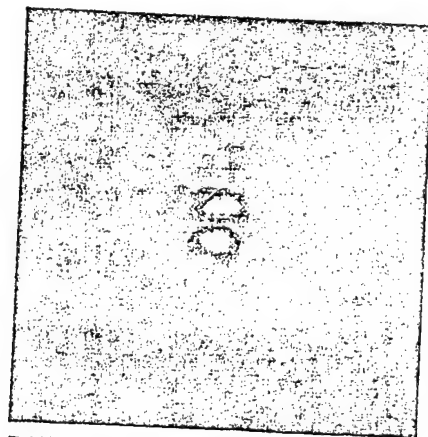
Difference image

Figure 1:d. Channel 3 outputs of Gabor filtered images and their absolute difference.
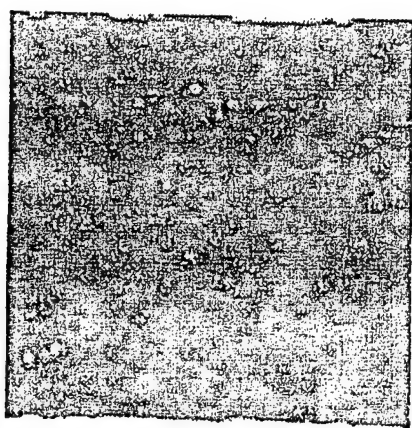
Unmasked Lenna: Channel 4
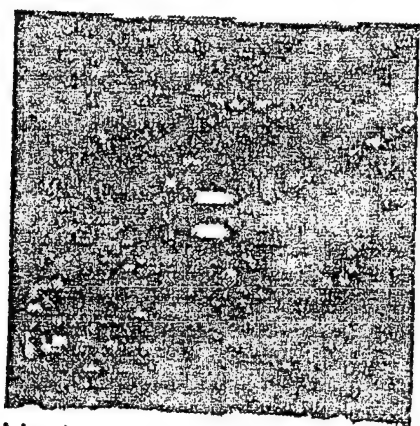
Masked Lenna: Channel 4
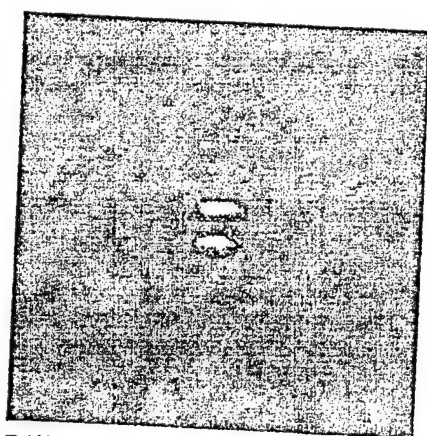
Difference image

Figure 1:e. Channel 4 outputs of Gabor filtered images and their absolute difference.
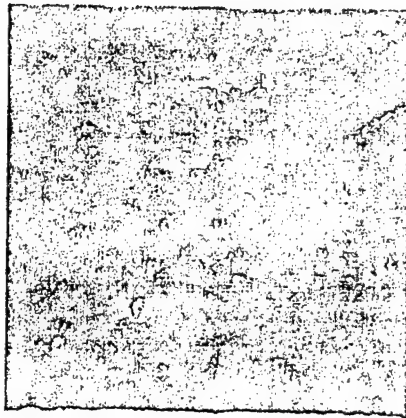
Unmasked Lenna: Channel 5

Masked Lenna: Channel 5
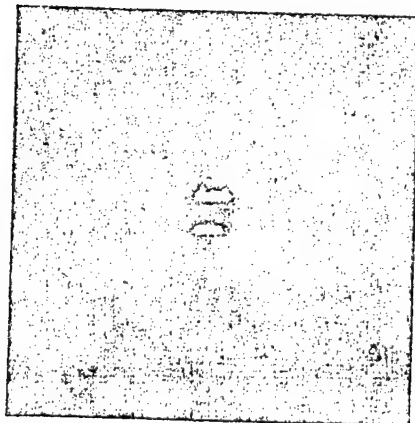
Difference image

Figure 1:f. Channel 5 outputs of Gabor filtered images and their absolute difference.

HUMAN VISUAL PROCESSING OF IMPULSIVE NOISE

James R. Dykes, Jr.

Susmitha Baddipudi

The University of Texas at San Antonio
San Antonio, Texas 78285

Abstract of Psychophysical Experiments

Any trauma (such as intravitreal blood resulting from laser damage) which adds noise to the retinal image will degrade performance, but the manner in which the human visual system codes the information available to the photoreceptors will have a profound effect in how resistant performance is to that noise. Two general classes of models of this coding have been proposed. The first (including threshold theory and median filtering) predicts minimal effects of low levels of noise, but a discontinuity in the function at the "break point". The second (including SDT and the logistic) predict no such disconitinuity; performance will gradually decline as more noise is added. While previous researchers have voiced opinions based on the steepness of the function, those data are insufficient to distinguish between the two models. The current research had observers discriminate between a pair of binary target stimuli as increasing levels of binary noise were XORed with the stimulus. Extending previous research, two additional independent variables were added: the number of distracters (0, 1, 3, or 15) and the nature of the distracters (blanks or hybrids). A pilot study was used to choose the appropriate four levels of noise and to refine the three pairs of targets. While the results of the main experiment are limited to the type of stimuli and noise chosen, the data were better fit by the SDT/logistic model than by the threshold/median filtering model. To the extent that diffuse intravitreal blood is appropriately modeled by binary impulsive noise, one can predict that increasing levels of noise will lead to a gradual and graceful decline in performance as opposed to level performance with a sudden drop.

Introduction

Many traumas to the eye can produce a hemorrhage causing blood diffusion in the vitreous humor of the eye. This in turn produces noisy images on the retina of the eye. One of the advantages of using a median filter in image processing is that it is resistant to noise. As the amount of noise added to an image is increased, the output of a median filter convolved with the image remains high in quality up to a fairly high level of noise. Beyond that break point, the output quality degrades precipitously. If the human visual system included a median filter, our perception should remain stable over low levels of noise and then should drop rapidly past the break point. This prediction is consistent with classic threshold theory. When image intensity, duration, and quality are above threshold, performance should be almost perfect. Below threshold, performance should be at chance. Both using a median filter and threshold theory predict that the performance function should have a discontinuity at the break point.

In contrast, the human visual system might employ operators that produce performance functions with no such discontinuity. One such operator (the logistic) has been widely employed in PDP models of visual function. Assuming the logistic, performance would degrade gradually and gracefully as a function of noise level. Such predictions are also consistent with Signal Detection Theory (SDT). According to SDT, the neural code is a continuous function (albeit digitized by neurons) of the input. There is no threshold or discontinuity. Although signal detection theory was developed for detection problems, it can be extended to discrimination situation. For this experiment, the observer has to say which of two stimuli was presented on a given trial. This is called a two-alternative forced-chice task in the psychophysical literature.

The efffects of adding noise to an image has been an important research question. As one example, Barber & de la Mahotiere (1982) conducted an experiment which measured the ease with which words, degraded by noise, could be recognized. More specifically, the motivation for this research came from data reported by Thompson & Stoessel (1987). They measured their drop in acuity as a function of viewing the Snellen charts through different dilutions of human blood. Blood from a normal subject was diluted with saline from 1/100 to 1/12,800. A total of seventeen concentrations were prepared. The two opthamologists tried to read the Snellen chart through a 4mm aperture and a cylinder containing the blood solution. Visual acuity was 20/20 when tested through normal saline and all tests with blood dilutions of 1/4,800 or higher. Visual acuity decreased with increasing concentrations of blood between

the dilutions of 1/3,200 and 1/100. At dilutions of 1/400 of less, visual acuity reduced to hand motions. Thus between dilutions of 1/4,800 to 1/400, acuity dropped from 20/20 to hand motions. This "rapid" change in performance through a greater than 10 fold change in concentration suggested that the visual system might be modeled by a median filter. While varyng blood concetration is the most direct way to mimic the density of an intravitreal hemorraghe, it might be possible to model these hemorraghes by varying the level of binary impulsive noise replacing image pixels. This provides more trials per subject and generates a broader base of observers.

Whether using concentrations of blood or implusive noise, it is not possible to distinguish between these two models (threshold and SDT) and operators (median filter and logistic) by simply looking at performance as a function of blodd concentration / noise level. Since there is always some error variance in the data, the performance function would not contain a clear discontinuity at the break point even if the human visual system <u>did</u> use a median filter and/or threshold. Simply looking at the performance function leaves one asking the unanswerable question: "How steep is steep?".

On the other hand, it might be possible to distinguish between the two models if the data were reliable and if a second independent variable (in addition to noise level) were manipulated that made differentiable predictions between the two models. The independent variable chosen for this study was number of possible locations (1, 2, 4, or 16). This variable has an established research history within SDT and the two models make quite different predictions. Burgess (1985(a), 1985(b), Burgess & Colburne (1988), Burgess & Ghandcharian (1984)) has demonstrated the theoretical importance of this variable in signal detection. In order to bracket performance, the distractors used were either blank cells with noise added or hybrids with noise added.

Pilot Experiment

The aim of the pilot experiment was to find a set of stimulus pairs, hybrids, and noise levels that generally produced performance from close to perfect (for 1 alternative and low noise level) to chance (for 15 hybrid distractors and high noise level). Independent noise sample replaced pixel element in the target and distractor locations.

Method

Subjects

Ninety six students from University of Texas at San Antonio participated in the experiment. They were given credit for partial fulfillment of the requirements for their freshman year. Visual acuity in all subjects was normal or corrected to normal.

Design and Procedures

The experiment was conducted in the Psychology lab at the University of Texas at San Antonio. This lab had six rooms and each room had an IBM PC clone with an Intel 286 processor and mother board. All of the rooms were well lighted and partially sound proofed (preventing the subjects from being distracted). The observers were led into the room which contained the computer and were asked to sit on a chair facing the screen. The stimuli were presented at the center of the monitor. Each stimulus display contained one of two pssible targets. Observers were instructed to place their index fingers on the "z" and "/" keys of the keyboard. The two possible targets were always present on the lower left hand and right hand corners of the screen. The "z" key corresponded to the target on the left hand corner of the screen

and the "/" key corresponded to the right hand corner of the screen. For a given stimulus pair, the position of the two possible targets was counterbalanced across observers. After deciding which target was present, the observer pressed the appropriate key. Stimuli were response terminated. Feedback was provided with two different kinds of sounds: a "chirp" for the correct response and a "buzzer" for the incorrect response.

Five independent variables were manipulated in the experiment: (i) stimulus pair, (ii) type of distractor, (iii) percentage of noise pixels, (iv) number of alternative positions/distractors, and (v) location of the target.

Three stimulus pairs were chosen. A particular observer was presented with either two alphabetic stimuli (T and F), a pair of airplanes inclined at 45° and 135° angles, or a pair of horizon angles (45° or 135°). The three sets of stimuli are shown below. T and F show high confusability (Gilmore et al., 1979). The windows containing the stimuli were 16 pixels wide and 18 pixels high including a 4 pixel border. The windows consisted of black pixels (value 0) against a white background (value 255).

Two types of distractors were chosen: blank windows and windows with hybrids. Blank windows were white with noise superimposed on them. Hybrids resembled both the alternatives and were composed of parts of each. The same noise level (but independent samples) replaced pixels in each distractor as in the target. The distractors also were the same size as the target.

Given binary images, impulsive noise involved XORing individual noise elements with image pixels. This is called "salt and pepper", because XORing flips the image pixels: a white pixel becomes black and a black pixel becomes white. The proportion of image elements XORed was independently, but uniformly distributed across each line of the stimulus window. The proportion of pixels XORed can vary betwen 0 and .5. Between .5 and 1, the "noisy" output becomes more recognizable but reverse in binary value. The possible combinations of the first three independent values (each of the three stimulus pairs, hybrids, and noise levels between 0 and .5) are shown in the following figure. Four different levels of
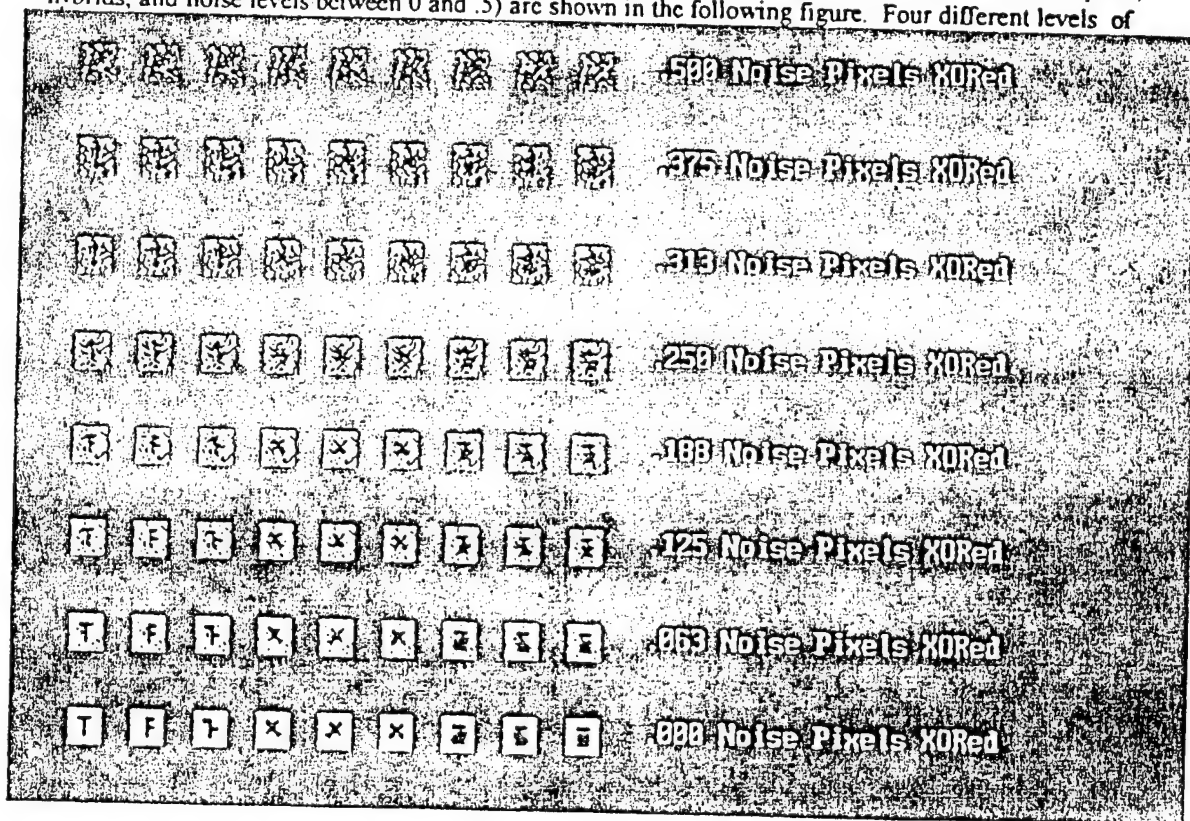
impulsive noise {0.125, 0.188, 0.25, and 0.313} were used in the pilot .

Let the number of windows or possible locations be denoted by the letter "m". Four different values for m were chosen. m= 1, 2, 4, and16. One stimulus was always present, thus the number of distractors was 0, 1, 3, or 15. Sixteen windows were arranged in four rows with each row containing four windows. These locations are numbered as shown below. For m = 1, only one of the windows numbered 0, 3, 12, or 15 was presented on the screen and this window contained the target. For m = 2, two windows

from the following set {(0,15),(3,12),(12,3),(15,0)} were presented and one contained the target, while the other contained a distracter. For m = 4, four windows numbered (0, 3, 12 ,and 15) were displayed on the screen. One of the windows contained a target and the remaining three contained distractors. For m = 16, all sixteen windows were displayed. One of the windows contained a target and the other 15 contained distracters. All possible stimuli are shown below for m= 1, 2, and 4. Only one stimulus is shown for m= 16. For each m size, all of the the stimuli were presented equally often.
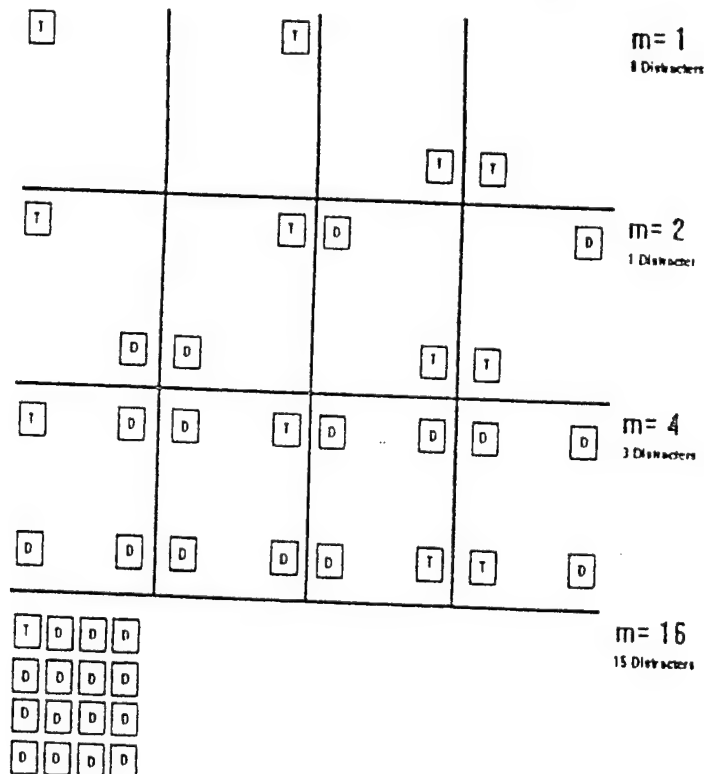
Each observer was given one type of stimuli and one type of distracter. Each was presented with a total of 576 trials broken into 8 blocks consisting of 8 practice trials and 64 test trials. No more than three stimuli of the same kind appeared in a row (ex: T,T,T,F,F,T,............), no more than three noise

levels of same value appeared in a row (ex: 0.125, 0.125, 0.250, 0.188, 0.188, 0.188, 0.125,........), and no more than three trials in a row had the same "m" value. (ex: m=2, m=2, m=2, m=1, m=1, m=4, ...). The alternatives, noise levels and m size, occurred equally often within each block. All locations (crossed with the other independent variables) occurred equally often across the 8 blocks.

Results and Discussion

For each stimulus type, the percentage of correct responses are displayed as a function of type of distracters (blank versus hybrid), noise level (.125, .188, .250. and .313), and m size in the following graphs. While performance generally declined as a function of noise level and m size, the data are noisy. In spite of these imperfections, the pilot study served its function. The two types of distracters, the four noise levels, and four m sizes clearly bracketed performance, On the other hand the data for the horizon angles were lowest and least regular. Consequently, the general design of the blocks and the angle and airplane stimuli were modifed for the main experiment.

Angle Stimuli in Pilot
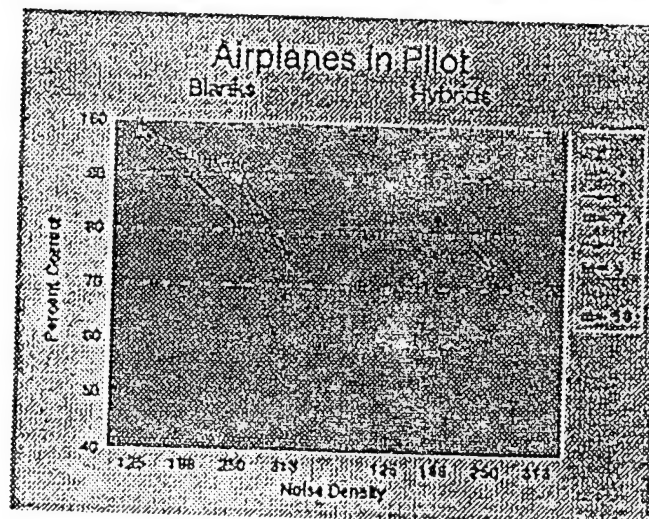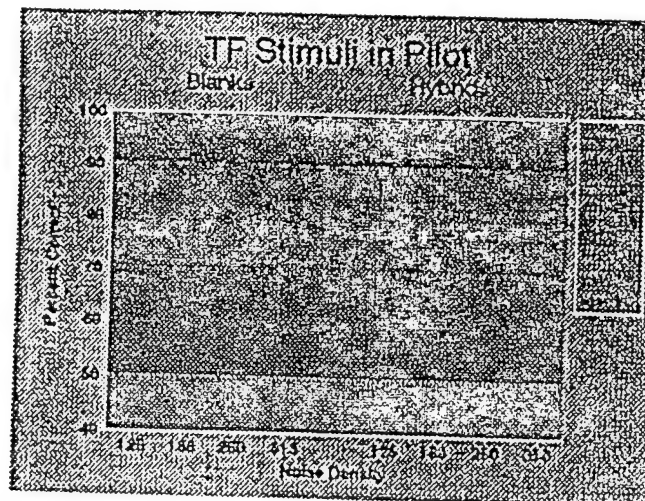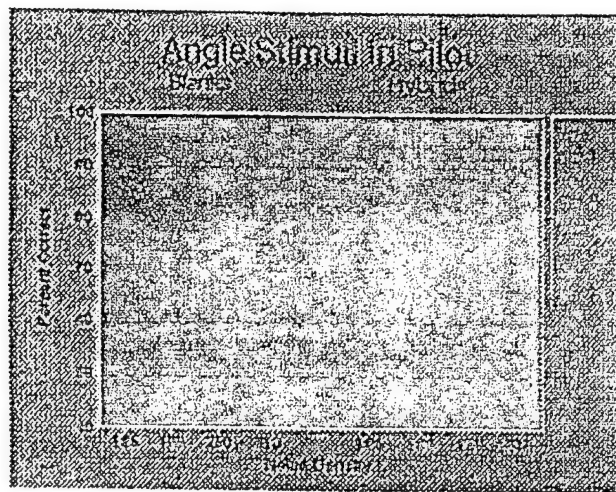
Main Experiment

Method

Design and Procedures

The number of trials in each block of the pilot was too long. The attention span of the subject diminished towards the end of the block. The number of times a target occurred at each location was not sufficient to generate stable data points. Also the rapid changes of m sizes within a block caused the results to be noisy for higher m sizes. These problems were corrected in the main experiment. The number of trials in each block was changed to 48 as opposed to 64 in the pilot in order to better match the attention span of the subject. The number of blocks was increased to 16 (compared to eight blocks in the pilot experiment). Increasing the total number of trials to 768 (compared to 576 in the pilot) provided more trials for each target at each location with each level of noise and m size. This should provide more stable estimates of accuracy. Each block consisted of only one m-size to also increase stability in the data. The order of m sizes across the 16 blocks was counter-balanced using a digram-balanced Latin Square. Each block was preceded by the observer completing two perfect runs of 12 practice trials. These trials were the same m size as in the test trials for that block, but contained no noise. These practice runs were designed to increase the onservers' familiarity with the task and m size.

Results for horizon angles and airplanes were worse than for the T/F stimulus set in the pilot.
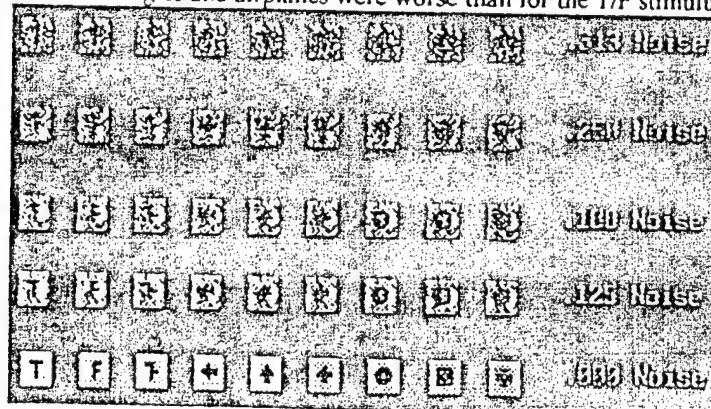
Given the small size of the displays, the angles and airplanes banking at 45 degrees and 135 degrees looked very similar and this caused the lowest accuracy. The planes were shifted to vertical and

143

horizontal in the main study to maximize the use of the pixels available. The horizon angles were changed to geometric figures. These are shown in the figure.

Subjects

One hundred and forty students from the University of Texas at San Antonio participated in the experiment. They were given credit for partial fulfillment of the requirements for their freshman year. Visual acuity in all subjects was normal or corrected to normal. The data for 44 of these observers were discarded due to poor baseline performance or extreme response bias. To be included the observer had to have at least 50% correct responses in the lowest noise condition (.125). No effect of noise could be obtained if the observer was at chance at the lowest level. Secondly the subject had to have at least 20% responses for each target in each condition. Since the targets were equiprobable, a more extreme than 80% / 20% split indicated a very extreme response bias and suggested that the observer may have just repeatedly pressed the same button without attending to the stimuli. All but 5 of the observers dropped were given the airplane targets. The remaining 96 observers consisted of 16 people given each of three stimulus sets by two distractor combinations.

Results

For each subject, the proportion of correct responses was computed for each m size at each noise level. As can be seen in the following figures, the dramatic drops in performance as a function of noise level and m size were more stable than in the pilot. On the other hand, the new airplane stimuli were still very difficult to discriminate (especially from the hybrid distractors). Even for the subjects meeting the criteria listed above, overall performance for the airplanes was low and unstable.
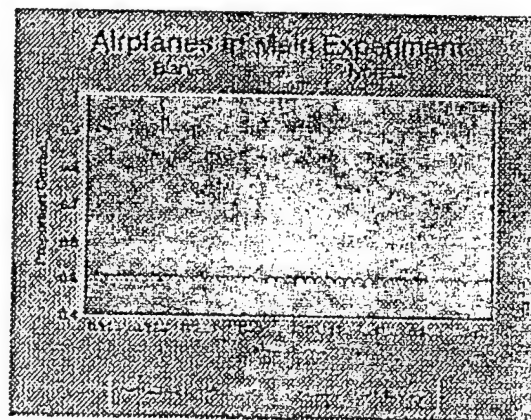
the correct location of the stimulus as a function of m size (d'm). Parallel to the assumptions for the Luce model, it is assumed that the observer knows the location (based on d'm) and is accurate based on stimulus discriminability (d') or thinks another location contains the target (also based on d'm) and guesses at chance (.5 in the 2AFC task). Given the assumption that the SDT distributions are guassian, it is necessary to scale proportion correct. A similar transformation occurs with the logistic. The proportion correct for a given d' and m size can be defined as

$$p(c)_{d_m} = [(p(c)m) * p(c)_{d_1}] + [.5 * (1 - p(c)m)].$$

where

$(p(c)m) \equiv$ the propbability of knowing the target location based on d'm

and

$p(c)_{d_1} \equiv$ the probability of knowing a single target based on d

Accuracy for m= 1 can be used to measure d'. d' and the proportion correct for m= 2 can be used to determine d'm. As with the Luce model, those can then be used to predict accuracy for m= 4 and 16.

The predictions for each model (Luce and SDT) were separately computed for each observer shown each stimulus type (airplane, T/F, and geometric) at each noise level (.125, .188, .250, and .313). As shown in the formulae above, each model (Luce and SDT) uses the data for 1 and 2 locations to predict the data for 4 and 16 locations. It should be noted that as performance in the m= 1 and m= 2 conditions approaches either ceiling or floor, the two predictions of the two models converge toward a common prediction for m= 4 and m= 16. More obviously, as the effect of m size diminishes; the ability to distinguish between the models also diminishes.

The levels of the independent variables were chosen to bracket the whole performance range: performance was close to ceiling with blank distractors & m= 1 and it was close to floor for hybrid distractors & m= 16. There were also differences between the stimuli: overall performance was worst for airplanes, medium for geometric, and best for T/F. The graphs for percent correct as a function of m size and noise level are shown below. Each graph shows the data for a given stimulus pair. Within each graph, the data for the blank distractors observers are shown on the left and the data for the hybrid observers are shown on the right.

Looking across the three graphs, the data for blank hybrids demonstrates an approximately linear drop in performance as a function of noise level. However, the slight differences due to m size are insignificant. Consequently the median filter/Luce model can not be evaluated against the logistic/SDT model for the blanks data.

In spite of the high drop rate for observers in the airplanes stimuli/hybrids condition, performance was still low for the m= 1 and noise= .125 conditions. Further, the functions were quite irregular and unreliable. In contrast, the data for distractors= hybrids were clean for the geometric and T/F targets. The effect of m size was stable and the effect of noise level spanned the range from almost perfect(1.0) to chance (0.50).

For these two targets (geometric/hybrids and TF/hybrids), a 2 (geometric versus TF) X 2 (model= Luce versus SDT) X 4 (noise= .13, .19, .25, or .31) X 2 (m size= 4 or 16) mixed ANOVA was performed to see if the predictions of the Luce or SDT model based on m=1 and 2 better fit the m= 4 and 16 data. Overall, there was no effect of target set ($\underline{F}$<1). As expected, the effects of noise level ($\underline{F}(3,51)$=3.27; $\underline{p}$< .03) and m size ($\underline{F}(1,17)$=6.68; $\underline{p}$< .02) were significant. The predictions of the SDT model approached being significantly closer to the data than the Luce model ($\underline{F}(1,17)$=3.18; $\underline{p}$< .10). It can be seen in the next graphs that the Luce model underpredicts actual performance for the noise level= .250 and .313 conditions. The data provide no hint of a discontinuity at the "break point" in noise level. While the
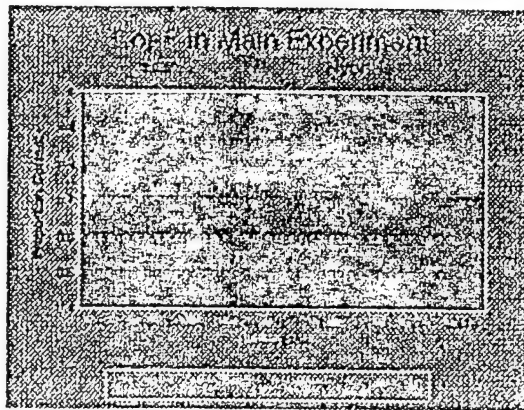
The main goal of the experiment was to find out whether visual performance with impulsive noise is better modeled by a discontinuous function (as predicted by threshold theory and median filters) or by a smooth curve with no break point (as predicted by SDT theory and the logistic). For a given subject (corresponding to a single stimulus and distractor type combination), it is possible to use the data for m= 1 and m= 2 for a given noise level to predict what performance should be found for m= 4 and m= 16 at that noise level. The models make different predictions for those m= 4 and m= 16 conditions.

Luce proposed a model of threshold theory. On a given trial, the stimulus quality is either above or below threshold. In terms of a median filter, the noise level of the image is either above or below the break point. When the stimulus on a given trial is above threshold, the observer is certain and performance will be perfect on that trial. When the stimulus on a given trial is below threshold, the observer will perform randomly (at chance) on that trial. At the threshold (break point), performance should rapidly shift from perfect to chance. For this experiment, Luce's model needs to be extended in order to deal with the distractors. To be sure of the target on a given trial, the target must be above threshold and <u>all</u> of the distractors must be below threshold for the incorrect response. Otherwise the observer must guess. Thus two probablities must be known: p is the probability that the target is above threshold and q is the probability that a distractor is below threshold. For a given noise level, the proportion correct for a given m size can be defined as

$$p(c)m = 1[p * q^{(m-1)}] + .5[1 - (p * q^{(m-1)})]$$

When sure, performance will be perfect (1). Otherwise performance will be at chance (.5 in this 2AFC task). p(c)1 provdies a measure of p (the probability that the target exceeds threshold for a given noise level. Given this estimate of p, p(c)2 can be used to measure q. Thus p(c)1 and p(c)2 can be used to measure p and q and thus predict performance for m= 4 and m= 16.

In contrast to the two-state threshold theory, Green & Swets (1966) proposed SDT. The decision axis is continuous for an interval of uncertainty about wheter or not a signal is present. The representation of both the signal and noise on this decision axis is assumed to be normally distributed with equal standard deviations. Performance is determined by the distance between the means of the signal and noise distributions on the decision axis scaled in standard deviation units. This quantity is called d'. The observer chooses a value on the axis called the criterion. On a trial the stimulus (either signal or noise) will sometimes be represented as a value exceeding the criterion and the observer will respond "signal". Those trials will produce hits and false alarms for signal and noise trials respectively. If the trial value is below criterion, the observer responds "noise" producing misses or correct rejections. For a given noise level, hit rate and false alarm rate can be used to measure d' and the criterion. As with the Luce model discussed above, the SDT model can be extended to deal with the identification task with various m sizes. The criterion is assumed to lead to the target 1 versus target 2 decision as opposed to signal versus noise. Table 1 in Swets (1964) provides a conversion between d' and probability of knowing

TF Hybrid

Geometric Hybrid
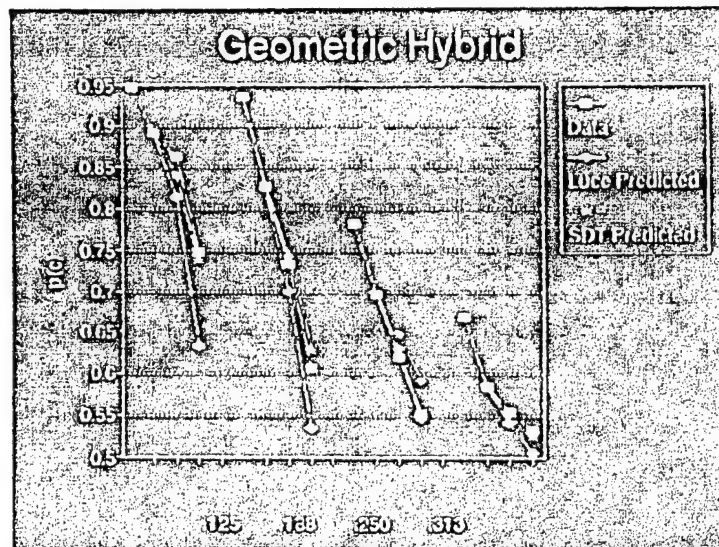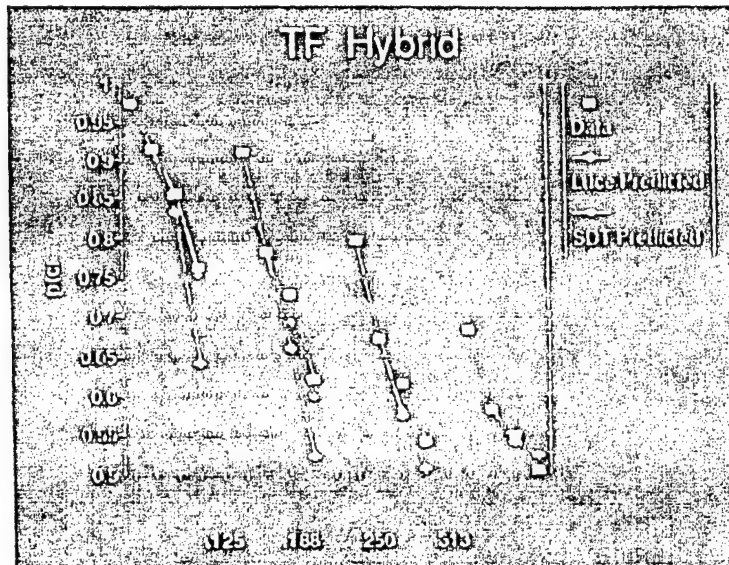
overall drop in performance as a function of noise level is not prescriptive, the relevant data to contrast the models involves the drop in performance as a function of m size. As can be seen in the next two graphs, the data for both noise level= .125 and .188 are better fit by the SDT model than by the Luce model for both the Geometric and T/F stimuli. Statistically, the superior predcitions of the SDT/logistic models (relative to the Luce/median filter models) are revealed in the significant interactions. The advantage of the SDT model over the Luce model interacted with level of noise ($F(3,51)=4.64$; $p< .006$) and m size ($F(1,17)=6.83$; $p< .019$). Finally, the Noise Level X m Size interaction ($F(3,51)=3.02$; $p< .04$) and the model X Noise Level X m Size interaction ($F(3,51)=4.01$; $p< .012$) were significant. For both stimulus types, the advantage of the SDT model was greater at low noise levels than at .313 and was larger for m= 16 than for m= 4.

Discussion

In summary, the use of a median filter in the human visual system predicts a discontinuity at the break point. No such discontinuity was found. The lack of such a discontinuity in such an overly simplistic analysis can be explained away as a result of error variance in the data. That is why m size was

included as an independent variable. Where there is a discriminable difference, these data are better fit by a continuous model (such as the logistic and SDT) than by a discontinuous model (median filter and threshold theory). For these stimuli, the human visual system does not use a median filter.

This conclusion must be qualified by two limitations in these experiments. First, the stimuli were binary, since this was the simplest way to implement impulsive noise. Retinal images are coded in neural firing rate which roughly varies between 0 and several hundred spikes per second. It is possible that the data might have been different if the images had been grey scale rather than binary. Secondly, it is possible that a different type of noise might produce different results. Intravitreal blood might be better modeled by a smoothing operator or by a normal distribution of impulsive noise. Evidence regarding the importance of these two possible limitations awaits future research.

Having stated the potential limitations of this research, it should be noted that the data from these conditions strongly suggest that the human visual system uses a continuous function (albeit digitized) to code retinal illuminance into neural firing rate. Based on PDP modeling, the best assumption is that this translation is adequately fit by the logistic. These data provide no evidence that the human visual system involves a median filter. While a median filter would provide certain image processing advantages, it would be very difficult to implement in a biological system and it predicts a faster drop off in performance as a function of m size than is actually found with binary images.

References

Barber, P. & de la Mahotiere, C. (1982). Ease of identifying words degraded by visual noise. British Journal of Psychology, 371- 381.

Burgess, A.E. (1988a). Effect of quantization noise on visual signal detection in noisy images. Journal of Optical Society of America, 2, 1424-1428.

Burgess, A.E. (1988b). Visual Signal Detection. III. On Bayesian use of prioir knowledge and cross correlation. Journal of Optical Society of America, 2, 1498-1507.

Burgess, A.E. & Colburne, B. (1988). Visual Signal Detection. IV. Observer inconsistency. Journal of Optical Society of America, 5, 617-627.

Burgess, A.E. & Ghandeharian, H. (1984). Visual Signal Detection. II. Signal location identification. Journal of Optical Society of America, 1, 906-910.

Gilmore, G.C., Hersh,H., Caramazza, A., & Griffin, J.. (1979). Multidimensional letter similarity derived from recognition errors, Perception and Psychophysics, 25 ,425-431.

Green, D.M. & Swets, J.A. (1966). Signal Detection Theory and Psychophysics. New York: John Wiley and Sons.

Swets, J.A. (1964). Signal Detection and Recognition by Human Observers. New York: John Wiley and Sons.

Thompson, J.T. & Stoessel, K.M. (1987). An analysis of the effect of intravitreal blood on visual acuity. American Journal of Opthamology, 104, 353- 357.

Reduced Visual Pigment Bleaching in Simulated Retinal Hemorrhage

Melissa A. de la garza
Andrew T.C. Tsin

April 1995

ABSTRACT:

Purpose. Studies were conducted to assess the effects of a simulated retinal hemorrhage on the level of photopigment bleaching in light adapted bovine eyes. Because visual sensitivity relies on photopigments in the retina, and the level of luminance, the effect of retinal hemorrhage on visual sensitivity is influenced by the level of bleached photopigment. Methods. Bovine eyes were obtained from a local purveyor, and dark adapted by storage on ice in a light tight box, for at least one hour. Whole bovine blood was injected into the eyes to occlude an area of the retina just anterior to the central retina, to simulate retinal hemorrhage. Parameters such as exposure time, light intensity, and blood volume, were varied to determine optimal conditions. Exposure for 10 min with a 150W standard light bulb, placed 100 cm away from eyes injected with 1ml of blood, yielded the maximal reduction of bleached photopigment. Following bleaching, retinals were extracted by the formaldehyde method, and the 11-*cis*- and all-*trans*-retinal were analyzed by high performance liquid chromatography (HPLC). Results. Dark adapted control eyes yielded an average of 6% all-*trans*-retinal (i.e. 94% 11-*cis*-retinal, the unbleached pigment chromophore). Light adaptation increased the bleached pigment proportion to about 80%. The addition of blood (to simulate retinal hemorrhage) reduced the bleached photopigment proportion by 5-12%. Conclusions. Simulated retinal hemorrhage resulted in a reduction in the proportion of bleached photopigment in the eye, suggesting that the level of light arriving at the retina is reduced by blood located anterior to the retina. The ability of patients with retinal hemorrhage to detect light due to a combination of reduced bleached pigment (or increased unbleached pigment) and reduced luminance will be explored further.

INTRODUCTION:

Clinical manifestations from a retinal hemorrhage resulting from injury to the eye, such as during laser surgery, would be of concern to many in the medical field. Simulation of retinal hemorrhage, by occlusion of light to an area of the central retina by blood and tissue fluid exudate, would attenuate luminance of photoreceptors. This may result in a decrease in visual sensitivity, or conversely, an increase in the threshold of visual sensitivity. The threshold of visual sensitivity is a log unit measurement, where normal vision has been arbitrarily designated as 1 log unit, (log threshold = 0), and impaired vision is measured in log increment increases up to about 5 log units in rats and 18-20 log units in man (Dowling, 1960, 1963, Dowling & Wald, 1960, and Rushton, 1961b). Visual threshold is defined as the lowest luminance of a flash of light (1/50-second) necessary to evoke a barely measurable electroretinogram (ERG) (Dowling & Wald, 1960). As rhodopsin content decreases, the visual sensitivity threshold increases (Dowling, 1960, 1963, Dowling &Wald, 1960), so that at a log unit of 3.3-3.5 (in rats) only 1-5% of the normal rhodopsin concentration can be extracted (Dowling & Wald). Rushton (1961b) found that in humans, for each 4% of rhodopsin that is bleached, there is a 1 log unit rise in visual threshold. Dowling & Wald (1960) concluded that the increase in visual threshold, could be completely accounted for by the decrease in rhodopsin concentration in rats; however, it has since been found that although there is a correlation, other factors must be considered,(Rushton, 1961a, and Dowling 1960) such as reorganization of nerve synapses (Rushton, 1961a), and instances of photochemical adaptation, where only small amounts of bleaching occur, yet human visual threshold is raised 2-3 log units instead of the projected 0.5 log units (Dowling, 1963).

Visual sensitivity is lowered after light adaptation, and is recovered during dark adaptation (Dowling, 1960, 1963). The dark adapted eye, contains 11-*cis*-retinaldehyde, and when the eye is exposed to light, the retinal chromophore undergoes conformational changes to become all-*trans*-retinaldehyde (retinal) (Bongiorno, 1991). This principle was applied to the present study, where changes in visual sensitivity due to simulated retinal hemorrhage, were assessed by extracting retinals from light adapted, hemorrhaged eyes for HPLC analysis of 11-*cis*- and all-*trans*- retinals.

To date most of this type of work is performed with rats, and, when possible, on humans. Difficulties arise in measurement of visual pigment concentrations in man (Dowling, 1960, 1963, Dowling & Wald, 1960, and Rushton, 1961a&b). Nevertheless, some studies have been conducted, such as the study by Rushton (1961b), with a human monochromat, or cone vision deficient, subject. The study employed retinal densitometry, in which visual pigments in a living eye can be measured (Rushton, 1961a&b). Briefly, rhodopsin density is measured during bleaching and regeneration events, by calculating relative differences in red and green light paths which are displaced by the density of rhodopsin through which the lights are shone (Rushton, 1961a). However, absolute rhodopsin concentrations cannot easily be obtained in humans.

The literature also reflects little data on vitamin A content in bleaching adaptation of bovine eyes (Bongiorno, 1991); however, since this laboratory studies retinoid metabolism in bovine eyes, the present study was conducted to measure changes in visual sensitivity with simulated retinal hemorrhage in bovine eyes. Visual sensitivity can be stated as a function of bleached photopigment in the retina as determined by the following relationship: $\log I/I_0 =$

$3.6[(y-y_o)/y_o]$. where I = threshold of visual sensitivity at different stages of bleaching (Dowling, 1960, Rushton, 1961a). In the present study, we took y_o and y to represent rhodopsin content in light adapted bovine retina in the presence and absence of exogenous blood, respectively. Retinal hemorrhage was simulated by injection of a small volume of blood into the area just anterior to the retina of the enucleated bovine eyes. Parameters were then varied to optimize conditions.

METHODS:

The present study was conducted in order that the relationship between photopigment concentration and simulated retinal hemorrhage could be assessed. Fresh bovine eyes were obtained from a local purveyor and transported to the laboratory on ice in a light tight box, thereby inducing the dark adapted state. A total of 15 bovine eyes were used in the present study. Retinal hemorrhage was simulated by the injection of whole bovine blood (100 μl, 500 μl, and 1 ml) directly in front of the central retina. The eyes were then exposed to standard white light, either 150 or 75 watts, 50 or 100 cm away. Exposure time was varied between 5, 10, and 20 min. The maximal effect was seen at 10 min of exposure with 150 watts, 100 cm away from eyes injected with 1 ml of blood. Degree of dark adaption was checked by injecting some eyes with blood but not exposing them to light, rather they were processed completely under dim red light. Each retina was dissected under appropriate lighting conditions and retinaldehydes were isolated via formaldehyde extraction (Suzuki, 1986). Retinas were homogenized, glass/teflon, with 4ml of 0.1M phosphate buffer, pH 6.8, and incubated for 5 min. Two milliliters of 37% formaldehyde was added, the mixture vortexed, and incubated at

room temperature for 5 min. Then 2ml of isopropyl alcohol was added, vortexed, and incubated at room temperature for 5 min. Eight milliliters of distilled water and 12ml of n-hexane were then added. Tubes were vigorously shaken and centrifuged at 2000 rpm, for 5 min, at 4°C. The hexane extraction was repeated twice and extracts were combined, evaporated with nitrogen, and resuspended in 1ml of n-hexane. Retinaldehydes from each sample were eluted from an alumina column with 10ml 3% D/H. This fraction was dried with nitrogen, and samples collected early in the study were resuspended in 100μl of 3% D/H, and 40μl were injected into a Beckman HPLC (25cm, 5μm, microsorb silica column, flow rate 2 ml/min, mobile phase 3% D/H). Samples collected later were resuspended in 500μl of 3% D/H and 200μl from that were injected through a Beckman 502 Autosampler into a Beckman HPLC with a photo diode array detector. Because samples were analyzed by two different methods using two separate calibration curves, percent differences in all-*trans*-retinaldehyde described in each table, were reported as differences in peak area and not molar concentration.

RESULTS:

The first set of experiments were conducted to assess the effects of exogenous blood on the retina and to establish the light adaptation procedure. Bovine eyes were injected with 100μl, 500μl and 1ml of bovine blood, and 1ml was found to give the best results (data not shown). Thus all simulated retinal hemorrhages were conducted with 1ml of blood. Percentages of bleached rhodopsin (all-*trans*-retinal) following blood injection and light adaptation were then assessed.

Differences in all-*trans*-retinal (AT-al) between dark adapted eyes and those exposed to

a 150W standard white light for 10 min were determined quantitatively. Retinas extracted from dark adapted eyes contained very little AT-al (see Fig. 1), whereas the light adapted retina contained predominantly AT-al (see Fig. 2). Once it was determined that the dark and light adaptation procedures yielded expected results, the effects of exogenous blood on bleached rhodopsin content were tested. Light adaptation in the presence of blood had a bleached rhodopsin content which was slightly less than that of the light adapted control eyes (see Fig. 2 & 3). Changes in rhodopsin content simply due to the presence of blood in a dark adapted eye were also tested. This treatment had the effect of increasing very slightly the AT-al content.

Subsequent experiments were conducted in order to optimize the bleaching conditions. Extracted retinaldehydes were injected into HPLC and analyzed quantitatively. Results from these experiments were reported in molar concentration of AT-al (bleached rhodopsin) relative to 11-c-al (unbleached rhodopsin). Table I shows the results of dark adapted eyes with exogenous blood injected. They were exposed to 150W of standard white light at a distance of 50 cm, for 5 and 10 minutes. Five minutes of exposure time did not seem adequate to significantly bleach the photopigment, for the difference in bleached rhodopsin in experimental eyes (Table I, column II) from control eyes (Table I, column I) was only a 9% decrease. However, when the eyes were exposed to 150W of light for 10 minutes this difference increased to 22%. A third treatment was also attempted (data not shown) where the eyes were exposed for 20 min. However, the tissue was presumably damaged from the heat-producing light, because the retina had deteriorated so that it was difficult to extract, hence retinal content could not be assessed.

Table II shows the results of experiments where bovine eyes were exposed to either

155

150W of standard white light 100 cm away, or 75W of standard white light 50 cm away, for 10 min. The light-adapted, hemorrhaged eye (Table II, column II) that was exposed to 150W @ 100 cm away, had 12% less bleached rhodopsin than did the light adapted control eye (Table II, column I). The light-adapted, hemorrhaged eye (Table II, column II) exposed to 75W @ 50 cm away only had a 5% difference in AT-al when compared to its control (Table II, column I). This suggests that the first treatment in this series of experiments offered a pathlength that was able to preserve more of the 11-cis, or unbleached, form of the photopigment.

Results of these studies taken together indicate that a bovine eyes injected with 1ml of blood, and exposed to 150W of white light, 50 cm away, for 10 min had the effect of inducing the greatest difference in bleached rhodopsin, when compared to eyes without retinal hemorrhage. In other words, these conditions preserve the greatest amount of photoreceptor, thus have the effect of increasing visual sensitivity.

DISCUSSION:

The present study was conducted to assess the effects of exogenous whole bovine blood in dark- and light-adapted bovine eyes, as a simulation of retinal hemorrhage. It has been well established that visual sensitivity is a function of photopigment concentration in the retina (Dowling 1960, Rushton 1961). We adapted the Rushton-Dowling equation for measuring threshold of visual sensitivity in our study: $\log I/I_o = 3.6[(y\text{-}y_o)/y_o]$. Where I = threshold of visual sensitivity at different stages of bleaching, and y_o and y = light adapted bovine retina in the presence and absence of exogenous blood, respectively. We found that our protocols for light and dark adaption were optimal at exposure for 10 min with a 150W standard white light,

placed 50 cm away from eyes injected with 1 ml of whole bovine blood (22% difference, Table I). Such treatments resulted in a significant reduction in bleaching of photopigment in the retina.

In the first set of experiments, we were able to establish a baseline dark adapted control, this sample contained only a small percentage of all-*trans*-retinaldehyde. The light adapted sample of this study had a significantly higher all-*trans*-retinaldehyde content, which was decreased slightly by the addition of 1 ml of blood (see Fig. I, II, & III). By repeating the experiments under different conditions, we were able to increase this difference in bleached rhodopsin to 22% (Table I and II). The studies reported in Table II included another group that was exposed for 20 min; however, there was an actual increase in AT-al content in eyes injected with blood. This negative result might be attributable to the effects of this more harsh treatment. The light produced much heat, which combined with the presence of exogenous blood appears to cause a more rapid degradation of tissues. The retina became unattached to the eye cup, and part of it discarded with the vitreous humor, making it impossible to fully extract retinals from the retina.

Using the Rushton-Dowling equation, we calculated that treatment under optimal experimental conditions induced a decrease in visual sensitivity threshold by 0.8 log units (or a 7.1 times increase in visual sensitivity).

A sample calculation using the Rushton-Dowling equation, is shown below.

$$\log I/I_o = 3.6[(y-y_o)/y_o]$$

$$\log I/I_o = 3.6[(0.93-0.71)/0.93]$$

$$\log I/I_o = 0.8516129 \cong 0.8$$

According to this equation, the threshold of visual sensitivity has decreased by a factor of 0.8

log units.

Results of the present study indicate that the addition of exogenous blood to the central retina of the eye also resulted in a decrease in light luminance at the level of the retina based on reduced bleaching of photopigment. However, the Rushton-Dowling equation suggested a compensatory increase in visual sensitivity based on an increase in the amount of unbleached pigment. Thus the net effects of reduced luminance and increased sensitivity determines the visual perception (such as contrast sensitivity function) of an individual.

Some experiments have been perform on humans, to determine how simulated retinal hemorrhage affects Contrast Sensitivity Function (CSF). Seventeen dilutions of blood were added to a chamber, placed in front of the eyes. Subjects were asked to identify the clarity with which they could discriminate objects at the various blood concentrations (Thompson & Stoessel, 1987). In this study, 12.5 μl of whole blood was enough to reduce visual acuity to mere hand motions. Using a Snellen acuity chart, 20/20 vision was only achieved with 1.40 μl of blood or less.

Theoretically, these experiments could also be conducted in patients who have retinal hemorrhages due to some natural causes, or by injury. In certain instances, where retinal hemorrhage only occurs in one eye, the other eye could be used as a control. Obviously, their retinas cannot be extracted (unless the injury is sufficiently serious to warrant enucleation) therefore, maybe the rhodopsin content can be assessed with a retinal densitometer, as described in the 1961(a) Rushton paper. Future studies regarding measurement of contrast sensitivity function and light scattering due to retinal hemorrhage, will provide more data in explanation of the effects of retinal hemorrhage on visual perception.

REFERENCES:

Bongiorno, A., Tesoriere, L., Livrea, M.A., and Pandolfo, L. (1991) Distribution of Vitamin A Compounds in Bovine Eyes After Bleaching Adaptation. *Vision Res.* 31(7/8): 1099-1106.

Dowling, J.E., and Wald, G. (1960) The Biological Function of Vitamin A Acid. *Proc. of the Natl. Acad. of Sci.* 46(5): 587-608.

Dowling, J.E. (1960) Chemistry of Visual Adaptation in the Rat. *Nature* 188: 114-118.

Dowling, J.,E. (1963) Neural and Photochemical Mechanisms of Visual Adaptation in the Rat. *J. Gen. Physiol.* 46: 1287-1301.

Rushton, W.A.H. (1961a) Dark-Adaptation and the Regeneration of Rhodopsin. *J. Physiol.* 156: 166-178.

Rushton, W.A.H. (1961b) Rhodopsin Measurement and Dark-Adaptation in a Subject Deficient in Cone Vision. *J. Physiol.* 156: 193-205.

Suzuki, T., Fujita, Y., Noda, Y., and Miyata, S. (1986) A Simple Procedure for the Extraction of the Native Chromophore of Visual Pigments: The Formaldehyde Method. *Vision Res.* 26 (2): 425-429.

Thompson, J.T., and Stoessel, K.M. (1987) An Analysis of the Effects of Intravitreal Blood on Visual Acuity. *Am. J. Ophthal.* 104: 353-357.

FIGURE I
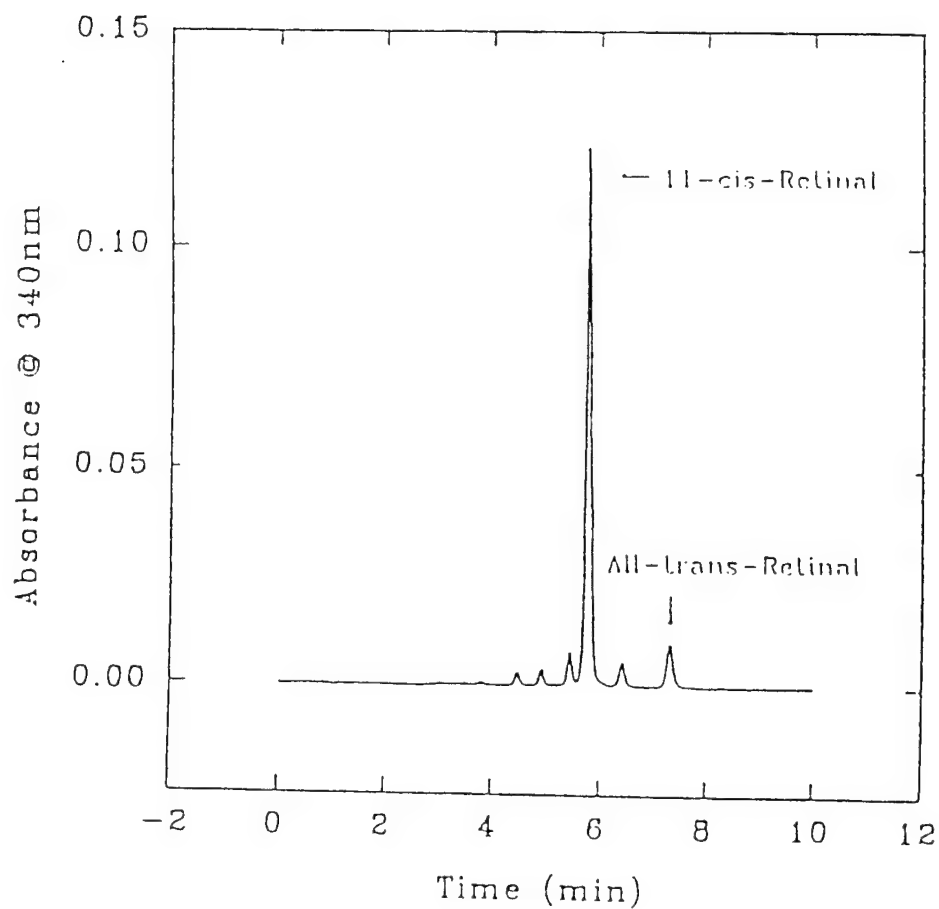
FIGURE I: Chromatographic analysis of retinaldehydes from a dark adapted bovine eye. Retention times for 11-*cis*- and all-*trans*-retinaldehyde, 5.77 min and 7.32 min, respectively. See methods for HPLC conditions.
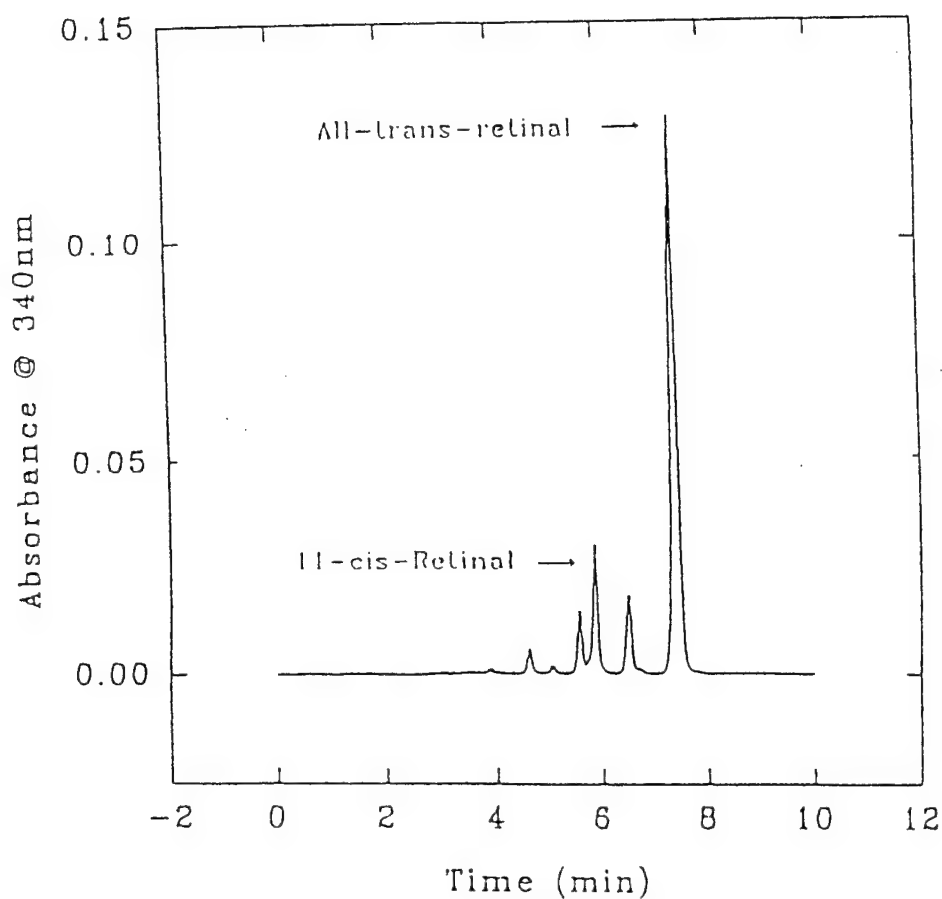
FIGURE II

FIGURE II: Chromatographic analysis of retinaldehydes from a light adapted bovine eye. Retention times for 11-*cis*- and all-*trans*- retinaldehyde, 5.86 min and 7.41 min, respectively. See methods for HPLC conditions.

FIGURE III
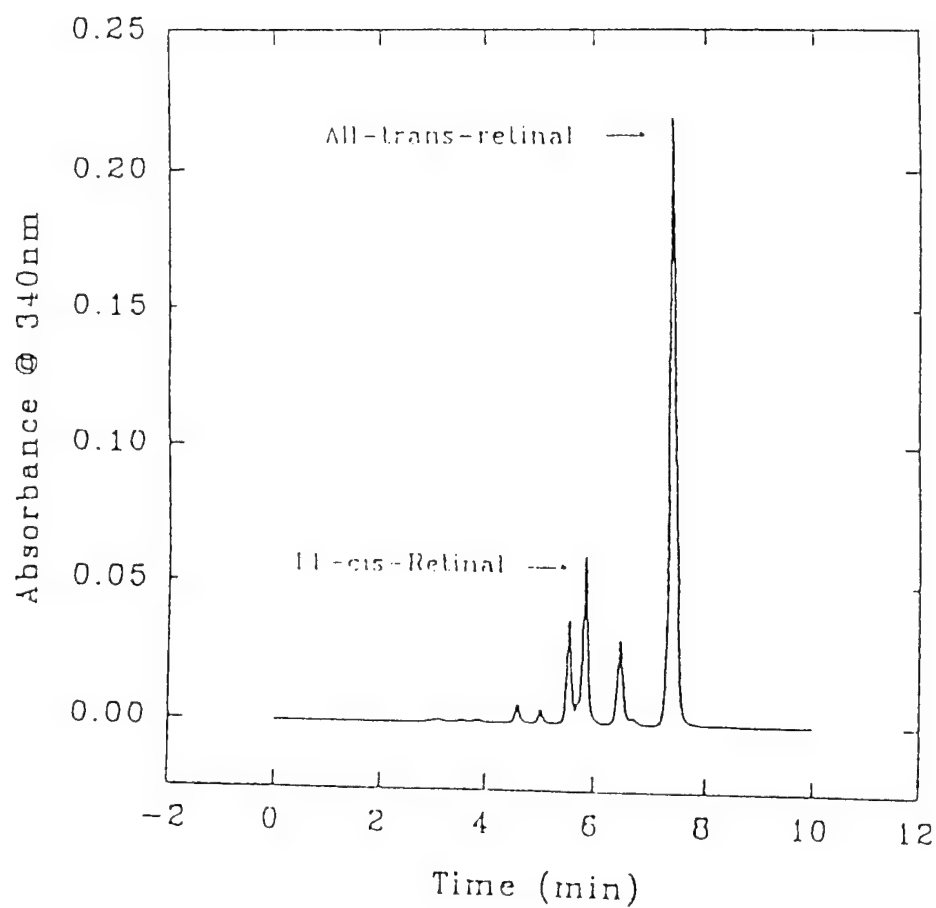
FIGURE III: Chromatographic analysis of retinaldehydes from a light adapted bovine eye, injected with 1 ml of whole bovine blood. Retention times for 11-*cis*- and all-*trans*-retinaldehydes, 5.84 min and 7.40 min, respectively. See methods for HPLC conditions.

TABLE I
Percentages of Bleached Rhodopsin
(All-*trans*-Retinaldehyde)
from Eyes Light Adapted for 5 and 10 min

Time	Light Adapted Without Blood (I)	Light Adapted With Blood (II)	% Difference
5 min:	77%	68%	9
10 min:	93%	71%	22

The table shows differences in relative picomolar concentrations between 11-*cis*-and all-*trans*-retinal when dark adapted bovine eyes were exposed to 150 watts of white light placed 50 cm away for 5 and 10 min. Experimental eyes received 1 ml of whole bovine blood. The 10 min exposure time with 1 ml of blood, allowed for the least amount of bleaching, thus blocking the most light from the retina. Retinals were processed as described in Methods, and analyzed by HPLC (25cm, 5μm microsorb column, flow rate 2ml/min, mobile phase 3% D/H) with a Beckman Autosampler.

TABLE II
Percentages of Bleached Rhodopsin
(All-*trans*-Retinaldehyde)
at Two Different Pathlengths

Pathlength	Light Adapted Without Blood (I)	Light Adapted With Blood (II)	% Difference
150W @ 100 cm:	82%	70%	12
75W @ 50cm:	82%	87%	5

Studies were conducted with variation of pathlength. The table shows the difference in relative peak areas between 11-cis- and all-trans-retinal when dark adapted bovine eyes were exposed to either 150W of standard white light 100 cm away, or 75W of standard white light 50 cm away, for 10 min. In this study, the first condition allowed for the greatest reduction in bleached pigment upon light adaptation, thus blocking more light from arriving at the retina. Retinals were extracted as described in Methods, and analyzed by HPLC (25cm, 5μm microsorb column, flow rate 2ml/min, mobile phase 3% D/H) using a Beckman Autosampler.

615 — 523

PAX 3 TRANSCRIPTION FACTOR BINDS TO HYALURONAN
((P.A. Knepper, C.S.K. Mavarui, R.W. Byrne, and W. Goossens))
Laboratory for Oculo-Cerebrospinal Investigation, Northwestern University
Med School, Chicago, IL

Purpose. Hyaluronan (HA) is known to influence important cellular events in
ocular development such as cell locomotion and differentiation. To explore the
possibility that certain transcription factors bind to HA, we used an HA affinity
column to isolate HA-binding proteins. Methods. Incubation day 3 to 7 chick
embryos were prepared as a whole homogenate in 0.32 M sucrose or as an
aspirate of vesicular fluid from the mesencephalon; both preparations were
centrifuged to remove nuclear debris; and the supernatants were applied to a
EAH-Sepharose-HA-affinity columns. The HA-bound proteins were eluted
fractionated by SDS polyacrylamide gel electrophoresis, transferred to
Immobilon P, and immunoblotted with a series of monoclonal and polyclonal
antibodies directed against transcription factors. Results. Notably, numerous
HA-binding proteins were immunopositive with the anti-transcription factor
antibodies. The immunoblot of an anti-PAX 3 antibody, directed against the
paired homeodomain of pax-3, suggested that PAX 3 transcription factor binds
to HA, and also that the expression of PAX 3 was developmentally regulated.
The reported amino acid sequence of pax-3 and CD44, the HA receptor, were
compared. A shared motif was a nine amino acid peptide stretch containing
three basic amino acids and no acidic amino acids. Conclusions. The results
indicate that certain transcription factors bind to HA. This binding may
indicate that HA serves a role as a carrier of transcription factors to coordinate
cellular activity in a paracrine-like fashion. Supported by National Children's
Eye Care Foundation and The Glaucoma Foundation.   none

616 — 524

Reduced Visual Pigment Bleaching in Simulated Retinal Hemorrhage. ((Melissa A.
de la Garza, Andrew T.C. Tsin, Harold G. Longbotham, Nathan L. Mata, Yolanda R.
Moreno, Shahed Ziari, Wally R. de la Garza, and Jennifer A. Ray)) Division of Life
Sciences, The University of Texas at San Antonio, San Antonio, Texas 78249

Purpose. Studies were conducted to assess the effects of a simulated retinal hemorrhage on
the level of photopigment bleaching in light adapted bovine eyes. Because visual sensitivity
relies on photopigments in the retina, and the level of luminance, the effect of retinal
hemorrhage on visual sensitivity is influenced by the level of bleached photopigment.
Methods. Bovine eyes were obtained from a local purveyor, and dark adapted by storage on
ice in a light tight box, for at least one hour. Whole bovine blood was injected into the eyes
to occlude an area of the retina just superior to the fovea, to simulate retinal hemorrhage.
Parameters such as exposure time, light intensity, and blood volume, were varied to determine
optimal conditions. Exposure for 10 min with a 150W standard light bulb, placed 100 cm
away from eyes injected with 1ml of blood, yielded the maximal reduction of bleached
photopigment. Following bleaching, retinals were extracted by the formaldehyde method, and
the 11-cis- and all-trans-retinal were analyzed by high performance liquid chromatography
(HPLC). Results. Dark adapted control eyes yielded an average of 6% all-trans-retinal (i.e.
94% 11-cis-retinal, the unbleached pigment chromophore). Light adaptation increased the
bleached pigment proportion to about 80%. The addition of blood (to simulate retinal
hemorrhage) reduced the bleached photopigment proportion by 5-12%. Conclusions.
Simulated retinal hemorrhage resulted in a reduction in the proportion of bleached
photopigment in the eye, suggesting that the level of light arriving at the retina is reduced by
blood located anterior to the retina. The ability of patients with retinal hemorrhage to detect
light due to a combination of reduced bleached pigment (or increased unbleached pigment) and
reduced luminance will be explored further. This research was supported by grants from The
NIH, Concerted Manufactures Inc. under contract # F41624-93-C-9015 @ Brooks AFB, and
The San Antonio Area Foundation. None

617 — 525

AMILORIDE-SENSITIVE Na+ CHANNEL IN RAT EYE TISSUES
((R. V Paul, I. Saito, and M. B. Wax)) Department of Ophthalmology and Visual
Sciences, Washington University Medical School, St. Louis, MO

Purpose. Amiloride-sensitive Na+ channels have an important role in sodium and
water homeostasis. They are present in epithelial cells of kidney, lung, colon etc.,
and also in blood-brain-barrier endothelial cells. Recently, complementary DNAs
encoding amiloride-sensitive Na+ channels have been cloned and characterized
from rat colon. We sought to determine the localization of this Na+ channel in rat
eye tissues. Methods. The cornea, lens, ciliary body, retina were isolated from
inbred male Lewis rats. Total RNA was isolated by a single-step extraction
method, using RNAzol B. The isolated RNA was reverse-transcribed by MuLV
reverse transcriptase, using random hexamers as a primer. The sense and antisense
primers were designed corresponding to the nucleotide sequence of alpha subunit
of rat amiloride-sensitive Na+ channel, resulting in a 633-bp DNA fragment. PCR
amplification was performed using an automated thermal cycler. PCR product of
rat glyceraldehyde 3-phosphate dehydrogenase was used as an internal control in
RNA-PCR. PCR products obtained after 35 cycles were separated by agarose gel
electrophoresis, purified and subjected to restriction endonuclease digestion.
Results. DNA fragment of 640-bp, corresponding to the expected size of the
amplified portion of this channel gene, was obtained from the cornea, lens ciliary
body, and retina. Further, the restriction map for this fragment was identical to the
known restriction map of this channel. Conclusion. These results indicate the
existence of this channel in the various ocular tissues of rat. DNA sequencing is
currently underway to further confirm these findings. Additional experiments
such as in situ hybridization will be carried out to determine the detailed
localization of this channel in ocular tissues

618 — 526

PROTECTION OF ACTIVITY DECREASE OF PHOSPHATE-ACTIVATED GLUTA-
MINASE BY PHOSPHOLIPIDS IN ISCHEMIC/REPERFUSED RAT RETINAS ((A.
Arakawa,[1] S.Ishiguro,[1] H.Watanabe,[1] H.Tomita,[1] K.Ohki,[2] and M.Tamai,[1])) Depart-
ment of Ophthalmology, School of Medicine[1]; Department of Physics, Graduate School
of Science[2],Tohoku University.

Purpose. Phosphate-activated glutaminase(PAG) activity decreases in the ischemic rat
retinas(Watanabe et al.ARVO 1994). Recently we found that phosphatidylcholine itself
protected the decrease of PAG activity during our experiment using liposomes. We have
investigated whether supply of various phospholipids to ischemic/reperfused retinas pro-
tects the decrease of PAG activity. Methods. The blood flow of central retinal artery of
SD rats was stopped for 90 minutes. The phospholipids were injected into the vitreous
before or after this ischemia. Injected phospholipids were all 5.7 nmoles in 3 μl Tris-
buffered saline. After 72 hours of reperfusion, the retinas were homogenized and dia-
lyzed against distilled water, then PAG activity of the homogenate was measured by am-
monia production. The assayed samples were as follows: 1) intact retinas; 2) ischemic re-
tinas; 3) phosphatidylcholine(PC)-injected retinas before ischemia; 4) phosphatidylserine
(PS)-injected retinas before ischemia; 5) phosphatidylethanolamine(PE)-injected retinas
before ischemia; 6) PC-injected retinas after 20 minute-reperfusion. Results. PAG ac-
tivity decreased markedly in the ischemic/reperfused rat retinas as previously reported
(group 1 and 2, p<0.001). PC and PS had protective effects on the decrease of PAG ac-
tivity(group 2 and 3, p<0.01, group 2 and 4, p<0.01),whereas PE did not. In addition,
PC recovered PAG activity even if administered after ischemia/20 minute-reperfusion
(group 2 and 6, p<0.01). Conclusion. PC and PS specifically protected the decrease
of PAG activity when injected into vitreous before retinal ischemia.

None

619 — 527

CHANGE OF LOW-AFFINITY NGF RECEPTOR EXPRESSION IN THE
ISCHEMIC RAT RETINAS ((H Tomita,T.Abe,S.Ishiguro,and M. Tamai))
Department of Ophthalmology,Tohoku University,School of Medicine, Sendai ,
Japan.

Purpose. It has been reported that the cell surface nerve growth factor (NGF)
receptor has two types, high affinity receptor (trk A) and low affinity NGF
receptor(p75^{NGFR}). NGF itself has protective effects on rat retinas from ischemic
injury and the effects are generated through trkA . p75^{NGFR} has revealed to increase
the affinity of trk A for NGF and reported the induction of apoptosis in PC12 cells
when NGF was unbound. We investigated the expression of p75^{NGFR} in ischemic
rat retinas to understand a functional role of p75^{NGFR} in ischemia. Methods. The
optic nerves of the left eyes were clamped for 90 minutes for ischemia to make
ischemic retinas. Sham operation was performed on contralateral eyes. The eyes
were enucleated after reperfusion at 0, 1.5, 3, 6 and 72 hours for the RNA
preparation. First strand cDNA was synthesized from 1.5mg of the total RNA by
using random hexamer . PCR reaction was performed on p75^{NGFR} and
glyceraldehyde-3-phosphate dehydrogenase (G3PDH) as a control by each specific
primer sets.The PCR products were always in the linear range of concentration
curve. An aliquot of each product was separated on 2% agarose gel and
photographed.The band of this image was calibrated optical density by NIH Image.
The corrected density of p75^{NGFR} receptor was normalized to G3PDH for each
PCR run. Result. p75^{NGFR} showed no differences between ischemic and
contralateral retinas right after reperfusion. Three hours after reperfusion, p75^{NGFR}
was decreased in both retinas. On the otherhand , p75^{NGFR} was significantly
increased in ischemic retinas 72 hours after reperfusion . Conclusion. Our
results suggested that p75^{NGFR} may play an important role in recovering from
ischemic retinal damage .

None

620 — 528

BLOOD-RETINAL BARRIER BREAKDOWN IN THE RCS RAT RETINA AFTER
PHOTOCOAGULATION STUDIED BY IMMUNOCYTOCHEMISTRY FOR IgG
((Y Chu, M.F. Humphrey and Constable, I.J.)) Centre for Ophthalmology and
Visual Science, Lions Eye Institute, Perth, Western Australia.

Purpose. To examined the distribution of immunoglobulins-immunoreactivity (IgG-
IR) following argon laser photocoagulation in the RCS rat. Methods. The superior
retina was irradiated with a grid pattern of 40 argon laser lesions of 50 um diameter
and 120 mW. Frozen sections of RCS rat eyes were cut at various times after laser
lesion and processed for IgG immunoreactivity using a one step technique by
incubating with rabbit anti-rat immunoglobulins conjugated directly to horseradish
peroxidase. Results. In both RCS and RCS-rdy+p+ rat retinas, at 6, 12 and 24 hrs
after lesions, IgG-IR was very intense in the lesions and flanks. The outer plexiform
layer and photoreceptor inner segments (IS) provided a ready pathway for lateral
spread of IgG. In the outer nuclear layer (ONL), however, the IgG was much more
restricted. Despite very intense IgG-IR in the ONL of the coagulated lesion core
there was always a very sharply delineated boundary where the label abruptly halted.
The GFAP labelling showed that this boundary was between healthy and dead cells
as there was a core where GFAP was not produced by Müller cells. By 2 days after
lesions, the coagulated cells in the lesion core were being removed by phagocytic
cells which were IgG-IR. Labelled phagocyte cells were also found among the IS
and OS on the lesion flanks. There was still IgG-IR in the lesion but the label was
weaker. No IgG-IR was found in the retina at 3, 4, 7 and 14 days. Conclusions.
The IgG was derived from the choroidal circulation because at no stage was IgG
localised around the retinal vasculature. The IgG labelling was surprisingly wide
spread and therefore did not correlate with photoreceptor rescue, although it
preceded the widespread Müller cell expression of GFAP and may therefore trigger
glial reactions. None

The Effect of Disease on Signal Processing
Characteristics of the Human Visual Systems

FINAL REPORT

Dmitry Gokhman
April 29, 1995

My work on this project included a background study of the visual system with all co-pi's,
theoretical work and preparations for an experimental study of signal decomposition in
the eye with Dr. Jim Dykes, and a preliminary investigation of available approaches to
the problem of scattering in the eye due to occlusions.

Background:

During the initial stages of the project the team made a literature search and conducted
a background study of the visual system. We had a seminar series and carefully went
through 'Spatial Vision' by R.L. De Valois and K.K. De Valois.

Signal decomposition:

I and Dr. Jim Dykes began work on the problem of signal decomposition in the visual
system. Our goal was to select a decomposition model for eventual incorporation into
ILPEM. The model would be chosen according to good agreement with experimental
data and computational facility.

We designed experiments to test hypotheses related to what kind of decomposition
occurs in the visual system. The experiments use a masking technique with patterns.
The patterns are designed so that depending on the kind of decomposition that takes
place, some would be recognized with greater facility by the subjects than others.

The kinds of decomposition that we wanted to compare were Fourier decomposition
and wavelet decomposition into various wavelet sets, e.g. Gabor wavelets, Daubechies
wavelets, B-spline wavelets etc.

We started by preparing a pattern display software for the running of subjects. Also we
manually generated several patterns to test the display.

We wrote software for faster and more systematic generation of patterns (PTRGEN)
and, as the first step, generated patterns to differentiate Fourier decomposition from

a Haar wavelet decomposition. We decomposed patterns into Fourier components as well as into wavelet components with respect to two orthogonal bases: D2 (Haar) and D4 (Daubechies). We selected pairs of patterns with similar Fourier content, yet very different wavelet coefficients.

We began work on incorporating Fourier decomposition into pattern generation software and adding wavelet decomposition with respect to various bases. The idea was to make it easier to generate patterns for testing that would distinguish various wavelet bases — a more subtle task than Fourier versus wavelet. In addition, we started looking into decomposition with respect to nonorthogonal bases. Concurrently we were making preparations to start the running of subjects.

After discussions at the September 2, 1994 meeting of the whole group and consultants at CMI it was decided to halt work on these experiments. In particular, Dr. Randy Glickman said that Fourier decomposition has been abandoned by most researchers in favor of wavelet decomposition. Further, we got the impression from him that it is of little consequence as to what kind of wavelet basis is appropriate.

Scattering:

After it was decided to abandon the signal decomposition project I started looking into the problem of scattering in the eye due to occlusions. This was not an area of expertise for me, so I looked into the theoretical literature on the subject and consulted with several people more knowledgeable in the field.

In November 1994 I attended several talks on scattering at the 23rd Midwest Differential Equations Conference at the University of Oklahoma, Norman. One of the talks was by Dr. Klibanov (UNC Charlotte) with whom I had a lengthy discussion. On December 2, 1994 I attended a lecture by Dr. Tom Roberts (Brooks AFB) 'Direct & Inverse Scattering for a Hyperbolic System of Integro-PDEs'. With Dr. Roberts' kind assistance I compiled a list of available MIE software for scattering in a sphere. On December 19, 1994 I attended a meeting with Dr. Ray Applegate (UTHSCSA) were we discussed occlusions in eye.

Deliverable items:

- ☐ Pattern generation software PTRGEN in Perl.
- ☐ Lists of available software for Fourier and wavelet decomposition and scattering.
- ☐ Bibliography reference lists on Fourier and wavelet decomposition, and scattering.

Conclusions:

☐ I am not completely convinced that it is not of consequence as to what type of decomposition occurs in the visual system. While it is generally accepted that some sort of wavelet decomposition is taking place, the guess as to what type of basis is involved is largely a matter of empirical matching of basis functions to CRF curves. Many researches choose the Gabor wavelet for this reason. However, for computer modeling it may be advantageous to select a basis with better computational aspects which acceptably matches experimental data.

☐ The ability to compute scattering in the eye due to occlusions is obviously of great importance to modeling the effects of disease or injury on vision. This is a nontrivial undertaking considering that scattering is a vast area of research. My own expertise in this area is limited to numerical algorithms that are often used to compute scattering, such as the finite element method. I would say that work on this project would require significant participation of a specialist in scattering.

Appendix IV

VEP Data Collection Effort

Title: Retinal variation of acuity mapped by the visual evoked potential
Final Report: SBIR Contract F41624-93-9015
To: Conceptual MindWorks, Inc.
               4318 Woodcock, Suite 210
               San Antonio, TX 78228-1316
Date: 29 Sept., 1995

Introduction

The visual evoked potential (VEP) has been used as an objective measure of visual functional parameters such as visual acuity and contrast sensitivity (Tyler et al., 1979; Nelson et al., 1984; DeBruyn et al., 1986; Glickman et al., 1991). Accordingly, the interaction between the VEP and the actual viewing or stimulus conditions has been examined in numerous studies. For example, contrast sensitivity measured by the lowest contrast producing a detectable VEP agreed closely with psychophysical contrast sensitivity for all spatial frequencies, and the change in sensitivity with change in orientation of the gratings was the same for contrast sensitivity (CS) determined psychophysically and by VEP measures (Campbell and Maffei, 1970). Also, the psychophysically determined visual acuity depended on the target area and luminance, such that for a given spatial frequency target, there was a critical target area below which the measured acuity depended on the number of cycles (for a periodic grating stimulus) in the target aperture (Pokorny, 1968). Similarly, for the overall modulation transfer function, i.e. contrast sensitivity, of the retina, the observed contrast sensitivity for sine-wave grating stimuli depended on the number of cycles contained in the stimulus when that number fell below a critical value. Early studies found that the contrast sensitivity function, when corrected for the number of cycles in the stimulus, showed no maximum (i.e. no low-frequency roll-off) (Hoekstra et al., 1974; Savoy & McCann, 1975). Later work, however, modified this view by showing that even when at least seven cycles are used at each spatial frequency (in order to prevent the artifact due to too few cycles) there was still a low spatial frequency roll-off in central CS, as well as dependence on retinal location (Rovamo et al., 1978; Kelly, 1984, 1985). Both visual acuity and contrast sensitivity decline with retinal eccentricity (Ludvigh, 1941; Kelly, 1985). These findings have implications for the determination of an overall retinal contrast sensitivity function; for example, due to technical limitations, an insufficient number of cycles in a low spatial frequency grating or checkerboard may be displayed on the stimulus device to determine the response adequately.

The visual electrophysiological responses exhibit a dependence on target diameter and retinal location in a manner comparable to that of the psychophysical measures. The classic VEP "tuning curve", i.e. a graph of VEP amplitude with respect to stimulus spatial frequency, typically has been described as having an inverted "U" shape (Harter, 1970), although the decline in amplitude at low spatial frequencies may well have resulted from the presentation of a less-than-optimal number of contrast changes (cycles) in the stimulus field (Katsumi et al., 1988). Nevertheless, by the use of spatially-restricted stimuli, e.g. an annular check-pattern that left the fovea unstimulated, a larger contribution by the macular region than by the retinal periphery to the VEP amplitude (Harter, 1970; Armington, 1968, 1981; Sakaue et al., 1990), as well as threshold (Cannon, 1983), was demonstrated . The peak of the spatial frequency tuning curve shifted to lower frequencies in the peripheral retina (Harter, 1970; Armington, 1981; Sakaue et al., 1990), consistent with lower visual acuity in the peripheral retina. The VEP

1

amplitude dropped sharply as the size of a central scotoma (centered on the fovea) increased up to a diameter of about 6 degrees (Sakaue et al., 1990). Beyond this size, the scotoma exerted much less effect on the VEP amplitude. This finding illustrated the macular dominance of the VEP, and also pointed to the value of the VEP in assessing the effect of macular lesions (Sokol, 1972). Recent investigations found abnormalities in the transient and steady-state VEPs in up to 78% of retinal disorders (mostly maculopathies) (Celesia & Kaufman, 1985). This corroborated the potential utility of the VEP in predicting acuity or contrast sensitivity after discrete lesions to the fovea or macular area. It may be noted that the macular dominance of the VEP may be due to a combination of cortical magnification on the central retinal projection (a physiological and anatomical phenomenon affecting to visual function), and the location of the foveal projection on the occipital pole where it is most accessible to recording by scalp electrodes.

The VEP was initially used in this research program to assess visual acuity in monkeys after focal laser lesions to the fovea and parafovea (Schmeisser, 1992; Glickman et al., In Press). The VEP proved to be a useful method for objectively tracking and estimating acuity after threshold and suprathreshold laser lesions. The data from this initial study was used to validate a concentric retinal model implemented on a microcomputer (referred to as the "CMI model") which, given the size and location of a retinal lesion, predicted the lesion's effect on the VEP amplitude, and by extrapolation, on the resulting visual acuity. The model's basic assumption is that retinal acuity varies only with eccentricity (as hypothesized by Kelly, 1985), so that by adjusting a scaling factor for each concentric retinal region, the contribution of that region to the VEP response is brought into accordance with the physiological response, and then used to predict the response to a particular lesion input by the user. While this approach has proven to be suitable for predicting the effects of foveal (central lesions), additional VEP data, specifically obtained from more peripheral regions, was needed to validate predictions for other retinal regions. Moreover, some meridional differences in sensitivity have been reported (Regan & Beverley, 1983), which could be responsible for variability in the VEP response not properly accounted for by the model. Therefore, we collected VEP data from normal subjects using a variety of stimulus fields covering, in different experimental runs, the central macula, annular regions (i.e. parafovea), and superior and inferior hemifields (as an attempt to measure meridional sensitivity). This dataset was then compared to similar VEP data collected from patients with selected retinal disorders. In addition to validating the CMI model, this study was also performed to demonstrate the capability of the model in predicting visual function in the presence of naturally occurring pathology limiting function primarily in central or peripheral regions of the visual field.

Methods

Visual Stimulation

The visual stimuli were displayed on a 19" diagonal, high-resolution color CRT display with a resolution of 1024 by 1024. The stimulus patterns themselves were produced by the "VisionProbe" stimulus generator (Conceptual MindWorks/VisionProbe Enterprises, San Antonio, TX). The monitor was maintained at a viewing distance of 1 m by an adjustable chin-head rest, so that the full extent of the visible raster on the CRT subtended about a 12 by 12 degree stimulus field. Subjects viewed the stimulus screen monocularly with the other eye patched. The VEPs were elicited by sine wave luminance gratings counterphased in a square

wave temporal profile at 7 Hz (14 reversals/sec). Space-averaged luminance of the gratings was about 6 fL (20.8 cd/m^2) (green CRT gun only). Surrounding areas in the room had a luminance of <2 fL. The VisionProbe was set to sweep the contrast of the sine wave gratings from 0% to 50% contrast in a 12 sec period, with the contrast increasing logarithmically. Logarithmic sweeps were used to increase the "dwell" time at the lower contrasts around threshold. The contrast threshold was determined at spatial frequencies of 0.5, 1, 3, 5, 8, 12, and 16 cycles per degree (cpd), depending on the field condition. Table 1 shows the stimulus matrix used in the experiments.

The grating patterns were presented in fields of different sizes and configurations (see Table I). Different field configurations were produced by masking the full 12 degree field with opaque templates (cf. pictorial representation of different stimuli in fig. 1). During the recording epoch, the subject was instructed to look at a small red fixation spot centered in the stimulus field. The chin-head rest also assisted the subject in maintaining stable fixation, as well as reducing artifacts arising from head or neck movements and muscle contractions.

Table I. Stimulus Matrix

Field Type	Spatial Frequencies	Contrast Range	Subjects Tested
Whole Field (12x12°)	0.5, 3, 8, 12, 16*	0-50%	Normals and Patients
3° Central Field	0.5, 3, 8, 12, 16*	0-50%	Normals and Patients
6° Central Field	0.5, 3, 8, 12, 16*	0-50%	Normals and Patients
6°-12° Annulus	1, 5, 8, 12*	0-50%	Normals and Patients
6°-12° Upper Hemifield	1, 5, 8, 12*	0-50%	Normals only
6°-12° Lower Hemifield	1, 5, 8, 12*	0-50%	Normals only

*These spatial frequencies were only tested if conditions warranted, i.e. a response was observed.

Figure 1. Pictorial representation of stimulus masks used in sweep-VEP experiment
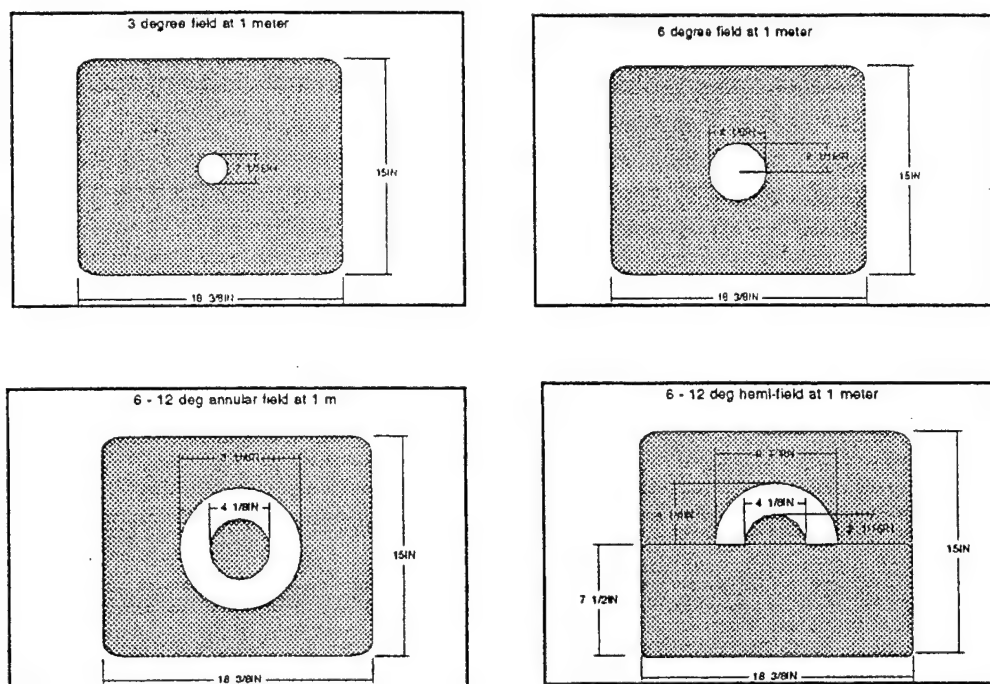
"Sweep-VEP" Recording

Because the VEPs were recorded with a dynamic stimulus, i.e. the contrast of the stimulus was increased gradually during data acquisition (i.e. "swept") over the range of 0 to 50%, these responses are called "sweep-VEPs". The VEPs were recorded with a type E5GH gold cup electrode (Grass Corp., Quincy, MA - now Grass Division of Astro-Med, Inc., West Warwick, RI) placed on the scalp 2 cm above the inion. Good contact between electrode and scalp was ensured by first cleaning the recording site with Redux Paste (Hewlett-Packard Medical Products Group, Waltham, MA), placing the recording electrode on the scalp with conductive electrode paste (Grass Corp., type EC-2), and covering the electrode with a piece of paper tape to ensure stability of the lead during recording. Gold-plated clip electrodes (Grass type E34D-G) on the ears served as reference (on the contralateral ear lobe - the subjects viewed the stimulus screen monocularly) and as ground (on the ipsilateral earlobe). Electrode impedance in all cases was less than 10K ohms and was usually below 5K ohms before VEP recording began.

The stimulus presentation and data acquisition system is shown schematically in Fig 2. The electrical signals were amplified with a Grass Model P5, AC-coupled amplifier with bandpass set from 1 to 1000 Hz. The raw VEP signal was then further low-pass filtered with a Wavetek model 452 active filter with the band limit set to 100 Hz. The output of this filter was fed into a SR530 lock-in amplifier (Stanford Research Systems, Palo Alto, CA). The lock-in amplifier was referenced to the stimulus counterphase frequency by an appropriate signal from the VisionProbe generator. The output of the lock-in consisted of DC voltages proportional to the amplitude and phase of the input signal whose frequency corresponded to that of the reference

frequency (cf. Nelson et al, 1984; Glickman et al., 1991). The raw VEP signal, the reference signal (an analogue signal - corresponding to the stimulus contrast - also generated by the VisionProbe), and a voice commentary were all recorded on standard, 1/4" audio tape. The VEP and control signals were converted to audio frequencies by voltage to frequency conversion (models 2D and 3 FM converters, Vetter Corp, Rebersburg, PA). The lock-in amplifier outputs were also captured with the "Experimenter's Workbench" (DataWave Corp., Longmont, CO) data acquisition system, and stored on computer. These computer files were analyzed to determine the point in the contrast sweep at which a recordable VEP occurred.
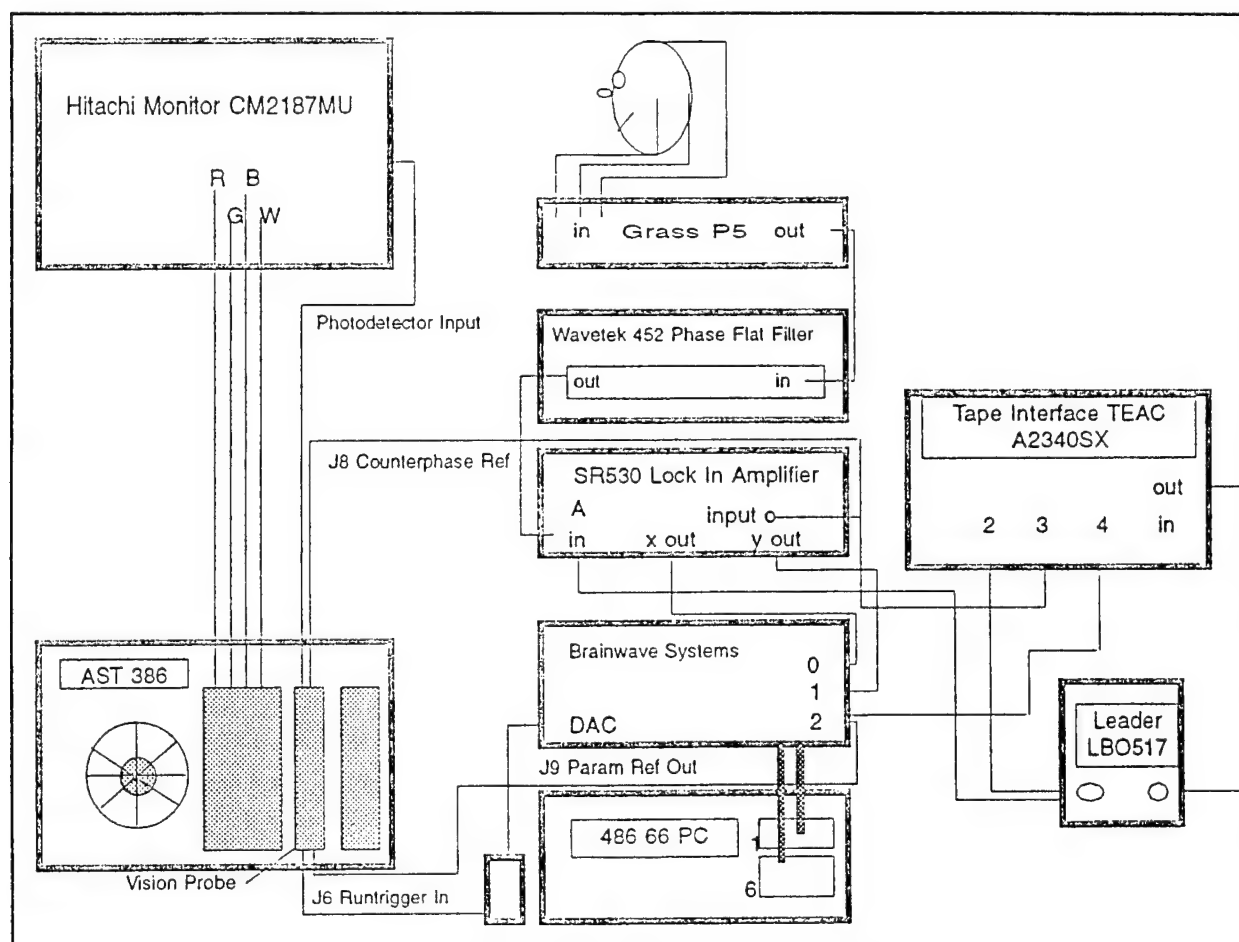
Figure 2. Schematic of experimental layout used to record sweep-VEP responses.

Analysis of VEP data

The original plan for this project called for developing a computer program for automatically determining contrast sensitivity from the sweep-VEP data files. Because the data from the normal subjects were obtained first, it was used to test the analysis software as it was developed. The following approach was adopted for the analysis algorithm. Due to the variability observed in the subjects' responses to a given stimulus, each subject's responses to a fixed, repeated stimulus were averaged, point by point, to get a "typical" response for that individual and a given

stimulus condition. Thus all of the sweeps in a file (typically 7-10 sweeps) were averaged, and the response detection algorithm was run on the average sweep response dataset.

The response detection algorithm used linear regression to fit a line to all the points in a window of given size. Lines were fit to all the points of the average sweep by using overlapping windows. Starting with the first window at the beginning of the sweep, the slope of the fitted line was compared to an arbitrary threshold value. If more than two consecutive windows had slopes above the threshold value, a response was assumed to have occurred. The response point was determined by calculating the intersection of the line in the first response window, with the line in the previous window (whose slope was below the threshold). The sample number where this intersection occurred was correlated to a stimulus parameter reference signal, also contained in the experimental records, the amplitude of which was proportional to the display contrast. This contrast value, ranging from 0 to 50%, was taken to be the contrast of a threshold stimulus for the particular spatial frequency and field size of the luminance grating on the display.

Due to noise spikes in the original data, a robust form of linear regression was used: the least median of squares (LMS) regression. This was predicted to give a better line fit in the presence of impulsive noise than ordinary least squares regression. The size of the line fit window and the minimum slope threshold were experimentally determined using sweep-VEP data from normal subjects. As it turned out, however, the algorithm developed for the normal subjects' dataset, proved to overestimate, by a large margin, the contrast sensitivity for the patient subjects. Therefore, the entire dataset collected in this study was analyzed by visual inspection by two observers, i.e. the observers looked at the individual and averaged VEP traces and determined if and at what contrast a VEP occurred (See Results, below). This manual analysis was performed in a masked fashion, i.e. the observers did not know the stimulus conditions for the VEP record being analyzed.

Statistical differences in the mean CS determined in the various subject groups were tested first by analysis of variance followed by three post-hoc tests (Least Significant Difference test, Tukey test, and Unequal N test) of the difference between means. Statistical tests were from the CSS Statistica Package. The raw data from all subject groups are tabulated in Attachment 2.

Subjects

Normals. Eleven subjects with no history of ophthalmic disease, other than corrected refractive errors, made up this group. They were mostly recruited from the University community and had their visual acuity measured, to ensure they had acceptable vision for the study. Visual acuity was measured using a Bailey-Lovie chart #4. Subjects were required to read the letters on the chart until they made a total of 7 errors or until they misidentified all 5 letters on one line. A numerical score was calculated based on the number of letters read correctly, and the score was converted into a conventional measure of visual acuity. Subjects wore their usual corrective eyeglasses (if any) during the experimental session. They received $25 upon completion of the session. The visual acuity of the normal subjects are shown in Table II.

Patients. There were fourteen patients referred from the UTHSCSA Eye Consultants Clinic, the Brady-Green Eye Clinic, and the Audie Murphy Veterans Administration Hospital with a diagnosis of a retinal disorder such as retinitis pigmentosa (RP), cystoid macular edema (CME)

with laser photocoagulation, ocular histoplasmosis syndrome, glaucoma with documented field loss, and one case of accidental laser exposure. In addition to the clinical history, all patients had their acuity tested on the day of the VEP recording, and, if necessary, wore their usual correction. Exclusion criteria for patients for this study were the presence of moderate to dense cataracts or visual acuity worse than 20/100. Patients received a $25 reward upon completion of the VEP recording session. The diagnoses and visual acuity of the patient subjects are shown in Table II.

Table II. Subjects

Subject ID	Visual Acuity	Log MAR	Visual Condition
BB1	20/18	-0.05	Normal
JH1	20/20	0	Normal
CG1	20/19	-0.01	Normal
DF1	20/15	-0.11	Normal
RG1	20/15	-0.11	Normal
BB2	20/15	-0.13	Normal
VH1	20/22	0.05	Normal
DR1	20/14	-0.15	Normal
LV1	20/20	0	Normal
MM1	20/16	-0.11	Normal
BP1	20/16	-0.09	Normal
MH1	20/18	-0.05	Patient: RP
VH2	20/20	0	Patient: RP - peripheral defect
NG1	20/68	0.53	Patient: RP - peripheral defect
FC1	20/16	-0.09	Patient: laser injury - macular defect
WS1	20/12	-0.21	Patient: retinal degeneration (probable RP) - peripheral defect
JS1	20/24	0.07	Patient: Toxoplasmosis, retinal degeneration, RP - peripheral defect
JW1	20/54	0.43	Patient: RP - peripheral defect; field constricted to 10°
LB1	20/98	0.69	Patient: RP - peripheral defect

MW1	20/18	-0.05	Patient: ARMD with subretinal scar adjacent to fovea - macular defect
KT1	20/47	0.37	Patient: RP & Usher's syndrome; field constricted to 5°
HP1	20/43	0.33	Patient: epiretinal membranes, drusen, RPE changes, & probable SRN - macular defect
YB1	20/44	0.34	Patient: parafoveal telangiectasis with SRN, laser ablation - macular defect
MG1	20/50	0.4	Patient: mild diabetic retinopathy, CME, post focal laser photocoagulation - macular defect
CM1	20/85	0.65	Patient: solar maculopathy - macular defect

Abbreviations:
ARMD: Age-Related Macular Degeneration
CME: Cystoid Macular Edema
RP: Retinitis Pigmentosa
SRN: Sub-Retinal Neovascularization

Psychophysical Determination of Contrast Sensitivity

In order to compare the electrophysiological and psychophysical estimates of contrast sensitivity, we determined the contrast sensitivity of each of the normal subjects psychophysically. We measured monocular contrast sensitivity using stimulus characteristics closely matching those of the 6° diameter targets producing pattern VEPs. The screen size was 5.6° at the 1.6 m viewing distance which was maintained constant by an adjustable chin-head rest. The circular target was produced by a 5.6° circular aperture in a diffusing Lucite mask. The spatially sinusoidal gratings were modulated with a square wave temporal profile at 7.5 Hz (15 reversals/s). The average luminance of the screen was 23 cd/m^2 ($\approx$ 195 td). The ambient luminance was kept dim (<2cd/m^2) to avoid loss of screen contrast due to ambient light reflected off the screen. The black and white monitor (15 MHz non-interlaced RCA TC1214 with a P4 phosphor) had a 60 Hz frame rate and displayed 240 lines vertically in 22.5 cm. The spatial modulation was synchronous with the raster modulation.

We used a two temporal interval forced choice adaptive staircase technique to measure contrast sensitivity. The two observing intervals were denoted by tones occurring before each. A blank screen was presented during one of each pair of observing intervals. The subject's task was to indicate by a button press which of the two intervals contained the stimulus. The contrast decreased by 0.3 log unit in the initial testing sequence until the subject made two errors. The contrast decrement and increment size was then changed to 0.15 log units. Two correct responses caused a 0.15 log unit decrease in contrast. One incorrect response caused a 0.15 log

unit increase in contrast. These decision rules result in an estimate of detection probability
(p(C)) of 71%. Data were collected until there were 7 reversals of contrast change with the 0.15
log unit steps. The final sensitivity was the mean of the sensitivity at the 7 reversal points. The
duration of each observation interval was 0.75 s with 0.4 s between intervals and 0.5 s between
trials. The stimuli were generated, the testing sequence was controlled, and the data were
collected using a NeuroScientific Corporation 8010 System. The NeuroScientific Corporation
8010 System is an eight bit PC compatible board controlled by NeuroScientific software. The
board was driven by a 386 DX33 PC.

Results

Computer vs. Manual Analysis of the Sweep-VEP.

As described in Methods, above, the computerized algorithm developed for this project was
accepted based on its performance with the sweep-VEP data recorded from the normal subjects.
That the contrast sensitivities returned by the automated method were reasonable - for the
normal dataset only - was demonstrated by subsequent comparison to the results obtained from
manual analysis. These results are shown graphically in Figure 3. For the 3, 6, and 12 degree
field conditions, the CS determined by computer and that measured manually either was
identical or largely overlapped. There was a consistent difference between the manual- and
computer-returned data in the 6-12 degree annulus condition (manual > computer, see Figure 3),
however, there was at least some overlap in the data for all spatial frequencies tested, i.e. the
difference was not large.

In contrast, the computer analysis returned CS determinations from the patient data that were
much higher (more sensitive) than were those of the normals, in some cases by a log unit or
more. This was patently incorrect, because for many of the patients with macular disease, there
were little or no VEP responses observed with many stimulus conditions. Therefore, the CS
measurements should have been lower compared to the normals. By examining the patient
datasets processed by the computer algorithm, we hypothesized that in the absence of a robust
response, the algorithm reported the first noise variation in the record as a response inflection,
thus returning an erroneous CS value. It was clear that further work would be required to make
the algorithm suitable for processing the weak responses often obtained from the patients, e.g. by
including additional "rules" to provide minimum response criteria, or, perhaps, by increasing the
length of the analysis windows used to detect excursions from baseline. In any event, without
the time or resources to develop the computer algorithm further, we decided to re-analyze the
entire dataset by hand, simply determining a response inflection by visual inspection of the
dataset.

Psychophysical Estimate of Contrast Sensitivity in Normal Subjects

The results of the psychophysical tests of contrast sensitivity are shown in Table III.
Although the intent had been to determine CS at 3 and 8 cpd, two of the spatial frequencies used
in the evoked potential studies, several of the subjects were actually tested at 1.5 and 6 cpd
instead before the error was noted. This error, however, permitted us to examine a wider range

9
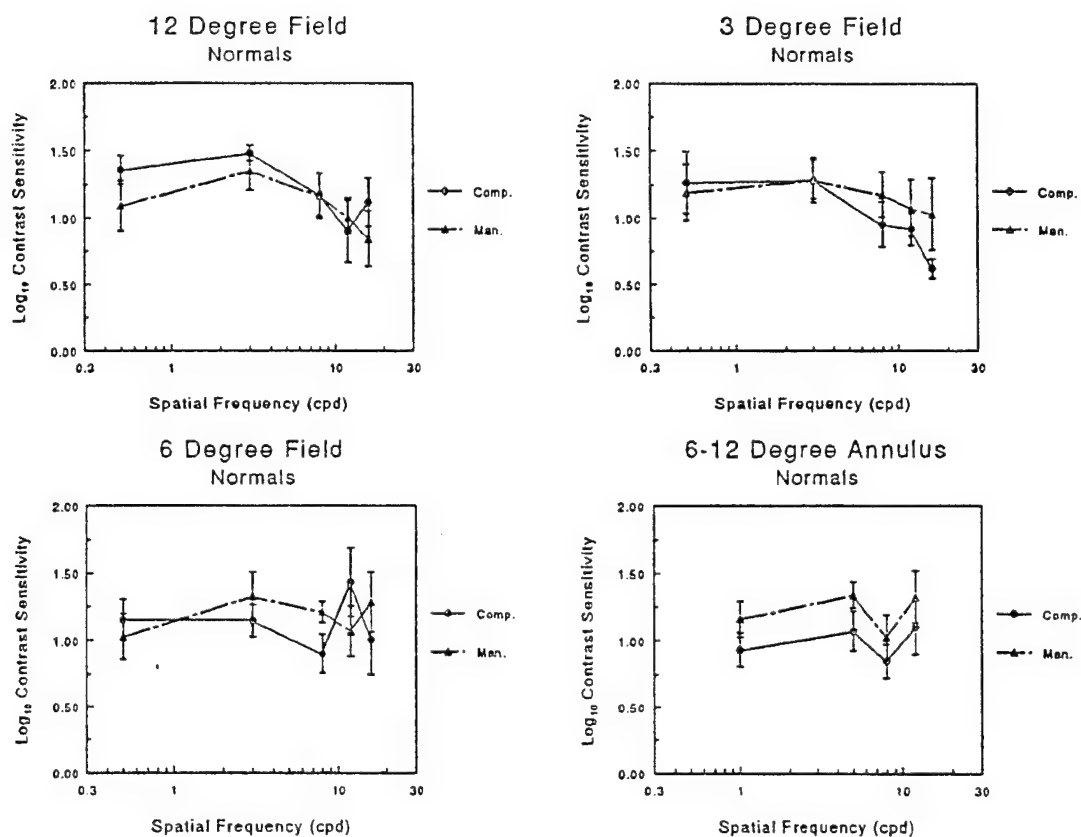
Figure 3. Comparison of CS determined by computer and visual inspection (Man.) for the normal subjects, for the 3°-, 6°-, 12°-central, and 6-12°-annular, field size condition. Error bars in this and all following figures indicate ±1 standard error of the mean.

of spatial frequencies, bracketing those used in the VEP study. All the measurements are shown in Table III

Table III. Contrast Sensitivity of Normal Subjects

Subject I.D.	1.5 cpd	6 cpd	3 cpd	8 cpd
0	277.24	107.05	n.d	n.d
JH1	333.01	51.05	n.d.	n.d.
CG1	333.01	107.05	n.d.	n.d.
DF1	273.37	124.13	n.d.	n.d.
RG1	247.68	107.05	n.d.	n.d.
BB2	158.87	175.34	n.d.	n.d.
VG1	213.60	68.67	n.d.	n.d.
DR1	n.d.	n.d.	184.21	145.98
LV1	n.d.	n.d.	158.87	65.36
MM1	n.d.	n.d.	175.34	6.43
BP1	n.d.	72.14	118.16	n.d.

Note: "n.d." = not done

Comparison of Electrophysiological and Psychophysical Measurements of Contrast Sensitivity.

In the normal subjects, over all spatial frequencies tested, the CS determined by the sweep-VEP was lower than that determined psychophysically. The difference was about a log unit at spatial frequencies of 3 cpd or less, and decreased to less than one half log unit at 8 cpd. A comparison of the two types of CS measurement are shown in Figure 4 (automated sweep-VEP analysis) and in Figure 5 (manual sweep-VEP analysis).

Comparison of CS in Normal and Patient Subjects.
For this analysis, the results from patients were separated into two groups: patients with disorders of the central retinal field (termed "macular" subjects, N=6), and those with disorders of the peripheral retinal fields (termed "peripheral" subjects, N=8). The CS measurements made by sweep-VEP and determined manually from the data are shown in Figure 6. Results for each stimulus field size are shown in separate insets in the Figure.

11
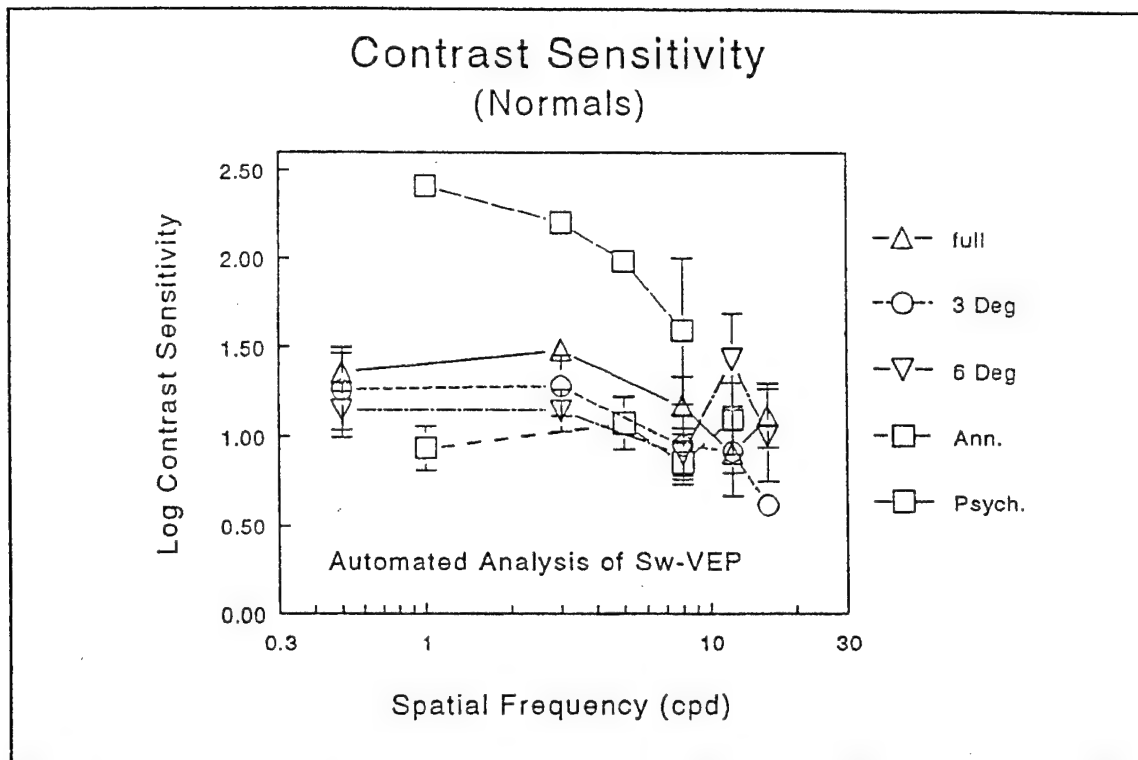
Figure 4. Comparison of psychophysical and <u>automated</u> sweep-VEP measures of CS for all field sizes tested (normal subjects only).
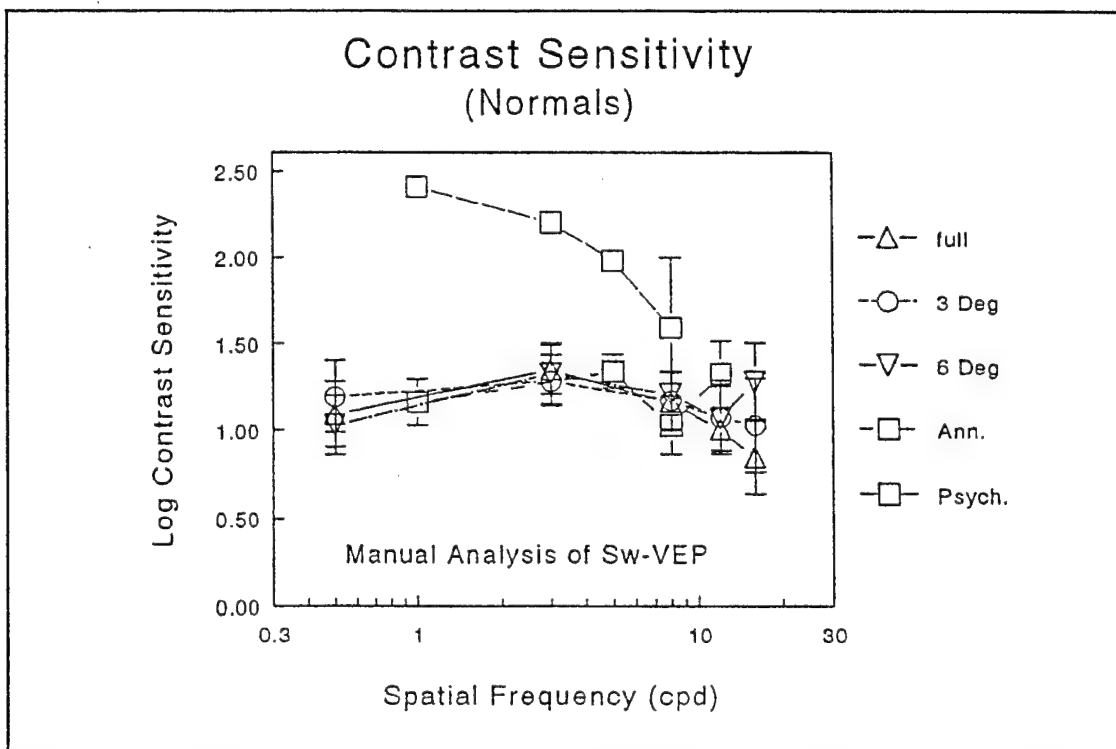
Figure 5. Comparison of psychophysical and <u>manual</u> sweep-VEP measures of CS determined for all field sizes (normal subjects only)

12
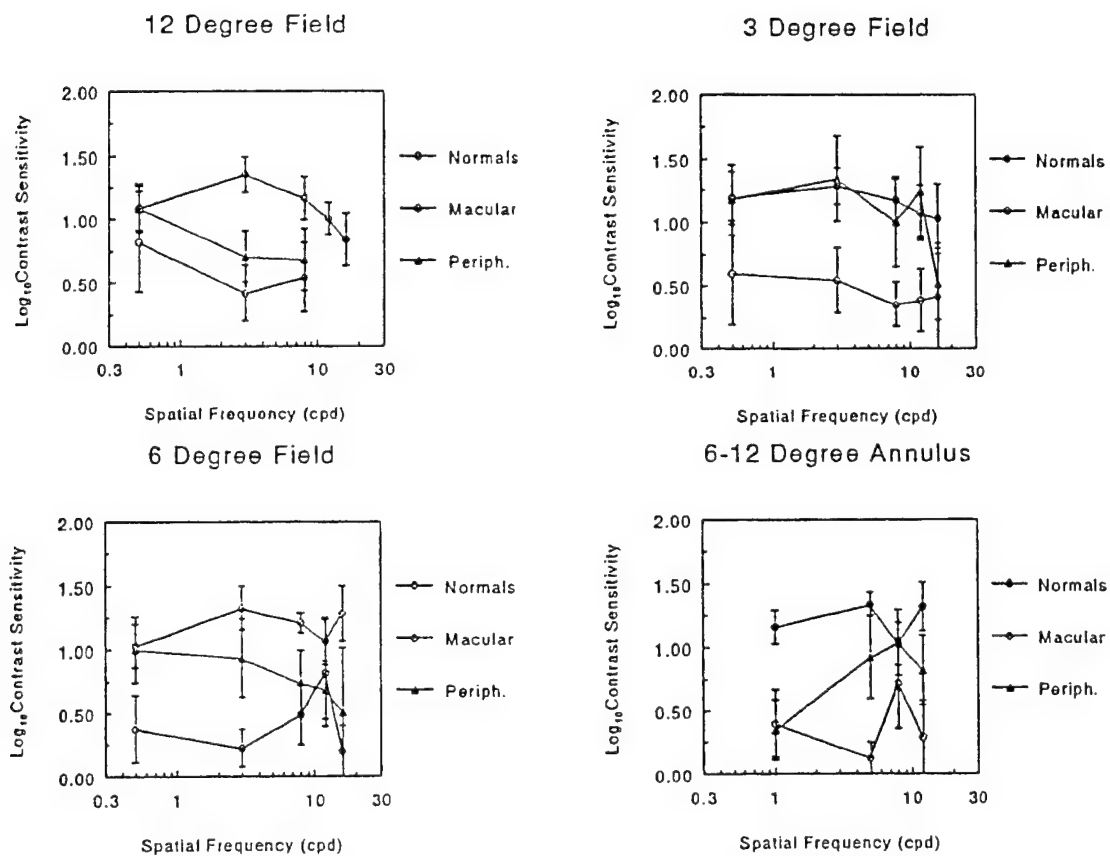
Figure 6. Comparison of CS data, determined by manual analysis of the sweep-VEP, of patient and normal subjects groups. Each inset shows the results from the indicated stimulus field size.

As shown in the four insets in Figure 6, corresponding to the 3°-, 6°-, 12°-central, and 6-12° annular fields, the mean CS of the "macular" subjects was much lower than the CS of normal subjects in all conditions. By analysis of variance followed by post-hoc tests on differences between the means, this difference was significant in all conditions (p<.05). The mean CS measured in the "peripheral" subjects did not differ significantly from the normals or from the "macular" subjects in any of the central field sizes tested, in spite of the apparent difference between peripherals and normals in the 12° field condition, although it should be noted that there is low statistical power to detect small differences because of the small sample size and large variability. With the 6-12°-annular field, however, the differences between normal, macular, and peripheral patients were all significant (p<.05).

Comparison of CS in upper and lower hemifields.

In the normal subjects, the CS was measured in upper and lower hemifields, consisting of half of the 6-12° annular mask, oriented so that the appropriate field was stimulated (see Figure 1). The results are shown in Figure 7. No significant difference was found in the CS measured in these two hemifields.
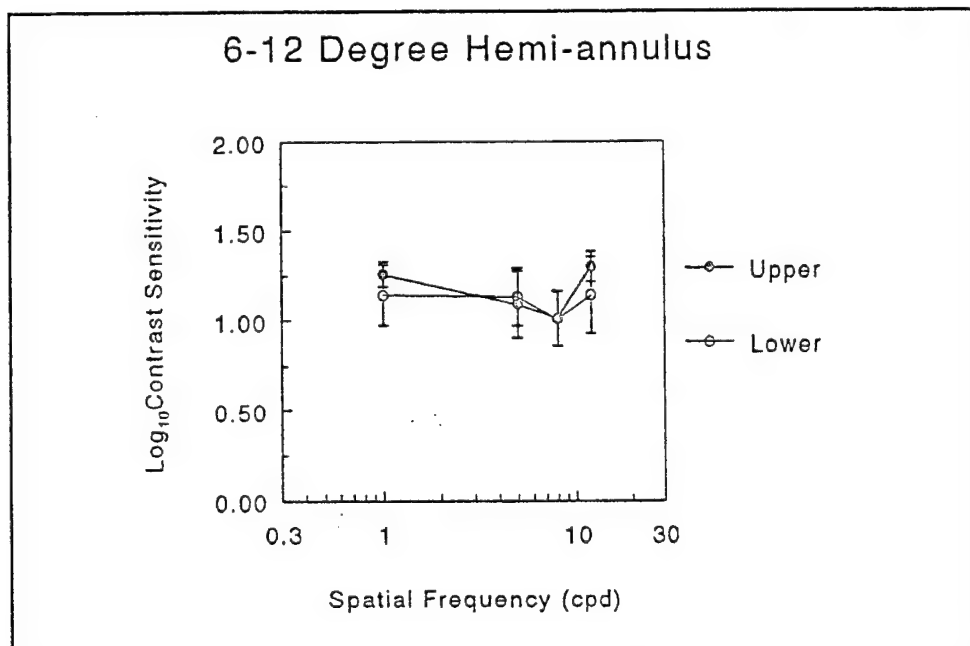
Figure 7. Comparison of upper and lower hemifield CS determined in the normal subjects.

Discussion

Suitability of Sweep-VEP for clinical testing.

The sweep-VEP technique is no more difficult to use with human subjects in clinical or laboratory settings than are other evoked potential recording techniques, because the actual

recording procedures, e.g. electrode preparation and application, are essentially similar to other (primarily flash and steady-state pattern VEP) recording procedures. The main difference is in the stimulus presentation, which does require a specialized pattern generator (cf. Glickman et al., 1991). However, in the usual clinical setting, we recommend that fewer conditions be tested, probably using only one field size, for example only the "full-field" (12°) size, or perhaps the 6° field if only the macular response is to be tested. Additional conditions may not add useful clinical information, and may cause the testing session to be unduly protracted. In our hands, the patient testing period was usually about three hours, which is far too long for the typical clinical test. Indeed, if the goal is to distinguish macular from peripheral dysfunction, testing 2 or 3 spatial frequencies with the 12° field will probably be sufficient.

Contrast Sensitivity measured with the sweep-VEP and by psychophysics.

In our study, the CS returned by the sweep-VEP was lower than that measured by a standard psychophysical test. The difference was about 1 log unit or less. This difference was not unexpected and is probably due to the difficulty of distinguishing an electrophysiological response near the threshold, as well as the possibility that the recorded electrophysiological response is not identical with the response of the "perceptron", i.e. the neural unit or units mediating the psychophysical response. An additional factor is that in all the psychophysical data cited here, except for Morris et al. (1987), thresholds were estimated by an up-down contrast adjustment series. The VEP thresholds and the psychophysical thresholds of Morris and Harrison (1987) were estimated from only increasing contrast series. The difference between these two estimates was only 0.5 - 0.75 log units. In any event, our electrophysiological measures of CS were similar to those reported by Seiple et al (1984), and our psychophysical measures of CS were also similar to published values of psychophysically-determined CS (Kelly, 1977; Seiple et al., 1984; Morris et al., 1987). Several datasets from the literature of psychophysical CS are graphed in Figure 8 along with the psychophysical and electrophysiological data obtained in the present study.

Sweep-VEP measures of CS and retinal pathology.

It has been shown in several studies that the VEP recorded from the occipital pole principally reflects activity in the central 6 degrees of the visual field (Meredith & Celesia, 1982; Yiannikas & Walsh, 1983). This may be due to (1) the projection in humans of the fovea to the cortex on the occipital pole, putting the electrical dipole of the foveal projection in closest proximity to a recording electrode on the occipital scalp, and (2) the disproportionately large representation of the fovea in the visual cortex (related to the greater cortical magnification factor of the central visual field). Thus, pathology impairing foveal function is expected to reduce the amplitude or other parameters of the VEP recorded from the scalp. Indeed, in the present study, the "macular" subjects had the lowest CS at all spatial frequencies and in all field sizes tested. In comparison, the "peripheral" subjects had CS measurements that were similar or identical to that of the normal subjects, except when the stimulus field was restricted to a 6-12° annulus centered in the parafoveal region. With this restricted field, some reduction in the CS was noted in the "peripheral" subjects, and marked reduction was noted in the "macular" subjects. Overall, the measurement of CS by the sweep-VEP was able to distinguish retinal pathology among the different subject groups, both by the relative robustness of the swept-VEP response in the

15

normals compared to the patients, as well as by the relative CS measured in the various testing condition.
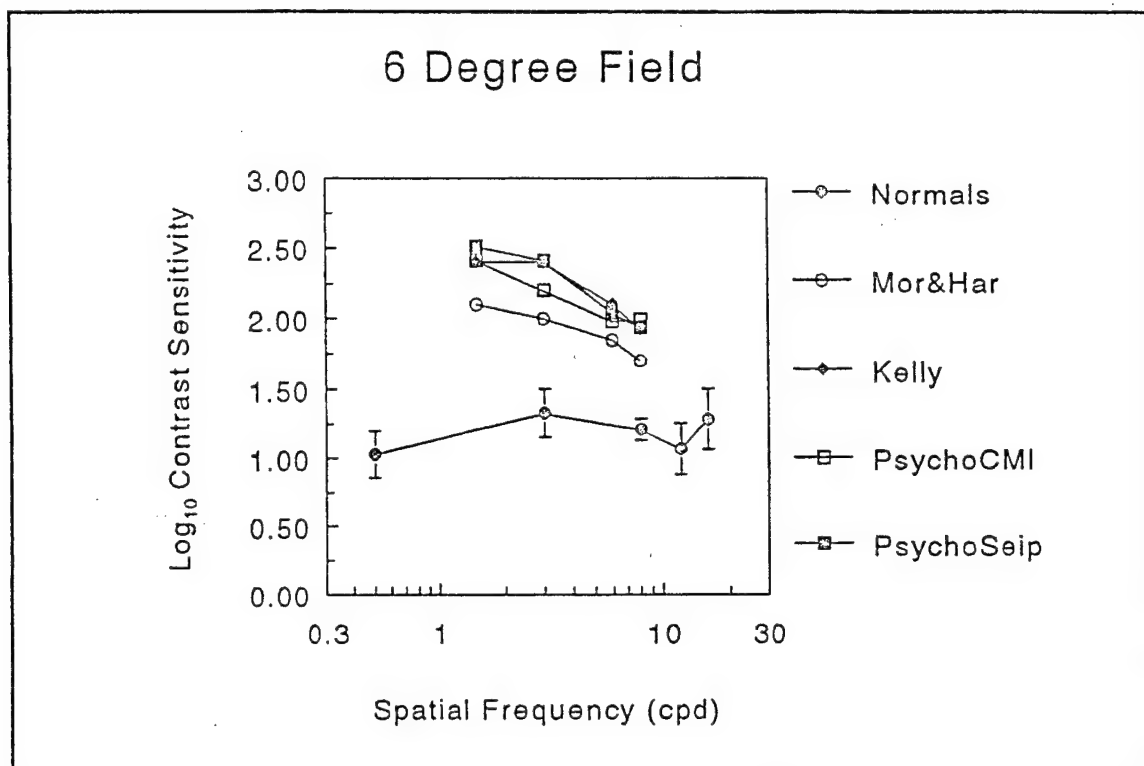
Figure 8. Comparison of CS data from the present study with selected data from the literature. Identification of datasets: "Normals": CS measured with sweep-VEP from the present study; "Mor&Har": pyschophysical CS from Morris et al. (1987); "Kelly": psychophysical CS from Kelly (1977); "PsychoCMI": psychophysical CS from the present study; and "PsychoSeip": psychophysical CS from Seiple et al., (1984). All the psychophysical CS measures were obtained under similar testing conditions.

The marked CS loss in the larger fields and annulus in the "macular" subjects was rather surprising; the clinical impression in these patients was that there was more or less normal retina beyond 5° eccentricity. One possible explanation of their poor performance is that these subjects may have used parafoveal retina for fixation, thus positioning their defective macular area closer to the annulus. Small errors in this maneuver may have resulted in part of the annular field being occluded by their scotomatous field, thus reducing the apparent VEP.

The similarity in the CS of the "peripheral" subjects compared to the normals was expected. Most of these subjects had retinitis pigmentosa with visual field sizes >10° in diameter. Thus, with central stimulus fields up to 12° in diameter, these subjects were able to use essentially normal retina to observe the stimulus screen. With the annular field, however, the field constriction of some of the subjects may have started to encroach on the visual subtense of the stimulus screen, resulting in loss of VEP. This reduction in VEP may account for the lower CS of the "peripheral" subjects in the 6-12° annular field test condition.

Using the sweep-VEP data to validate the CMI model.

The data from the normal human subjects can be compared directly to the output of the CMI retinal contrast sensitivity model in order to assess how reasonable was the selection of the scaling factors assigned to each of the concentric retinal segments of the model which adjust the model output to match the physiological data. For the patient data, the site and extent of the lesions may be inferred from their clinical data (see attachment 1), and this lesion information entered into the model. Then, the subject's measured CS data, as determined from the sweep-VEP data, may be compared to the CS (at any selected retinal location) predicted by the CMI model. If discrepancies occur between the model and the experimental data, they may have been due to a mismatch between the physical extent of the "observed" lesion and the actual extent of the pathological process, or to larger than expected effects of retinal lesions upon the VEP. Some adjustment of the scaling factors to reduce any discrepancies may have to be considered. Nevertheless, these comparisons will help improve the application of the CMI model to the prediction of visual function in the presence of various stressors or retinal lesions, as well as its anticipated use in visualizing visual disorders as an aid to educating patients and their families.

References

Armington, J.C. The electroretinogram, the visual evoked potential and the area luminance relation. Vis. Res. 8:263-276; 1968.

Armington, J.C. Effects of stimulus location and pattern upon the visually evoked cortical potential and the electroretinogram. Intern. J. Neurosci. 14:169-178; 1981.

Cannon M.W. Evoked potential contrastsensitivity in the parafovea: Spatial organization. Vision Res. 25:1441-1449, 1983.

Campbell F.W.; Maffei L. Electrophysiological evidence for the existence of orientation and size detectors in the human visual system. J Physiol (Lond). 207:635-52, 1970.

Celesia, G.G.; Kaufman, D. Pattern ERGs and visual evoked potentials in macuolopathies and optic nerve diseases. Invest. Ophthalmol. Vis. Sci. 26:726-735; 1985.

DeBruyn, E.J.; Gajewski, Y.A.; Bonds, A.B. Anticholinesterase agents affect contrast gain of the cat cortical visual evoked potential. Neurosci. Lett. 71:311-316, 1986.

Fagan, J.E.; Allen, R.G.; Yolton, R.E. Factors contributing to amplitude variability of the steady-state visual evoked response. Am. J. Optom. Physiol. Optics 61:453-464; 1984.

Glickman, R.D.; Rhodes, J.W.; Coffey, D.J. Noninvasive techniques for assessing the effect of environmental stressors on visual function. Neurosci. Biobehav. Rev. 15:173-178; 1991.

Glickman, R.D.; Cartledge, R.M.; Zuclich, J.A. Visual acuity following laser-induced hemorrhagic lesions in the fovea and parafovea: An experimental study. In: Charschan, S., ed., International Laser Safety Conference -1992. Cincinnati: Rockwell Laser Industries; In Press.

Harter, M.R. Evoked cortical responses to checkerboard patterns: Effect of check-size as a function of retinal eccentricity. Vis. Res. 10:1365-1376; 1970.

Hoekstra, J.; van der Goot, D.P.J.; van den Brink, G.; Bilsen, F.A. The influence of the number of cycles upon the visual contrast threshold for spatial sine wave patterns. Vis. Res. 14:365-368; 1974

Katsumi, O.; Hirose, T.; Tsukada, T. Effect of number of elements and size of stimulus field on recordability of pattern reversal visual evoked response. Invest. Ophthalmol. Vis. Sci. 29:922-927; 1988.

Kelly, D.H. Visual contrast sensitivity. Optica Acta 24:107-129, 1977.

Kelly, D.H. Retinal inhomogeneity. I. Spatiotemporal contrast sensitivity. J. Opt. Soc. Am. A 1:107-113; 1984.

Kelly, D.H. Retinal inhomogeneity. III. Circular-retina theory. J. Opt. Soc. Am. A 2:810-819; 1985.

Ludvigh, E. Extrafoveal visual acuity as measured with Snellen test-letters. Am. J. Ophthalmol. 24:303-310; 1941.

Meredith, J.T. and Celesia, G.G. Pattern-reversal visual evoked potentials and retinal eccentricity. Electroencephalogr. Clin. Neurophysiol. 53:427-435, 1983.

Morris, M.A.; Harrison, J.M.; and Ballentine, C.S. Effects of glare on spatiotemporal contrast sensitivity. Final Report: Georgia Instititute of Technology, Subcontract A-3529-200-S1, "Laser veiling glare studies", 1987.

Nelson, J.I.; Seiple, W.H.; Kupersmith, M.J.; Carr, R.E.; Lock-in techniques for the swept stimulus evoked potential. J. Clin. Neurophysiol. 1(4):409-436, 1984.

Pokorny, J. The effect of target area on grating acuity. Vis. Res. 8:543-554; 1968.

Regan, D.; Beverley, K.I. Visual fields described by contrast sensitivity, by acuity and by relative sensitivity to different orientations. Invest. Ophthalmol. Vis. Sci. 24:754-759; 1983.

Rovamo, J.; Virsu, V.; Nasanen, R. Cortical magnification factor predicts the photopic contrast sensitivity of peripheral vision. Nature 271:54-56; 1978.

Sakaue, H.; Katsumi, O.; Mehta, M.; Hirose, T. Simultaneous pattern reversal ERG and VER recordings. Invest. Ophthalmol. Vis. Sci. 31:506-511; 1990.

Savoy, R.L.; McCann, J.J. Visibility of low-spatial-frequency sine-wave targets: Dependence on number of cycles. J. Opt. Soc. Am. 65:343-350; 1975.

Schmeisser, E.T. Acute laser lesion effects on acuity sweep VEPs. Invest. Ophthalmol. Vis. Sci. 33:3546-3554; 1992.

Seiple, W.H.; Kupersmith, M.J.; Nelson, J.I.; and Carr, R.E. The assessment of evoked potential contrast thresholds using real-time retrieval. Invest. Ophthal. Vis. Sci. 26:627-631, 1984.

Sokol, S. An electrodiagnostic index of macular degeneration. Arch. Ophthalmol. 88:619-624; 1972.

Tyler, C.W.; Apkarian, P.; Levi, D.M.; Nakayama, K. Rapid assessment of visual function: an electronic sweep technique for the pattern visual evoked potential. Invest. Ophthalmol. Vis. Sci. 18:703-713; 1979.

Yiannikas, C. and Walsh, J.C. The variation of the pattern shift visual evoked response with the size of the stimulus field. EEG and Clin. Neurophysiol. 55:427-435, 1983.

Spatial Frequency (cpd)

	0.5	3	8	12	16
Normals: 12 Degree Field, Log Contrast Sensitivity					
BB1	1.3872	1.5376	2.1549		
BB2	1.3872	1.4202	1.2757	0.9245	0.6536
BP1	1.3979	1.4815	1.0410	0.8386	1.6990
CG1	1.3872	1.3279	0.6615	0.5654	
DF1	1.2291	1.5229	0.9208	0.5072	
DR1	1.9586	1.4815	1.1487	0.6840	0.7825
JH1			0.5638	0.5513	0.4949
LV1	0.8827	1.4559	1.0269	0.4522	0.6596
MM1		1.9208	2.1549	3.0000	1.5850
RG1		1.1871	0.9626	0.4711	1.4685
VH1	1.2366	1.5086	1.0044	1.0555	1.5850
Avg	1.3583	1.4844	1.1741	0.9050	1.1160
Std	0.2789	0.1770	0.4997	0.7251	0.4774
s.e.m.	0.1054	0.0590	0.1580	0.2417	0.1804

Spatial Frequency (cpd)

	0.5	3	8	12	16
Normals: 3 Degree Field, Log Contrast Sensitivity					
BB1	1.9208	2.2218		1.3872	
BB2	0.8601	1.2757		0.7799	0.4330
BP1	2.3010	1.4437	1.9208	1.0223	
CG1	1.4685	0.9586	0.6757	0.6716	
DF1	2.0969	0.8386	0.8894	0.7258	
DR1	0.6737	1.6021	1.3768	0.6478	0.7423
JH1	0.6038		0.6478	0.5467	
LV1	0.9431	0.5884	0.4949	0.5058	0.7212
MM1					
RG1	0.5229	1.6778	0.5935	1.2676	
VH1		0.9547	1.0088	1.6021	0.5735
Avg	1.2656	1.2846	0.9509	0.9157	0.6175
Std	0.6534	0.4782	0.4517	0.3631	0.1248
s.e.m.	0.2310	0.1691	0.1707	0.1210	0.0721

Spatial Frequency (cpd)

Normals: 6 Degree Field, Log Contrast Sensitivity

	0.5	3	8	12	16
BB1	1.2007	0.5686	0.8356	0.7852	
BB2	0.6946	1.4815	0.7620	1.7447	0.6799
BP1	0.9318	1.3665	1.4949	2.0000	2.0000
CG1		0.7447	0.6478	1.2291	
DF1	0.8697	1.3279	2.0000	2.3979	
DR1	0.8416	1.5686	1.0757	0.5560	0.6308
JH1	0.5638	0.6676	0.4522		
LV1	1.6021		0.4868	0.5817	1.0177
MM1	2.0000	1.1367	0.7932		
RG1	0.9706	1.5229	0.4389	1.0458	0.7077
VH1	1.8239	1.0757	0.9393	2.5229	
Avg	1.1499	1.1461	0.9024	1.4293	1.0072
Std	0.4678	0.3526	0.4551	0.7182	0.5146
s.e.m.	0.1559	0.1175	0.1439	0.2539	0.2573

Spatial Frequency (cpd)

Normals: 6-12 Degree Annulus, Log Contrast Sensitivit

	1	5	8	12
BB1		0.7932	0.7696	
BB2	1.1249	1.2596	0.7986	0.5544
BP1	0.8729	1.1739		1.5528
CG1		1.8239		
DF1	1.6021		1.0706	1.5850
DR1	0.8210	0.6716	1.6198	1.4949
JH1	0.5229	0.4962	0.6517	
LV1	1.1805		0.7375	0.7375
MM1				
RG1	0.6696	1.2840	0.5800	
VH1	0.6799	1.0969	0.5969	0.6737
Avg	0.9342	1.0749	0.8531	1.0997
Std	0.3285	0.3915	0.3239	0.4485
s.e.m.	0.1242	0.1480	0.1224	0.2006

Spatial Frequency (cpd)

Normals: 6-12 Degree Upper Hemifield, Log Contrast Sensitivity
MM1

	1	5	8	12
LV1	1.1739	0.0000	0.7305	1.1135
DR1	1.7447	1.5376	1.7959	1.5086
VH1	1.3279	1.6576	0.9393	1.3468
BB2	1.0555	0.8477	1.0362	1.2291
RG1	1.0000	0.8210	1.2076	
DF1	1.4559	1.6990	1.1549	
CG1	1.0915	0.7620	0.6778	
JH1	1.3665	1.4685	1.2840	
BB1	1.1549		0.0000	
BP1	1.2218	1.0315	1.3188	
Avg.	1.2593	1.0917	1.0145	1.2995
St. Dev.	0.2114	0.5235	0.4541	0.1462
S.E.M	0.0705	0.1851	0.1514	0.0844

Spatial Frequency (cpd)

Normals: 6-12 Degree Lower Hemifield, Log Contrast Sensitivity
MM1

	1	5	8	12
LV1	1.3565	1.6990	0.8356	1.1079
DR1	0.9355	0.9957	0.9706	1.0506
VH1	1.1427	1.4437	1.4815	1.7212
BB2	0.8153	0.7235	1.2596	0.6946
RG1	1.8539	1.2924	1.2840	
DF1	1.2518	1.0315	0.6021	
CG1	0.8508	1.6990	1.0757	
JH1	1.6021	1.4089	1.6576	
BB1	1.6198	0.0000	0.0000	
BP1	0.0000	1.0315	0.9281	
Mean	1.1428	1.1325	1.0095	1.1436
St dev	0.5043	0.4827	0.4482	0.3692
S.E.M.	0.1681	0.1609	0.1494	0.2131

	Spatial Frequency (cpd)				
	0.5	3	8	12	16
Peripherals: 12 Degree Field, Log Contrast Sensitivity					
JS1	0.8356	0.9066	0.0000		
JW1	0.6364	1.4949	1.2007		
KT1	1.3768	0.0000	0.0000		
LB1	1.4318	0.0000	0.0000		
MH1	1.4437	0.6517	1.9208		
NG1	1.4089	0.0000	1.3979		
VH2	1.6021	1.3468	0.0000		
WS1	0.0000	1.3010	0.9547		
Mean	1.0919	0.7126	0.6843		
St Dev	0.5180	0.6047	0.7290		
SEM	0.1727	0.2016	0.2430		

	Spatial Frequency (cpd)				
	0.5	3	8	12	16
Peripherals: 3 Degree Field, Log Contrast Sensitivity					
JS1	0.9393	1.8861	0.0000	0.8794	1.3768
JW1	2.6990	0.0000	1.3372	2.0000	0.7100
KT1	0.0000	0.0000	0.0000	0.0000	0.0000
LB1	0.9101	2.2218	0.6904	0.0000	0.0000
MH1	0.9788	1.9586	1.7696	1.5086	0.0000
NG1	1.4318	1.0132	2.6990	2.5229	0.0000
VH2	1.6990	2.3979	1.5528	2.3010	2.0458
WS1	0.7878	1.2757	0.0000	0.7033	0.0000
Mean	1.1807	1.3442	1.0061	1.2394	0.5166
St Dev	0.7380	0.8860	0.9350	0.9297	0.7458
SEM	0.2789	0.3349	0.3534	0.3514	0.2819

Spatial Frequency (cpd)				
	0.5	3	8	12	16

Peripherals: 6 Degree Field, Log Contrast Sensitivity

	0.5	3	8	12	16
JS1	2.0969	0.7212	0.7986	1.0088	0.0000
JW1	0.7620	1.5229	0.0000	1.1135	
KT1	1.3279	0.0000	0.0000	0.0000	
LB1	0.0000	0.0000	1.1249	0.0000	
MH1	1.2291	2.1549	0.0000	0.4711	
NG1	0.0000	1.6778	2.0458	1.2924	
VH2	1.5086	0.0000	1.1308	0.0000	0.0000
WS1	1.0809	1.3979	0.8239	1.5686	1.5229
Mean	1.0007	0.9343	0.7405	0.6818	0.5076
St Dev	0.6787	0.8115	0.6763	0.6012	0.7179
SEM	0.2565	0.3067	0.2556	0.2272	0.5076

Spatial Frequency (cpd)			
	1	5	8	12

Peripherals: 6-12 Degree Annulus, Log Contrast Sensitivity

	1	5	8	12
JS1	0.0000	0.6904	1.5376	1.1938
JW1	0.0000	2.5229	0.8297	0.5086
KT1	0.0000	0.0000	0.0000	0.0000
LB1	1.6576	1.4685	2.0458	0.0000
MH1	0.0000	1.0915	1.3565	1.7696
NG1	1.1487	1.6021	1.1367	1.6198
VH2	0.0000	0.0000	1.4202	1.4815
WS1	0.0000	0.0000	0.0000	0.0000
Mean	0.3508	0.9219	1.0408	0.8217
St Dev	0.6208	0.8629	0.6820	0.7274
SEM	0.2346	0.3261	0.2578	0.2749

Spatial Frequency (cpd)

Maculars: 12 Degree Field, Log Contrast Sensitivity

	0.5	3	8	12	16
CM1	2.2218	0.0000	0.5638	1.3979	
MG1	0.0000	0.6308	0.0000	0.0000	
YB1	0.0000	0.0000	0.0000	0.0000	
HP1	1.5850	0.6440	1.3768	0.0000	
MW1	0.0000	0.0000	0.0000	0.0000	
FC1	1.1487	1.3188	1.3468	1.0362	
Mean	0.8259	0.4323	0.5479	0.4057	
St Dev	0.8828	0.4883	0.6091	0.5832	
SEM	0.3948	0.2184	0.2724	0.2608	

Spatial Frequency (cpd)

Maculars: 3 Degree Field, Log Contrast Sensitivity

	0.5	3	8	12	16
CM1	0.0000	1.4318	0.3979	0.0000	0.0000
MG1	0.0000	0.0000	0.0000	0.0000	0.0000
YB1	1.2218	0.0000	0.0000	0.9355	0.0000
HP1	0.0000	0.0000	0.7905	1.3872	2.5229
MW1	0.0000	0.8153	0.9355	0.0000	0.0000
FC1	2.3979	1.0410	0.0000	0.0000	0.0000
Mean	0.6033	0.5480	0.3540	0.3871	0.4205
St dev	0.9183	0.5768	0.3887	0.5628	0.9402
sem	0.4107	0.2580	0.1738	0.2517	0.4205

Spatial Frequency (cpd)

	0.5	3	8	12	16
Maculars: 6 Degree Field, Log Contrast Sensitivity					
CM1	1.5686	0.0000	0.5800	0.0000	0.0000
MG1	0.0000	0.0000	0.0000	0.0000	0.0000
YB1	0.0000	0.0000	0.0000	0.0000	0.0000
HP1	0.0000	0.0000	1.3279	1.2757	0.0000
MW1	0.0000	0.6021	0.0000	1.1135	0.0000
FC1	0.6990	0.7670	1.0315	2.5229	1.2147
Mean	0.3779	0.2282	0.4899	0.8187	0.2024
St Dev	0.5905	0.3262	0.5360	0.9319	0.4527
SEM	0.2641	0.1459	0.2397	0.4168	0.2024

Spatial Frequency (cpd)

	1	5	8	12
Maculars: 6-12 Degree Annulus, Log Contrast Sensitivity				
CM1	1.4815	0.0000	2.0000	0.0000
MG1	0.0000	0.0000	0.0000	0.0000
YB1	0.0000	0.0000	0.7670	0.0000
HP1	0.9172	0.0000	0.0000	0.0000
MW1	0.0000	0.0000	0.0000	1.7447
FC1	0.0000	0.7620	1.5376	0.0000
Mean	0.3998	0.1270	0.7174	0.2908
St Dev	0.5884	0.2840	0.8025	0.6502
SEM	0.2631	0.1270	0.3589	0.2908

Appendix V

The Visualization Tool User's Guide
(withdrawn from published report)

Appendix VI

The Inhomogenous Retinal Cortical Model User's Guide
(withdrawn from published report)

Appendix VII

The VisionProbe™ User's Guide
(withdrawn from published report)